End-to-end Speech Separation with Neural Networks

Yi Luo

Submitted in partial fulfillment of the
requirements for the degree of
Doctor of Philosophy
under the Executive Committee
of the Graduate School of Arts and Sciences

COLUMBIA UNIVERSITY

2021

Abstract

End-to-end Speech Separation with Neural Networks

Yi Luo

Speech separation has long been an active research topic in the signal processing community with its importance in a wide range of applications such as hearable devices and telecommunication systems. It not only serves as a fundamental problem for all higher-level speech processing tasks such as automatic speech recognition, natural language understanding, and smart personal assistants, but also plays an important role in smart earphones and augmented and virtual reality devices.

With the recent progress in deep neural networks, the separation performance has been significantly advanced by various new problem definitions and model architectures. The most widely-used approach in the past years performs separation in time-frequency domain, where a spectrogram or a time-frequency representation is first calculated from the mixture signal and multiple time-frequency masks are then estimated for the target sources. The masks are applied on the mixture's time-frequency representation to extract the target representations, and then operations such as inverse short-time Fourier transform is utilized to convert them back to waveforms. However, such frequency-domain methods may have difficulties in modeling the phase spectrogram as the conventional time-frequency masks often only consider the magnitude spectrogram. Moreover, the training objectives for the frequency-domain methods are typically also in frequency-domain, which may not be inline with widely-used time-domain evaluation metrics such as signal-to-noise ratio and signal-to-distortion ratio.

The problem formulation of time-domain, end-to-end speech separation naturally arises to tackle the disadvantages in the frequency-domain systems. The end-to-end speech separation networks take the mixture waveform as input and directly estimate the waveforms of the target sources. Following the general pipeline of conventional frequency-domain systems which contains a waveform encoder, a separator, and a waveform decoder, time-domain systems can be design in a similar way while significantly improves the separation performance. In this dissertation, I focus on multiple aspects in the general problem formulation of end-to-end separation networks including the system designs, model architectures, and training objectives. I start with a single-channel pipeline, which we refer to as the time-domain audio separation network (TasNet), to validate the advantage of end-to-end separation comparing with the conventional time-frequency domain pipelines. I then move to the multi-channel scenario and introduce the filter-and-sum network (FaSNet) for both fixed-geometry and ad-hoc geometry microphone arrays. Next I introduce methods for lightweight network architecture design that allows the models to maintain the separation performance while using only as small as 2.5% model size and 17.6% model complexity. After that, I look into the training objective functions for end-to-end speech separation and describe two training objectives for separating varying numbers of sources and improving the robustness under reverberant environments, respectively. Finally I take a step back and revisit several problem formulations in end-to-end separation pipeline and raise more questions in this framework to be further analyzed and investigated in future works.

Table of Contents

List of Tables

List of Figures

Acknowledgements

It all started from the afternoon of December 4, 2015 - I went to LabROSA's office to seek for some research opportunities on music information retrieval, and I met Zhuo Chen there and learned about his ongoing work on Deep Clustering, one of the very first successful neural network speech separation systems. I knew nothing about neural networks at that moment, but Zhuo still kindly offered me the chance to help him extend the application of Deep Clustering to the task of music separation. That was the start of my career on the research of source separation. The works I've done as an assistant of Zhuo have led to my very first academic conference, my very first transaction paper, and eventually a position in NAPLab as a PhD student. I would say that my career and life would be completely different without Zhuo's help - not only about that afternoon, but also about all the suggestions and advice throughout these years. Words cannot express how grateful I am, thank you so much for all the efforts.

It is my great honor to have Prof. Nima Mesgarani to be my PhD advisor. Nima is not only a world-class researcher but also an extremely good mentor - he always knows the best way to mentor different students according to their own aptitudes. Working with Nima is always a pleasure. I can clearly remember the extremely detailed help from Nima in 2017 and 2018 when I was a newly admitted PhD student and working on the first transaction paper and the first TasNet models. Those days allowed me to know what I should do as both a PhD student and a researcher. After that I got a clearer idea about the general problem of speech separation and gained more experience on managing research projects, and then Nima offered me numerous suggestions on how to become an independent researcher and gave me enough freedom to work on the problems that I personally feel interesting. I would not be what I am now without all the efforts from Nima, and I can say that NAPLab *is* the best place for me and I am really fortunate to be a member here and being mentored by Nima.

I would like to thank the committee for my PhD defense: Prof. John Wright, Prof. Nima Mesgarani, Prof. John Paisley, Prof. Julia Hirschberg, and Prof. Shih-Chii Liu, for your time, encouragement, and insightful comments. I would like to also say thank you to all my collaborators. Dr. Jonathan Le Roux and Dr. John Hershey, thank you for being my very first collaborators and guided me to the world of source separation, I was really lucky enough to work with both of you at the very beginning of my career. Dr. Takuya Yoshioka, thank you for mentoring during my internship in Microsoft Research, I really enjoyed my days there and really learned a lot from you. Prof. Shih-Chii Liu and Dr. Enea Ceolini, I really missed the days we worked together. Really looking forward to meet you offline again and grab a beer together. Cong Han, I have witnessed your growth as a researcher and it is really great that we have you in the lab. NAPLab is a special place that we have people working on all different types of problems under a same large topic - understanding how the brain processes speech, and building computational models to analyze and mimic that. Every week's lab meeting was always a fresh experience as we can always expect some project from a different perspective than our own interest. I would like to thank all our previous and current lab members for not only sharing those very interesting works every week but also made our lab like a cozy home to stay. Zhuo, Bahar, Laura, James, Tasha, Hassan, Rajath, Kathleen, Prachi, Menoua, Jingping, Sam, Ali, Cong, Vinay, and Xiaomin, thank you for all the good memories in these years.

Special thanks to my parents for all the supports without asking for anything in return. I'm returning home now, and it's time for me to take up my duties for the family. Also special thanks to Yuxuan Tang for supporting me throughout these year. Video chatting with you is now a daily routine after these years, and you were always by my side in all my best memories. It's almost the end of the days we are apart, and let's build more memories together in the rest of our lives.

Covid-19 had a significant influence on the world. I never thought before 2019 that I will spend one and a half year working towards my PhD in my bedroom in China, and I never thought that the ASRU 2019 workshop in Singapore was the last place I met Nima in person. This is an unexpected experience for me and a hard time for the entire world. Thanks to Nima again for his considerations on this situation and allowing me to work and even graduate remotely, and thanks to Jingping on helping me with the packing and shipping of my belongings in NYC. Hope that the world will return to normalcy soon.

Chapter 1: Introduction to Speech Separation

In this chapter I will provide an introduction to the task of speech separation. I will first make a brief overview on the non-deep-learning speech separation algorithms and methods, and then show how recent developments on neural networks can either be applied to the conventional algorithms or propose new problem formulations to the task. I will then introduce the commonly used evaluation metrics and datasets for speech separation.

1.1 The Speech Separation Problem: A Brief Overview

The problem of speech separation has been investigated for decades [9], [19], [22], [25], [27], [41], [215]. Its problem formulation is straightforward and simple: given a set of observations of mixture signals $\{\mathbf{y}^m\}_{m=1}^{M}$ where M denotes the number of channels or microphones available, C target sources $\{\mathbf{x}_c\}_{c=1}^{C}$ should be extracted or separated from the mixture signals. With a standard assumption of additive sources, each mixture $\mathbf{y}_i$ contains its observation of all the sources with an optional additive noise signal:

$$\mathbf{y}^m = \sum_{c=1}^{C} \mathbf{x}_c^m + \mathbf{n}^m \tag{1.1}$$

where $\mathbf{x}_c^m$ and $\mathbf{n}^m$ denote the c-th target source and the additive noise observed by the m-th channel, respectively. Depending on the number of available channels M, the speech separation problem can be categorized into *single-channel* separation ($M = 1$) or *multi-channel* separation ($M > 1$). The target sources $\{\mathbf{x}_c\}_{c=1}^{C}$ can either be their observations in a certain channel, e.g., $\{\mathbf{x}_c^1\}_{c=1}^{C}$, or the modulated signals generated from the target sources from all channels, e.g., via *beamforming* algorithms [20], [38], [66], [142].

Real-world environments typically contain reverberations. A common definition of target sources included both the direct-path signal, early reverberation signal, and the late reverberation signal, which requires the speech separation system to separation all signals that are directly related to or generated by the clean target signal. For the task of joint speech separation and dereverberation, either the direct-path signal or the sum of direct-path signal and early reverberation signal can be used as the target sources. In this dissertation, we assume that the late reverberation is always included in the target sources except for certain methods in Chapter 3 and 5.

1.2 Existing Methods for Speech Separation

Due to the recent development of neural networks, speech separation systems can now be broadly categorized by whether a deep neural network is applied. I first make an overview on the methods that do not explicitly use neural networks, and then introduce the literature on deep learning systems.

1.2.1 Non-deep-learning Methods

Non-deep-learning algorithms proposed for the speech separation problem can be roughly categorized into three categories: *statistical* methods, *clustering* methods, and *factorization* methods.

1. In *statistical* methods, the target speech signal is modeled with probability distributions such as generalized Gaussian distributions [43], [46], [152], [178], [189] or methods such as independent component analysis (ICA) [12], [21], [26], [37], [39], [56] and independent vector analysis (IVA) [31], [40], [54], [70], [85], [141], [320], where the interference signal is assumed to be statistically independent from the target speech. Maximum likelihood estimation method is typically applied based on the known statistical distributions of the target.

   A standard problem formulation for an ICA system is as follows. The mixture signal $\mathbf{y}^m$ is rewritten as the weighted summation of the sources $\{\mathbf{x}_c^m\}_{c=1}^C$:

$$\mathbf{y}^m = \sum_{c=1}^{C} h_c^m \mathbf{x}_c^m \tag{1.2}$$

where the scalar h_c^m denotes the *transfer characteristic* from source $\mathbf{x}_c^m$ to $\mathbf{y}^m$, and the mixing condition is defined as *instantaneous mixing*. When reverberation exists, the transfer characteristic becomes a finite impulse response (FIR) filter:

$$\mathbf{y}^m = \sum_{c=1}^{C} \mathbf{h}_c^m \circledast \mathbf{x}_c^m \tag{1.3}$$

where $\circledast$ denotes the convolution operation, and the mixing condition is defined as *convolutive mixing*. While the convolutive mixing problem is hard to solve in time domain, the equivalent instantaneous mixing condition in frequency domain can be derived from the convolution theorem:

$$\mathbf{Y}^m(t,f) \approx \sum_{c=1}^{C} \mathbf{H}_c^m(f)\mathbf{X}_c^m(t,f) \tag{1.4}$$

where $\mathbf{Y}^m \in \mathbb{C}^{T\times F}$ and $\mathbf{X}_c^m \in \mathbb{C}^{T\times F}$ denote the spectrogram of $\mathbf{y}^m$ and $\mathbf{x}_c^m$ calculated by the short-time Fourier transform (STFT), respectively, and $\mathbf{H}_c^m \in \mathbb{C}^F$ denotes the spectrum of the FIR transfer characteristic. Note that equation 1.4 is an approximation since the window size used for STFT is typically shorter than the length of the FIR filter.

By jointly considering all available channels, an ICA system attempts to find an *unmixing* matrix at each frequency $\mathbf{W}(f) \in \mathbb{C}^{C\times M}$ that reverse the mixing procedure:

$$\hat{\mathbf{X}}(t,f) = \mathbf{W}(f)\hat{\mathbf{Y}}(t,f) \tag{1.5}$$

where $\hat{\mathbf{Y}}(t,f) = [\mathbf{Y}^1(t,f),\ldots,\mathbf{Y}^M(t,f)] \in \mathbb{C}^{M\times 1}$. $\hat{\mathbf{X}}(t,f) \in \mathbb{C}^{C\times 1}$ denotes the time-frequency (T-F) bin for the C estimated sources at frame t and frequency f.

2. In *clustering* methods, the characteristics of the target speakers, such as pitch and signal continuity, are estimated from the observation and used to separate the target signals in the mixture. One of the most important methods in this category is computational auditory scene analysis (CASA) [25], [36], [55], [60], [69], [74], where a T-F representation of the input

mixture is first calculated and the T-F bins are classified to different target sources. The ideal or oracle source assignments of the T-F bins can be defined as *T-F masks* [24], [45], and multiple ideal T-F masks such as ideal binary mask (IBM) [89], ideal ratio mask (IRM) [81], and Wiener-filter-like mask (WFM) [18] have been proposed for the task. Moreover, by alleviating the constraint that the T-F masks have to be the source assignments and thus have ranges between 0 and 1, phase-sensitive mask (PSM) [98] and complex ideal ratio mask (cIRM) [113] are further proposed to consider the phase information in the masks.

To be more specific, consider a target source at a certain channel $\mathbf{x}_c^1$ with its corresponding spectrogram $\mathbf{X}_c^1 \in \mathbb{C}^{T\times F}$ and the spectrogram of noise $\mathbf{n}^1$ denoted as $\mathbf{N}^1$. The ideal T-F masks can then be defined as:

$$\text{IBM}_c^1 \triangleq \begin{cases} 1, & \text{if } |\mathbf{X}_c^1| \geq |\mathbf{X}_j^1| \text{ for } \forall j \neq c \text{ and } |\mathbf{X}_c^1| \geq |\mathbf{N}^1| \\ 0, & \text{otherwise} \end{cases} \tag{1.6}$$

$$\text{IRM}_c^1 \triangleq \frac{|\mathbf{X}_c^1|}{\sum_{i=1}^{C} |\mathbf{X}_i^1| + |\mathbf{N}^1|} \tag{1.7}$$

$$\text{WFM}_c^1 \triangleq \frac{|\mathbf{X}_c^1|^2}{\sum_{i=1}^{C} |\mathbf{X}_i^1|^2 + |\mathbf{N}^1|^2} \tag{1.8}$$

$$\text{PSM}_c^1 \triangleq \text{Re}\left(\frac{\mathbf{X}_c^1}{\mathbf{Y}^1}\right) \tag{1.9}$$

$$g(\text{cIRM}_c^1) \triangleq 10\,\frac{1 - e^{-0.1\cdot g(\mathbf{X}_c^1/\mathbf{Y}^1)}}{1 + e^{-0.1\cdot g(\mathbf{X}_c^1/\mathbf{Y}^1)}}, \text{ where } g(\cdot) \text{ is } \text{Re}(\cdot) \text{ or } \text{Im}(\cdot) \tag{1.10}$$

where the matrix divisions are performed in an element-wise fashion. The T-F masks are estimated from the mixture observations $\{\mathbf{Y}^m\}_{m=1}^{M}$ and applied to the mixture's spectrogram by element-wise multiplication. The separated source waveforms are obtained by applying inverse STFT to the masked spectrograms with the phase spectrogram of the mixture.

3. *Factorization* models, such as non-negative matrix factorization (NMF) [15], [34], [42], [44], [90], [92], formulate the separation problem as a matrix factorization problem in which the T-F representation of the mixture is factorized into a weighed sum (i.e., *activations*) of a set

of *basis signals*:

$$\mathbf{W}^1, \mathbf{H}^1 = \underset{\mathbf{W}^1, \mathbf{H}^1}{\operatorname{argmin}} D(|\mathbf{Y}^1|, \mathbf{W}^1\mathbf{H}^1), \quad \text{s.t.}\, \mathbf{W}^1, \mathbf{H}^1 \geq \mathbf{0} \tag{1.11}$$

where $\mathbf{W}^1 \in \mathbb{R}^{T\times K}$ and $\mathbf{H}^1 \in \mathbb{R}^{K\times F}$ denote the nonnegative basis matrix and the nonnegative activation matrix, respectively, and $D(\mathbf{A}, \mathbf{B})$ denotes a distance measure between the two matrices $\mathbf{A}$ and $\mathbf{B}$. K denotes the number of basis signals and also puts constraint on the rank of the two matrices. Dictionary learning methods can be applied to learn the basis signals $\mathbf{W}^1$ in advance [64], [65], [75], [77], and equation 1.11 is modified to only estimate the activation matrix $\mathbf{H}^1$:

$$\mathbf{H}^1 = \underset{\mathbf{H}^1}{\operatorname{argmin}} D(|\mathbf{Y}^1|, \mathbf{W}^1\mathbf{H}^1), \quad \text{s.t.}\, \mathbf{H}^1 \geq \mathbf{0} \tag{1.12}$$

Sparsity constraints can also be enforced on the activation matrix $\mathbf{H}^1$ [13], [17], [28], [32], [33], [106]:

$$\mathbf{H}^1 = \underset{\mathbf{H}^1}{\operatorname{argmin}} D(|\mathbf{Y}^1|, \mathbf{W}^1\mathbf{H}^1) + \lambda|\mathbf{H}^1|_1, \quad \text{s.t.}\, \mathbf{H}^1 \geq \mathbf{0} \tag{1.13}$$

where $|\cdot|_1$ denotes the L^1 norm and $\lambda \in \mathbb{R}$ denotes the weight of the sparsity term in the optimization objective. The multi-channel extension to single-channel NMF is typically formulated in complex-domain, and the basis signals are modified to include the spatial properties of the different channels [50], [62], [63], [72], [103], [191].

Another important method for multi-channel speech separation is *beamforming* or *spatial filtering* methods [5], [7], [14], [23], [53], [142]. A beamforming algorithm estimates M filters for the M mixture observations to extract a target source by enhancing the signal coming from the direction of the target source and filtering out the interference signals in other directions. The most widely-used configuration is the linear *filter-and-sum* beamformer operated in frequency domain, which has the same formulation as equation 1.5 where $\mathbf{W}(f)$ denotes the beamforming filter coefficients for all the C sources. Various filter-and-sum beamformers, such as the multi-channel Wiener filter (MWF) beamformer, minimum variance distortionless response (MVDR) beamformer, and linearly constrained minimum variance (LCMV) beamformer, have been proposed to satisfy certain constraints and requirements on the filtered sources.

1.2.2 Deep-learning Systems

There are mainly two ways that deep neural networks can be applied to the speech separation task. The first way is to build new pipelines that purely rely on the modeling capacity of modern neural networks without the conventional design paradigms. Thanks to the capacity of modern deep neural networks, conventional operations in a standard speech separation pipeline, such as STFT and T-F masking, may not be necessary and can be implicitly done within a neural network. Such systems typically take the mixture waveform as the input and directly estimate the waveforms of the target sources. After the success of 1-D CNN architectures on the task of sample-level speech synthesis [130], various 1-D CNN architectures have been proposed and compared in the task of waveform-level speech separation [211], [240], [294].

The second way is to replace certain stages or operations in the non-deep-learning methods by a neural network. For methods that contain iterative parameter update procedures, e.g., various NMF algorithms, the iterations can be *unfolded* as different *layers* in a deep neural network [79], [105], [169]. Moreover, NMF algorithms can first be applied to learn the basis signals or the activations of the target sources, and a neural network can take both the mixture signals and the NMF outputs as inputs and perform a better separation [82], [126], [160], [203]. Neural network designs that directly apply the nonnegativity constraints to the intermediate feature like the NMF systems have also been proposed [163], [167]. For methods that rely on handcrafted features, e.g., CASA systems that use pre-calculated features for T-F bin classification, the feature extraction process can be done by neural networks and can even be jointly optimized with the clustering process [121], [123], [140], [198]. The T-F source assignments can also be directly generated by a neural network without an explicit clustering process [80], [102], [148], [173]. The T-F representation for

T-F mask calculation is typically calculated by STFT, while other learnable signal transformations defined by neural networks can also be designed to learn better signal representations [201], [214], [243], [266], [280], [299].

The training of neural network speech separation models typically rely on the supervised training framework, where the target speakers are used as the training labels during the training phase. A sequential order, or *permutation*, is then implicitly introduced to both the system outputs and the training labels. When additional speaker-specific information is available, the permutation of the system outputs can be easily determined, and the corresponding training label permutation can be set to match that of the system outputs. However, when the speaker-specific information is not available, the system output permutation can be different from the training label permutation, and the training can fail due to this permutation mismatch.

Two important systems, *deep clustering (DPCL)* [121] and *permutation invariant training (PIT)* [173], were proposed to solve this permutation problem and enabled the recent advanced of deep learning separation systems. DPCL follows the problem formulation of CASA-based approaches where T-F masks are estimated from the mixture's spectrogram. The masks are obtained by performing K-means clustering on a set of *discriminative embeddings* generated by a neural network. Each embedding corresponds to a T-F bin, and the training objective is designed to maximize the similarity between the embeddings whose T-F bins are dominated by the same source, and minimize the similarity between the embeddings whose T-F bins are dominated by different sources:

$$\mathcal{L}_{DPCL} = |VV^T - YY^T|_W^2 \tag{1.14}$$

where $V \in \mathbb{R}^{TF\times K}$ denotes the K-dimensional embeddings for all T-F bins, $Y \in \mathbb{R}^{TF\times 1}$ is the IBM defined in equation 1.6 representing the oracle source assignments, and $|\cdot|_W$ denotes the Frobenius norm of a matrix. During inference phase, the embeddings are extracted and directly sent to the K-means algorithm to achieve the classification assignments of the T-F bins, which are used as the estimated binary T-F masks for the sources. Since the affinity matrices VV^T and YY^T are permutation-free, DPCL does not require an explicit source permutation during training. Alternative training objectives have been proposed to either learn better embeddings or allow more robust clustering results [123], [140], [151], [185], [198], [218], [242].

PIT attempts to alleviate the permutation problem in another way. It first calculates the standard training objective, such as the mean-square error (MSE) between the separated and target source spectrograms, for all possible permutations for the C sources ($C!$ permutations). The source permutation with the lowest value for the objective is then selected as the actual objective and used for network training:

$$\mathcal{L}_{PIT} = \min_{\pi \in \Pi_C} D(\{\hat{\mathbf{s}}_c\}_{c=1}^{C}, \pi(\{\mathbf{s}_c\}_{c=1}^{C})) \tag{1.15}$$

where Π_C denotes the $C!$ permutations for the C sources, $\{\mathbf{s}_c\}_{c=1}^{C}$ denotes the C target sources, $\{\hat{\mathbf{s}}_c\}_{c=1}^{C}$ denotes the C separated sources, $\pi(\cdot)$ corresponds to the operation of permuting the target sources with the selected permutation, and $D(\cdot)$ is a training objective function to be minimized. The permutations can be calculated on either frame-level [173] or utterance-level [148] depending on the network architecture. Since PIT is only a training trick and does not depend on the forms of the model inputs, outputs, and the actual training objective to be used, it can be applied to any network architectures and separation pipelines.

Most of the modern neural-network-based speech separation systems follow either the DPCL or the PIT pipeline to estimate a set of T-F masks or multiplicative masks, and they vary on the actual network architectures. Since the spectrograms are often treated as a sequential data, various forms of deep recurrent neural networks (RNNs) have been widely adopted in the separation systems [91], [123], [199], [287], [293], [303], [313]. After the success of convolutional neural networks (CNN) in the task of image recognition [119], CNN architectures have also been applied in the task of source separation [137], [165], [212], [305], [315], [316]. With the tremendous of self-attention-based models, or *Transformers* [166], in the natural language processing tasks, Transformer-based models have also been tested on the separation task [265], [267], [268], [300]. While these systems were mainly proposed for single-channel separation, their extensions to the multi-channel or multi-modal separation task can be straightforward by incorporating cross-channel or cross-modal features into either the encoder or the separator module [171], [186], [219], [231], [257], [273], [274], [304], [311].

Besides the use of cross-channel features to perform multi-channel speech separation with neural networks, conventional beamforming algorithms can also benefit from the advances in neural source separation systems. Conventional beamforming algorithms often require a robust and accurate estimation of the statistics of the target source. When the target and the interference are partially-overlapped, this can be done by detecting the periods where only the target source is active. However, when the two signals are fully-overlapped, the estimation of the target source can be hard and inaccurate, resulting in a poor estimation of DOA or spatial features required to calculate the beamforming filters. The so-called *masked-based beamforming* systems use the estimated T-F masks at each channel as the estimate for the target sources for the calculation of spatial features and beamforming filters [100], [117], [118], [122], [136], [143], [156], [157], [159], [170], [176], [181], [188], [202], [333]. Mask-based beamforming systems have been successful in both synthetic and real datasets and have been deployed to many devices and applications in the real world. For separation systems that do not generate T-F masks, the separation outputs can also be directly used for a selected conventional beamforming algorithm [205], [298], [319]. Moreover, the beamforming filters can also be directly learned by a neural network without the need of T-F masks or conventional problem formulations of beamforming, leading to the so-called *learning-based beamforming* systems [111], [125], [134], [135], [154], [161], [190], [241], [286].

1.3 Evaluation Metrics for Speech Separation Systems

The most widely-used evaluation metrics for modern speech separation systems are signal-to-noise ratio (SNR), signal-to-distortion ratio (SDR) and scale-invariant signal-to-distortion ratio (SI-SDR). These three metrics are designed to measure the signal quality of the separated sources compared to the targets.

1. SNR between an estimated signal $\hat{\mathbf{x}}$ and the clean target $\mathbf{x}$ is defined as:

$$\text{SNR}(\hat{\mathbf{x}}, \mathbf{x}) = 10 \log_{10} \left(\frac{||\mathbf{x}||_2^2}{||\mathbf{x} - \hat{\mathbf{x}}||_2^2} \right) \tag{1.16}$$

2. SDR has been used as a default metrics for source separation systems [35]. SDR allows a linear distortion on the target source $\mathcal{F}(\cdot)$, typically defined as the least-square mapping between delayed versions of $\mathbf{x}$ and $\hat{\mathbf{x}}$, and is defined as:

$$\text{SDR}(\hat{\mathbf{x}}, \mathbf{x}) = 10 \log_{10} \left(\frac{||\mathcal{F}(\mathbf{x})||_2^2}{||\mathcal{F}(\mathbf{x}) - \hat{\mathbf{x}}||_2^2} \right) \tag{1.17}$$

   Existing toolboxes provide sample implementations to the metric [35], [87].

3. SI-SDR was proposed as a modification to SDR to not only address the misuse of the metric but also improve its robustness and accuracy on the evaluation results [236]. SI-SDR is defined as:

$$\text{SI-SDR}(\hat{\mathbf{x}}, \mathbf{x}) = 10 \log_{10} \left(\frac{||\alpha\mathbf{x}||_2^2}{||\alpha\mathbf{x} - \hat{\mathbf{x}}||_2^2} \right) \tag{1.18}$$

   where $\alpha \triangleq \frac{\hat{\mathbf{x}}^T\mathbf{x}}{||\mathbf{x}||_2^2}$ is an optimal rescaling factor.

Beyond the three metrics, other evaluation metrics used for speech enhancement and source separation systems such as perceptual evaluation of speech quality (PESQ) [16], short-time objective intelligibility (STOI) [58], and perceptual evaluation methods for audio source separation (PEASS) [59], can also be applied to speech separation systems.

1.4 Datasets for Speech Separation

Most modern speech separation networks rely on simulated multi-speaker datasets for both training and evaluation. Although different systems may create their own datasets, there are a few benchmark datasets used by a variety of speech separation systems for fair performance comparison.

1. WSJ0-2mix [121]: WSJ0-2mix contains 30 hours of 8 kHz training data (20000 utterances) that are generated from the Wall Street Journal (WSJ0) si_tr_s set. It also has 10 hours of validation data (5000 utterances) and 5 hours of test data (3000 utterances) generated by using the si_dt_05 and si_et_05 sets, respectively. Each mixture is artificially generated by randomly selecting different speakers from the corresponding set and mixing them at a random relative signal-to-noise ratio (SNR) between -5 and 5 dB. All the utterances are assumed to be clean and anechoic, and all the mixtures contain a 100% overlap ratio between the two speakers.

2. WHAM! & WHAMR! [256], [291]: The WSJ0 Hipster Ambient Mixtures (WHAM!) dataset and its reverberant counterpart (WHAMR!) extend the anechoic and noise-free WSJ0-2mix dataset with real-world noise and artificial reverberations. The WHAM! noise dataset is split into 58 hours of training data (20000 utterances), 15 hours of validation data (5000 utterances), and 9 hours of test data (3000 utterances), respectively, following the original configuration of wsj0-2mix dataset. The artificial reverberantions are generated by simulating the room impulse response (RIR) filters from random-sized rooms [208].

3. SMS-WSJ [229]: The Spatialized Multi-Speaker Wall Street Journal (SMS-WSJ) dataset contains 33561, 982, and 1332 train, validation, and test mixtures, respectively, with highly randomized configurations of artificial room sizes, RIR filters, and microphone and speaker locations. It also contains truncated RIR filters that represent the early reflections and can potentially be used for joint separation and dereverberation task.

4. LibriMix [269]: The LibriMix dataset is generated by clean speech utterances in the Librispeech dataset [109] and noise signals from WHAM!. It contains both two-speaker and three-speaker mixtures with 170 and 186 hours of training data, respectively. It also contains a partially-overlapped test set where the overlap ratio between the speakers are uniformly

sampled between 0% and 100%. This configuration is designed to mimic the realistic and conversation-like scenarios.

5. LibriCSS [268]: The LibriCSS dataset is particularly designed for continuous speech separation task, which is defined as the separation problem on long, unsegmented recordings. It contains 10 hours of multi-channel audio recorded from real playbacks of utterances sampled from the Librispeech dataset from a loud speaker in real meeting rooms. The recording are split into 10 1-hour sessions, and each session is further segmented into 6 10-minute-long mini-sessions with different overall speaker overlap ratios. Each mini-session contains 8 active speakers with a maximum overlap ratio of 40%. This dataset is purely proposed for evaluation purpose, and the evaluation can be done at either utterance-level (with oracle utterance boundaries) or session-level with both signal quality metrics and automatic speech recognition accuracy.

Other public available datasets for the task of multi-talker speech recognition, e.g., the Computational Hearing in Multisource Environments (CHiME) datasets [51], [68], [73], [96], [180], can also be used for speech separation systems. However, some of the datasets might not contain clean target sources and the calculation of signal-quality metrics can be inaccurate, and the evaluation of the speech separation systems in such conditions can be done by evaluating the word error rate (WER) of the separated sources by a selected speech recognition engine.

Chapter 2: Single-channel System: Time-domain Audio Separation Network

In this chapter I will introduce a time-domain single-channel system, the time-domain audio separation network (TasNet), for source separation. TasNet has a simple motivation of replacing the complex-valued STFT with a real-valued, trainable module (namely the *adaptive encoder and decoder*) jointly learned with the separation module, and use a time-domain training objective function to perform end-to-end optimization. According to how the adaptive encoder and decoder and the separation module are designed, three versions of TasNet have been proposed: the *LSTM-TasNet* [201] was the very first version of TasNet which validated the applicability of such end-to-end training, the *Conv-TasNet* [243] was the second version of TasNet and was also the first deep learning system that surpassed the performance of several ideal magnitude time-frequency masks, and the *DPRNN-TasNet* [287] was the third version that significantly improved the sequence modeling power and boosted the performance.

2.1 LSTM-TasNet: Applicability of End-to-end Separation

Prior to LSTM-TasNet, all state-of-the-art systems for speech separation operated on frequency domain. LSTM-TasNet served as a step towards validating the applicability of end-to-end separation by replacing the STFT and inverse STFT stages by learnable encoding and decoding modules, while keeping the separation module almost unchanged. Experiment results showed that LSTM-TasNet can achieve better or on par performance comparing with other frequency-domain networks, proving the applicability of the end-to-end separation paradigm.

2.1.1 System Pipeline

The problem of single-channel speech separation can be formulated in terms of estimating C sources $s_1(t), \dots, s_C(t) \in \mathbb{R}^{1\times T}$, given the discrete waveform of the mixture $x(t) \in \mathbb{R}^{1\times T}$, where

$$x(t) = \sum_{c=1}^{C} s_c(t) \tag{2.1}$$

Following the same windowing process in STFT, the input mixture can be divided into overlapping windows of length L, represented by $\mathbf{x}_k \in \mathbb{R}^{1\times L}$, where $k = 1, \dots, \hat{T}$ denotes the window index and $\hat{T}$ denotes the total number of windows in the input. Instead of applying a discrete Fourier transform on each $\mathbf{x}_k$, LSTM-TasNet transforms $\mathbf{x}_k$ to a nonnegative hidden representation via a gated layer:

$$\bar{\mathbf{x}}_k = \frac{\mathbf{x}_k}{||\mathbf{x}_k||_2} \tag{2.2}$$

$$\mathbf{w}_k = \text{ReLU}(\bar{\mathbf{x}}_k\mathbf{U}) \odot \sigma(\bar{\mathbf{x}}_k\mathbf{V}) \tag{2.3}$$

where $\mathbf{w}_k \in \mathbb{R}^{1\times N}$ is the hidden representation for $\mathbf{x}_k$, $\mathbf{U}, \mathbf{V} \in \mathbb{R}^{L\times N}$ are two learnable weight matrices, $\text{ReLU}(\cdot)$ corresponds to the rectified linear unit function, $\sigma(\cdot)$ corresponds to the Sigmoid function, $||\cdot||_2$ denotes the L^2-norm of a vector, and $\odot$ denotes the Hadamard product. The L^2-norm normalization is applied to ensure that the calculation of $\mathbf{w}_k$ is invariant to the input power. Note that since the multiplication between $\mathbf{x}_k$ and each column in $\mathbf{U}$ and $\mathbf{V}$ can be viewed as a linear convolution operation, equation 2.3 can be viewed as an operation similar to DFT, and each column in $\mathbf{U}$ and $\mathbf{V}$ can be formulated as a convolutional kernel of length L.

Given that $\mathbf{w}_k$ is always nonnegative due to the gating operation, $\mathbf{w}_k$ can be treated as a replacement of the nonnegative magnitude spectrogram of the mixture, and C multiplicative mappings similar to the time-frequency masks can be estimated by methods identical to the conventional time-frequency masking systems. Given the sequence of hidden representations $\mathbf{W} \in \mathbb{R}^{\hat{T}\times N}$, a deep bi-directional LSTM (BLSTM) network is used as the separation module and applied on $\mathbf{W}$

to estimate C nonnegative "multiplicative masks" $\mathbf{M}_c \in \mathbb{R}^{\hat{T}\times N}$, , $c = 1, \ldots, C$. The estimated hidden representation $\mathbf{S}_c$ for source c is then obtained by calculating the Hadamard product between the mixture hidden representation $\mathbf{W}$ and the multiplicative mask $\mathbf{M}_c$:

$$\mathbf{S}_{c,k} = (\mathbf{W}_k \odot \mathbf{M}_{c,k}) \cdot ||\mathbf{x}_k||_2 \tag{2.4}$$

The L^2-norm of each frame is multiplied back to the masked hidden representations to reverse the L^2-norm normalization operation.

A linear transformation is finally applied to $\mathbf{S}_c$ to reconstruct the waveform of source c:

$$\hat{\mathbf{s}}_c(t) = OLA(\mathbf{S}_c\mathbf{P}) \tag{2.5}$$

where $\mathbf{P} \in \mathbb{R}^{N\times L}$ is the learnable weight matrix in the deecoder, and OLA stands for the overlap-add operation on the neighbouring windows for waveform reconstruction.

The training objective function is the negative SI-SDR score between the separated outputs $\hat{\mathbf{s}}_c(t)$ and the target outputs $\mathbf{s}_c(t)$ under the permutation invariant training (PIT) framework:

$$\mathcal{L} = -\max_{\pi\in\Pi_C} \text{SI-SDR}(\{\hat{\mathbf{s}}_c(t)\}_\pi, \{\mathbf{s}_c(t)\}) \tag{2.6}$$

where $\{\hat{\mathbf{s}}_c(t)\}_\pi$ denotes the permuted separated outputs $\{\hat{\mathbf{s}}_c(t)\}$ under the given index permuation π, and Π_C denotes all the possible index permutations for the C sources. Figure 2.1 shows the flowchart of LSTM-TasNet.

2.1.2 Design of the Separation Module

The separation module follows the standard design of deep recurrent networks in prior works. A standard deep recurrent network contains stacked recurrent layers such as LSTM or GRU layers, either uni-directional or bi-directional, to capture hierarchical sequential dependencies within the input sequence $\mathbf{W}$. As the name indicates, LSTM-TasNet uses LSTM layers for sequence

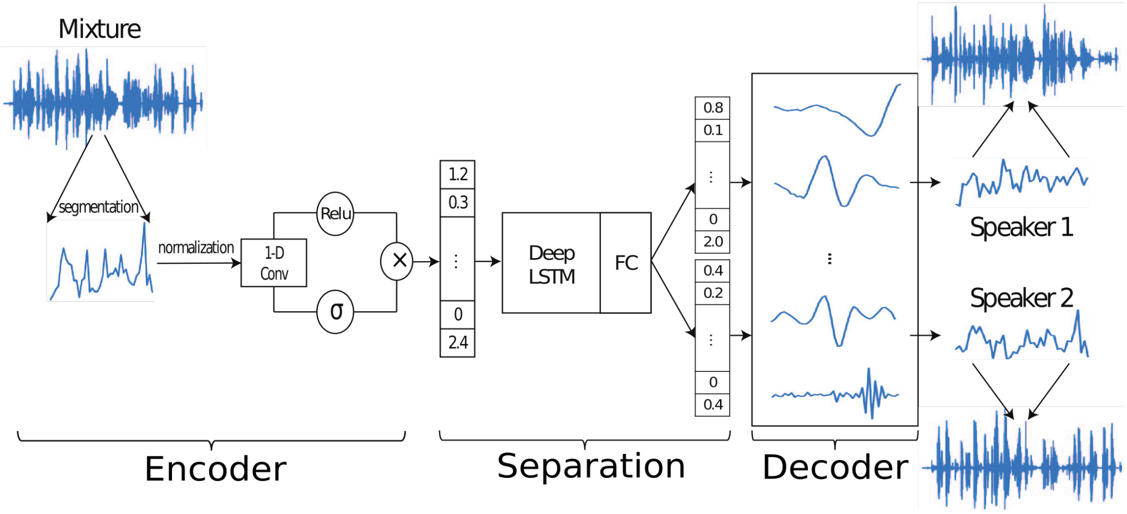

Figure 2.1: LSTM-TasNet performs end-to-end separation with a three-module design. A gated nonnegative encoder maps the input mixture waveform into a hidden representation. A separation module consists of stacked LSTM layers maps the hidden representation to a set of multiplicative masks. The masks are then applied to the mixture hidden representation to estimate the hidden representations of the target sources. A linear decoder transforms the hidden representations back to the waveforms.

modeling. A layer normalization operation is applied on the input sequence $\mathbf{W}$ to speed up and stabilize the training process:

$$\hat{\mathbf{w}}_k = \frac{\mathbf{g}}{\sigma} \otimes (\mathbf{w}_k - \mu) + \mathbf{b} \tag{2.7}$$

$$\mu = \frac{1}{N}\sum_{j=1}^{N} \mathbf{w}_{k,j} \quad \sigma = \sqrt{\frac{1}{N}\sum_{j=1}^{N}(\mathbf{w}_{k,j} - \mu)^2} \tag{2.8}$$

where parameters $\mathbf{g} \in \mathbb{R}^{1\times N}$ and $\mathbf{b} \in \mathbb{R}^{1\times N}$ are gain and bias vectors that are jointly optimized with the network. This normalization step enables the separation network to be scale invariant to the power of $\mathbf{W}$, and $\hat{\mathbf{W}}$ is used as the actual input sequence to the LSTM layers. A fully-connected (FC) layer is applied on the output of the last LSTM layer to generate the C masks $\{\mathrm{M}_c\}_{c=1}^{C}$. A Softmax function is used in the FC layer in order to mimic the property of T-F masks, hence the unit summation constraint $\sum_{c=1}^{C} \mathrm{M}_c = \mathbf{1}$ satisfies. Moreover, an identity skip connection [120] is added between every two LSTM layers in order to enhance the gradient flow and accelerate the

Table 2.1: SI-SDR (dB) and SDR (dB) for different methods on WSJ0-2mix dataset.

Method	Causal	SI-SDRi	SDRi
uPIT-LSTM [148]	✓	–	7.0
LSTM-TasNet	✓	7.7	**8.0**
DPCL++ [123]	×	**10.8**	–
DANet [140]	×	10.5	–
uPIT-BLSTM-ST [148]	×	–	10.0
BLSTM-TasNet	×	**10.8**	**11.1**

training process.

2.1.3 Experiment Configurations and Results

LSTM-TasNet is evaluated on the benchmark WSJ0-2mix dataset described in Chapter 1.4. The parameters of the network include the window length L, the dimension of the hidden representation N, and the configuration of the deep LSTM separation network. Here L is set to 40 samples (5 ms at 8 kHz) and N is set to 500. The deep LSTM separation module contains 4 uni-directional or bi-directional LSTM layers, where for the uni-directional configuration there are 1000 hidden units in each layer, and for the bi-directional configuration there are 500 hidden units in each direction. The FC layer contains 1000 hidden units that generates two 500-dimensional multiplicative masks.

During training, the batch size is set to 128, and the initial learning rate is set to $3e^{-4}$ for the causal system (uni-directional LSTM) and $1e^{-3}$ for the noncausal system (bi-directional LSTM). The learning rate is halved if the performance on the validation set is not improved in 3 consecutive epochs. The criteria for early stopping is no decrease in the cost function on the validation set for 10 epochs. Adam [83] is used as the optimization algorithm. Negative SI-SDR is used as the training objective. No further regularization or training procedures were used.

Similar to prior works [123], [140], the curriculum training strategy [47] is applied for network optimization. The training of the models starts on 0.5 second long utterances until convergence, and is resumed on 4 second long utterances afterwards.

Table 2.1 shows the performance of LSTM-TasNet as well as three frequency-domain systems, Deep Clustering (DPCL++, [123]), Permutation Invariant Training (PIT, [148]), and Deep Attractor Network (DANet, [140]). Here LSTM-TasNet represents the causal configuration with uni-directional LSTM layers and BLSTM-TasNet corresponds to the system with bi-directional LSTM layers. The best reported performance on WSJ0-2mix is reported for other systems. With causal configuration, LSTM-TasNet significantly outperforms another frequency-domain causal system, the uPIT model with LSTM as sequence modeling module. Under the noncausal configuration, LSTM-TasNet outperforms all the other systems. As the deep LSTM module of LSTM-TasNet is almost identical to the separation module in the three frequency-domain systems listed above, the results proves the applicability of end-to-end separation comparing with frequency-domain modeling.

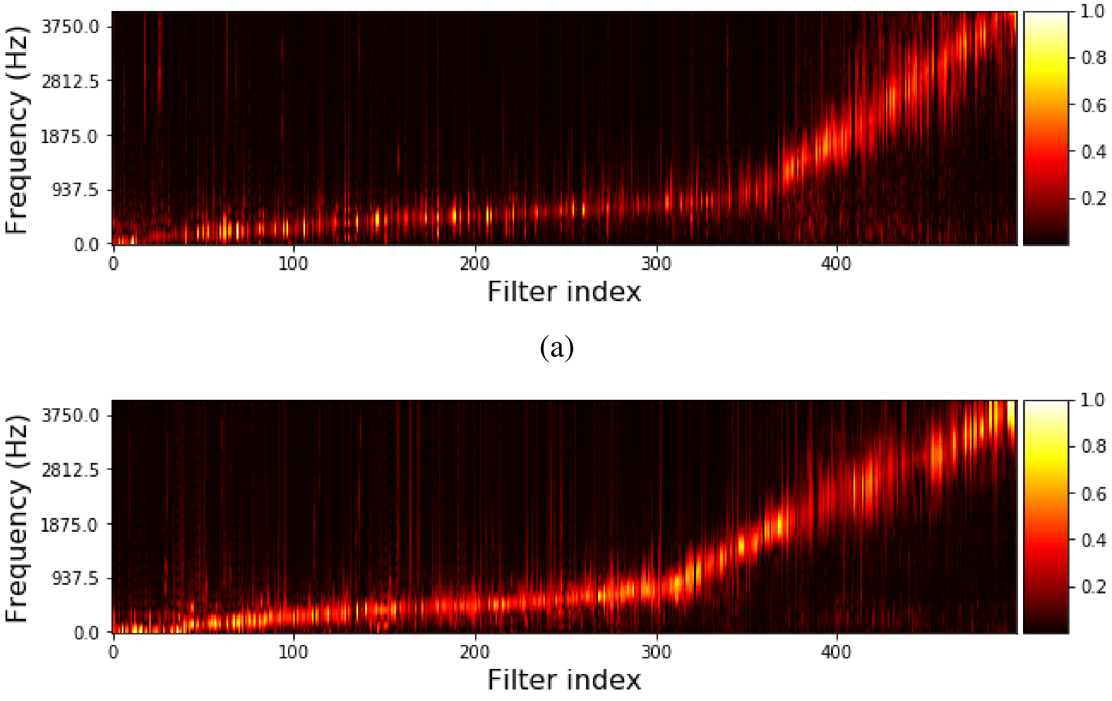

(a)

(b)

Figure 2.2: Frequency response of row vectors (i.e. basis kernels) in decoder weight $\mathbf{P}$ in (a) causal and (b) noncausal configurations.

The decoder weight $\mathbf{P}$ can be treated as the basis kernels for waveform reconstruction. Figure 2.2 shows the frequency response of the basis signals in $\mathbf{P}$ sorted by their center frequencies (i.e. the bin index corresponding to the the peak magnitude). There is clearly a continuous transition from low to high frequency, showing that the network has learned to perform a spectral decomposition of the waveform, similar to the finding in other time-domain speech processing systems [112]. The frequency bandwidths of the basis kernels also increase with their center frequencies similar to mel-filterbanks. In contrast, the basis signals in LSTM-TasNet have a higher resolution in lower frequencies compared to Mel and STFT. In fact, 60% of the basis signals have center frequencies below 1 kHz, which may indicate the importance of low-frequency resolution for accurate speech separation.

2.2 Conv-TasNet: Surpassing Ideal Magnitude Time-frequency Masking

While LSTM-TasNet already outperformed multiple frequency-domain speech separation methods in both causal and noncausal implementations, the use of the deep LSTM separation module significantly limited its applicability. First, choosing smaller window size L in the encoder increases the length of the mixture hidden representations $\hat{T}$, which makes the training of the stacked LSTM module unmanageable. Second, the large number of parameters in the deep LSTM module significantly increases its computational cost and limits its applicability to low-resource, low-power platforms such as wearable hearing devices. The third problem is caused by the long temporal dependencies of LSTM networks which often results in inconsistent separation accuracy, for example, when changing the starting point of the mixture. To alleviate the limitations of LSTM-TasNet, a fully-convolutional TasNet (Conv-TasNet) is proposed here that uses a convolutional network for the separation module. Motivated by the success of temporal convolutional network (TCN) models [124], [149], [179], Conv-TasNet uses stacked dilated 1-D convolutional blocks to replace the deep LSTM networks for the separation step. The use of convolution allows parallel processing on consecutive frames or segments to greatly speed up the separation process and also significantly reduces the model size. To further decrease the number of parameters and the computational cost, the original convolution operation is substituted with depthwise separable convolution [115], [144]. With these modifications, Conv-TasNet significantly increases the separation accuracy over the LSTM-TasNet in both causal and noncausal configurations. Moreover, the separation accuracy of Conv-TasNet surpasses the performance of ideal magnitude T-F masks, including the ideal binary mask (IBM [29]), ideal ratio mask (IRM [48], [89]), and Winener filter-like mask (WFM [98]) in both signal-to-distortion ratio (SDR) and subjective (mean opinion score, MOS) measures.

2.2.1 Modifications upon LSTM-TasNet

The general system pipeline of Conv-TasNet follows the design of LSTM-TasNet except for two main modifications. The first one is on the design of the separation module, where a TCN is used instead of the stacked LSTM layers in LSTM-TasNet. TCN was proposed as a replacement for RNNs in various sequence modeling tasks. Each layer in a TCN consists of 1-D convolutional blocks with increasing dilation factors. The dilation factors increase exponentially to ensure a sufficiently large temporal context window to take advantage of the long-range dependencies of the speech signal. In Conv-TasNet, M convolutional blocks with dilation factors $1, 2, 4, \ldots, 2^{M-1}$ are repeated R times. The input to each block is zero padded accordingly to ensure the output length is the same as the input. The output of the TCN is passed to a convolutional block with kernel size 1 ($1 \times 1-conv$ block, also known as *pointwise* convolution) for mask estimation. The $1 \times 1-conv$ block together with a nonlinear activation function estimates the C multiplicative masks as in LSTM-TasNet.

The design of the 1-D convolutional blocks follows [130], where a residual path and a skip-connection path are applied: the residual path of a block serves as the input to the next block, and the skip-connection paths for all blocks are summed up and used as the output of the TCN. To further decrease the number of parameters, depthwise separable convolution (S-$conv(\cdot)$) is used to replace standard convolution in each convolutional block. Depthwise separable convolution (also referred to as separable convolution) has proven effective in image processing tasks [115], [144] and neural machine translation tasks [147]. The depthwise separable convolution operator decouples the standard convolution operation into two consecutive operations, a depthwise convolution

(D-*conv*$(\cdot)$) followed by pointwise convolution ($1 \times 1-conv(\cdot)$):

$$D\text{-}conv(\mathbf{Y}, \mathbf{K}) = concat(\mathbf{y}_j \circledast \mathbf{k}_j), j = 1, \ldots, N \tag{2.9}$$

$$S\text{-}conv(\mathbf{Y}, \mathbf{K}, \mathbf{L}) = D\text{-}conv(\mathbf{Y}, \mathbf{K}) \circledast \mathbf{L} \tag{2.10}$$

where $\mathbf{Y} \in \mathbb{R}^{G \times M}$ is the input to S-*conv*$(\cdot)$, $\mathbf{K} \in \mathbb{R}^{G \times P}$ is the convolution kernel with size P, $\mathbf{y}_j \in \mathbb{R}^{1 \times M}$ and $\mathbf{k}_j \in \mathbb{R}^{1 \times P}$ are the rows of matrices $\mathbf{Y}$ and $\mathbf{K}$, respectively, $\mathbf{L} \in \mathbb{R}^{G \times H \times 1}$ is the convolution kernel with size 1, and $\circledast$ denotes the convolution operation. In other words, the D-*conv*$(\cdot)$ operation convolves each row of the input Y with the corresponding row of matrix K, and the $1 \times 1-conv$ block linearly transforms the feature space. In comparison with the standard convolution with kernel size $\hat{\mathbf{K}} \in \mathbb{R}^{G \times H \times P}$, depthwise separable convolution only contains $G \times P + G \times H$ parameters, which decreases the model size by a factor of $\frac{H \times P}{H + P} \approx P$ when $H \gg P$.

A nonlinear activation function and a normalization operation are added after both the first 1×1-*conv* and D-*conv* blocks respectively. The nonlinear activation function is the parametric rectified linear unit (PReLU) [99]:

$$PReLU(x) = \begin{cases} x, & \text{if } x \geq 0 \\ \alpha x, & \text{otherwise} \end{cases} \tag{2.11}$$

where $\alpha \in \mathbb{R}$ is a trainable scalar controlling the negative slope of the rectifier. The choice of the normalization method in the network depends on the causality requirement. For noncausal configuration, a global layer normalization (gLN) operation is introduced to utilize the global sequence information across both the channel and time dimensions:

$$gLN(\mathbf{F}) = \frac{\mathbf{F} - E[\mathbf{F}]}{\sqrt{Var[\mathbf{F}] + \epsilon}} \odot \gamma + \beta \tag{2.12}$$

$$E[\mathbf{F}] = \frac{1}{NT} \sum_{NT} \mathbf{F} \tag{2.13}$$

$$Var[\mathbf{F}] = \frac{1}{NT} \sum_{NT} (\mathbf{F} - E[\mathbf{F}])^2 \tag{2.14}$$

where $\mathbf{F} \in \mathbb{R}^{N \times T}$ is a sequential feature, $\gamma, \beta \in \mathbb{R}^{N \times 1}$ are trainable parameters, and ϵ is a small constant for numerical stability. This is identical to the standard layer normalization applied in computer vision models where the channel and time dimension correspond to the width and height dimension in an image [114]. In causal configuration, gLN cannot be applied since it relies on the future values of the signal at any time step. Instead, a cumulative layer normalization (cLN) operation is designed operation to perform step-wise normalization:

$$cLN(\mathbf{f}_k) = \frac{\mathbf{f}_k - E[\mathbf{f}_{t \leq k}]}{\sqrt{Var[\mathbf{f}_{t \leq k}] + \epsilon}} \odot \gamma + \beta \tag{2.15}$$

$$E[\mathbf{f}_{t \leq k}] = \frac{1}{Nk} \sum_{Nk} \mathbf{f}_{t \leq k} \tag{2.16}$$

$$Var[\mathbf{f}_{t \leq k}] = \frac{1}{Nk} \sum_{Nk} (\mathbf{f}_{t \leq k} - E[\mathbf{f}_{t \leq k}])^2 \tag{2.17}$$

where $\mathbf{f}_k \in \mathbb{R}^{N \times 1}$ is the k-th frame of the entire feature $\mathbf{F}$, $\mathbf{f}_{t \leq k} \in \mathbb{R}^{N \times k}$ corresponds to the feature of k frames $[\mathbf{f}_1, \ldots, \mathbf{f}_k]$, and $\gamma, \beta \in \mathbb{R}^{N \times 1}$ are trainable parameters applied to all frames. To ensure that the separation module is invariant to the scaling of the input, the selected normalization method is applied to the encoder output $\mathbf{w}$ before it is passed to the separation module.

At the beginning of the separation module, a linear 1×1-*conv* block is added as a bottleneck layer. This block determines the number of channels in the input and residual path of the subsequent convolutional blocks. For instance, if the linear bottleneck layer has B channels, then for a 1-D convolutional block with H channels and kernel size P, the size of the kernel in the first 1×1-*conv* block and the first D-*conv* block should be $\mathbf{O} \in \mathbb{R}^{B \times H \times 1}$ and $\mathbf{K} \in \mathbb{R}^{H \times P}$ respectively, and the size of the kernel in the residual paths should be $\mathbf{L}_{Rs} \in \mathbb{R}^{H \times B \times 1}$. The number of output channels in the skip-connection path can be different than B and is denoted as $\mathbf{L}_{Sc} \in \mathbb{R}^{H \times Sc \times 1}$. Figure 2.3 shows the flowchart of the entire system as well as the design of the 1-D convolutional blocks.

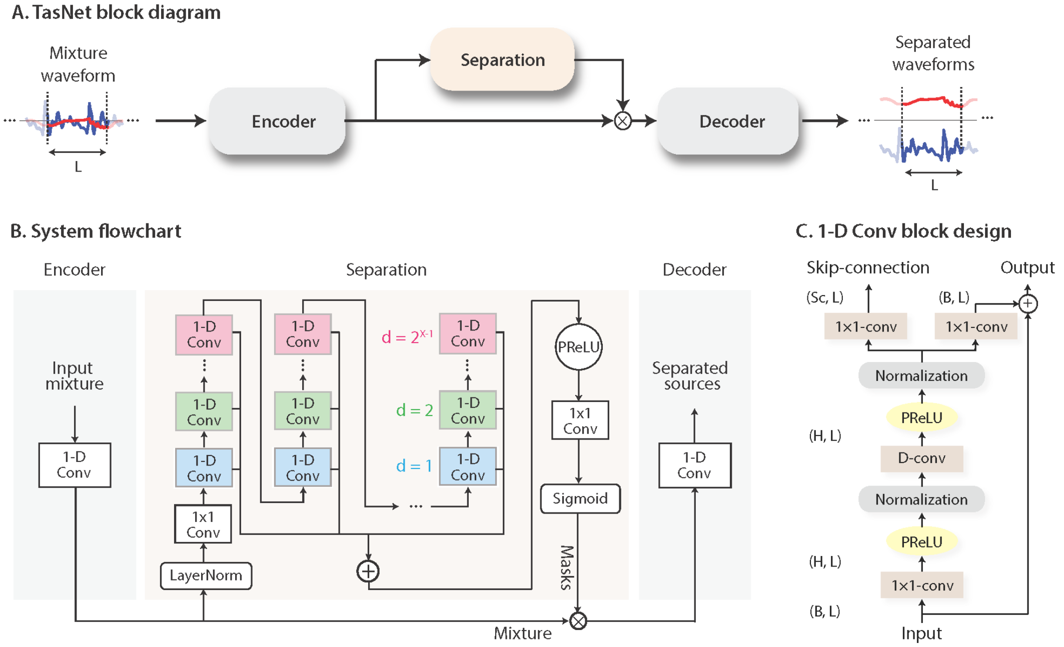

Figure 2.3: (A): The block diagram of Conv-TasNet, which follows the encoder-separator-decoder design of LSTM-Tasnet. (B): The flowchart of Conv-TasNet. A linear encoder and decoder model the waveforms and a temporal convolutional network (TCN) separation module estimates the masks based on the encoder output. Different colors in the 1-D convolutional blocks in TCN denote different dilation factors. (C): The design of the 1-D convolutional block. Each block consists of a 1×1-$conv$ operation followed by a depthwise convolution ($D - conv$) operation, with nonlinear activation function and normalization added between each two convolution operations. Two linear $1 \times 1{-}conv$ blocks serve as the residual path and the skip-connection path respectively.

The second difference is the design of the encoder and the nonlinearity function in the mask estimation layer of the separation module. LSTM-TasNet used a gated nonlinear encoder in order to ensure that the mixture hidden representations are nonnegative. Moreover, the Softmax nonlinear function was used in as the activation function in the mask estimation layer in LSTM-TasNet to follow the unit-summation assumption in conventional magnitude T-F masks. However, whether such assumptions are valid and lead to optimal separation performance is unknown. After multiple ablation experiments on different choices of the nonlinear functions on the encoder and the mask estimation layer, a linear encoder and a Sigmoid nonlinear function for the mask estimation layer are selected for the Conv-TasNet. Details will be introduced in the following section.

2.2.2 Experiment Configurations and Results

Conv-TasNet is also evaluated on the benchmark WSJ0-2mix dataset for a fair comparison with the LSTM-TasNet as well as other models. Moreover, the WSJ0-3mix dataset is also used for three-speaker separation task. All models are trained for 100 epochs on 4-second long utterances with a initial learning rate of $1e^{-3}$. The learning rate is halved if the accuracy of validation set is not improved in 3 consecutive epochs. Negative SI-SDR is used as the training objective. Adam [83] is used as the optimizer. A 50% stride size is used in the encoder and decoder (i.e. 50% overlap between consecutive windows). Gradient clipping with maximum L^2-norm of 5 is applied during training. The hyperparameters of the network are shown in table 2.2.

To better evaluate the models, scale-invariant signal-to-distortion ratio improvement (SI-SDRi) and signal-to-distortion ratio improvement (SDRi) [35] are used as objective measures of separation performance, and perceptual evaluation of subjective quality (PESQ, [16]) and the mean opinion score (MOS) [335] are used as the subjective measures. MOS are obtained by asking 40 normal hearing subjects to rate the quality of the separated mixtures. All human testing procedures were approved by the local institutional review board (IRB) at Columbia University in the City of New York.

Table 2.2: Hyperparameters of the network.

Symbol	Description
N	Number of basis kernels in encoder and decoder
L	Window length (in samples)
B	Number of channels in bottleneck and the residual paths' 1×1-$conv$ blocks
Sc	Number of channels in skip-connection paths' 1×1-$conv$ blocks
H	Number of channels in convolutional blocks
P	Kernel size in convolutional blocks
X	Number of convolutional blocks in each repeat
R	Number of repeats

The first experiment on the configurations of Conv-TasNet is the nonnegativity of the encoder. The non-negativity of the encoder output was enforced in [201] using a gated operation with ReLU and Sigmoid nonlinear functions. This constraint was based on the assumption that the masking operation on the encoder output is only meaningful when the mixture and target waveforms can be represented with a nonnegative combination of the basis functions, since an unbounded encoder representation may result in unbounded masks. However, by removing the nonlinear function in the encoder, another assumption can be made: with an unbounded but highly overcomplete representation of the mixture, a set of nonnegative masks can still be found to reconstruct the clean sources. In this case, only $\mathbf{U}$ is used in the encoder and $\mathbf{V}$ is discarded, and the overcompleteness of the representation, i.e. the ratio between N and L, becomes crucial. If there exist only a unique weight feature for the mixture as well as for the sources, the non-negativity of the mask cannot be guaranteed. Also note that in both assumptions, there is no constraint on the relationship between the encoder and decoder basis functions $\mathbf{U}$ and $\mathbf{P}$, meaning that they are not forced to reconstruct the mixture signal perfectly. One way to explicitly ensure the autoencoder property is by choosing $\mathbf{P}$ to be the pseudo-inverse of $\mathbf{U}$ (i.e. least square reconstruction). The choice of encoder/decoder design affects the mask estimation: in the case of an autoencoder, the unit summation constraint must be satisfied; otherwise, the unit summation constraint is not strictly required. To illustrate this point, there are five possible encoder-decoder configurations:

1. Linear encoder with its pseudo-inverse (Pinv) as decoder, i.e. $\mathbf{w} = \mathbf{x}(\mathbf{P}^T\mathbf{P})^{-1}\mathbf{P}^T$ and $\hat{\mathbf{x}} = \mathbf{w}\mathbf{P}$, with Softmax function for mask estimation.

2. Linear encoder and decoder where $\mathbf{w} = \mathbf{x}\mathbf{U}$ and $\hat{\mathbf{x}} = \mathbf{w}\mathbf{P}$, with Softmax or Sigmoid function for mask estimation.

3. Encoder with ReLU activation and linear decoder where $\mathbf{w} = \text{ReLU}(\mathbf{x}\mathbf{U})$ and $\hat{\mathbf{x}} = \mathbf{w}\mathbf{P}$, with Softmax or Sigmoid function for mask estimation.

Separation performance of different configurations in table 2.3 shows that pseudo-inverse autoencoder leads to the worst performance, indicating that an explicit autoencoder configuration does not necessarily improve the separation score in this framework. The performance of all other configurations is comparable. Because linear encoder and decoder with Sigmoid function achieves a slightly better accuracy over other methods, this configuration is used in all the following experiments.

Table 2.3: Separation performance for different system configurations. SI-SDRi and SDRi are reported on decibel scale.

Encoder	Mask	Model size	SI-SDRi	SDRi
Pinv	Softmax	1.5M	12.1	12.4
Linear	Softmax		12.9	13.2
	Sigmoid		**13.1**	**13.4**
ReLU	Softmax		13.0	13.3
	Sigmoid		12.9	13.2

The second experiment on the network configuration is on the effect of hyperparameters on the overall performance. Table 2.4 shows the performance of the systems with different parameters, from which several observations can be made:

(i) Encoder/decoder: Increasing the number of basis signals N in the encoder/decoder increases the overcompleteness of the basis signals and improves the performance.

(ii) Hyperparameters in the 1-D convolutional blocks: A possible configuration consists of a small bottleneck size B and a large number of channels in the convolutional blocks H. This matches the observation in [207], where the ratio between the convolutional block and the bottleneck H/B was found to be best around 5. Increasing the number of channels in the skip-connection block improves the performance while greatly increases the model size. Therefore, a small skip-connection block is selected as a trade-off between performance and model size.

(iii) Number of 1-D convolutional blocks: When the receptive field is the same, deeper networks lead to better performance, possibly due to the increased model capacity.

(iv) Size of receptive field: Increasing the size of receptive field leads to better performance, which shows the importance of sequence modeling in the speech signal.

(v) Length of each segment: Shorter segment length consistently improves performance. Note that the best system uses a filter length of only 2 ms ($\frac{L}{fs} = \frac{16}{8000} = 0.002s$), which makes it very difficult to train a deep LSTM network with the same L due to the large number of time steps in the encoder output.

(vi) Causality: Using a causal configuration leads to a significant drop in the performance. This drop could be due to the causal convolution and/or the layer normalization operations.

Table 2.4: The effect of different configurations in Conv-TasNet. "Norm" stands for the normalization method and "RF" stands for the receptive field. SI-SDRi and SDRi are reported on decibel scale.

N	L	B	H	Sc	P	X	R	Norm	Causal	RF (s)	Size	SI-SDRi	SDRi
128	40	128	256	128	3	7	2	gLN	×	1.28	1.5M	13.0	13.3
256	40	128	256	128	3	7	2	gLN	×	1.28	1.5M	13.1	13.4
512	40	128	256	128	3	7	2	gLN	×	1.28	1.7M	13.3	13.6
512	40	128	256	256	3	7	2	gLN	×	1.28	2.4M	13.0	13.3
512	40	128	512	128	3	7	2	gLN	×	1.28	3.1M	13.3	13.6
512	40	128	512	512	3	7	2	gLN	×	1.28	6.2M	13.5	13.8
512	40	256	256	256	3	7	2	gLN	×	1.28	3.2M	13.0	13.3
512	40	256	512	256	3	7	2	gLN	×	1.28	6.0M	13.4	13.7
512	40	256	512	512	3	7	2	gLN	×	1.28	8.1M	13.2	13.5
512	40	128	512	128	3	6	4	gLN	×	1.27	5.1M	14.1	14.4
512	40	128	512	128	3	4	6	gLN	×	0.46	5.1M	13.9	14.2
512	40	128	512	128	3	8	3	gLN	×	3.83	5.1M	14.5	14.8
512	32	128	512	128	3	8	3	gLN	×	3.06	5.1M	14.7	15.0
512	16	128	512	128	3	8	3	gLN	×	1.53	5.1M	**15.3**	**15.6**
512	16	128	512	128	3	8	3	cLN	✓	1.53	5.1M	10.6	11.0

Table 2.5 compares the performance of the best configuration of Conv-TasNet with other state-of-the-art methods on the same WSJ0-2mix dataset. For all systems, the best reported results in the literature are listed. The numbers of parameters in different methods are based on reimplementations, except for [194] which is provided by the authors. The missing values in the table are either because the numbers were not reported in the study or because the results were calculated with a different STFT configuration. The previous LSTM-TasNet model is denoted by the (B)LSTM-TasNet. While the BLSTM-TasNet already outperformed IRM and IBM, the noncausal Conv-TasNet significantly surpasses the performance of all three ideal T-F masks in SI-SDRi and

SDRi metrics with a significantly smaller model size comparing with all previous methods. Table 2.6 further compares the performance of Conv-TasNet with those of other systems on the WSJ0-3mix dataset for three-speaker separation task. The noncausal Conv-TasNet system significantly outperforms all previous STFT-based systems in SDRi. While there is no prior result on a causal algorithm for three-speaker separation, the causal Conv-TasNet significantly outperforms even the other two noncausal STFT-based systems [123], [148].

Table 2.5: Comparison between Conv-TasNet and other methods on WSJ0-2mix dataset. SI-SDRi and SDRi are reported on decibel scale.

Method	Size	Causal	SI-SDRi	SDRi
DPCL++ [123]	13.6M	×	10.8	–
uPIT-BLSTM-ST [148]	92.7M	×	–	10.0
DANet [140]	9.1M	×	10.5	–
ADANet [198]	9.1M	×	10.4	10.8
cuPIT-Grid-RD [222]	47.2M	×	–	10.2
CBLDNN-GAT[194]	39.5M	×	–	11.0
Chimera++ [218]	32.9M	×	11.5	12.0
WA-MISI-5 [220]	32.9M	×	12.6	13.1
BLSTM-TasNet [200]	23.6M	×	13.2	13.6
Conv-TasNet-gLN	**5.1M**	×	**15.3**	**15.6**
uPIT-LSTM [148]	46.3M	✓	–	7.0
LSTM-TasNet [200]	32.0M	✓	**10.8**	**11.2**
Conv-TasNet-cLN	**5.1M**	✓	10.6	11.0
IRM	–	–	12.2	12.6
IBM	–	–	13.0	13.5
WFM	–	–	13.4	13.8

Table 2.6: Comparison between Conv-TasNet and other systems on WSJ0-3mix dataset. SI-SDRi and SDRi are reported on decibel scale.

Method	Size	Causal	SI-SDRi	SDRi
DPCL++ [123]	13.6M	×	7.1	–
uPIT-BLSTM-ST [148]	92.7M	×	–	7.7
DANet [140]	9.1M	×	8.6	8.9
ADANet [198]	9.1M	×	9.1	9.4
Conv-TasNet-gLN	**5.1M**	×	**12.7**	**13.1**
Conv-TasNet-cLN	**5.1M**	✓	**7.8**	**8.2**
IRM	–	–	12.5	13.0
IBM	–	–	13.2	13.6
WFM	–	–	13.6	14.0

The third experiment is on the joint subjective and objective evaluations of Conv-TasNet. Table 2.7 shows the PESQ score for Conv-TasNet and IRM, IBM, and WFM, where IRM has the highest score for both WSJ0-2mix and WSJ0-3mix dataset. However, since PESQ aims to predict the subjective quality of speech, human quality evaluation can be considered as the ground truth. Therefore, a psychophysics experiment is conducted in which 40 normal hearing subjects are asked to listen and rate the quality of the separated speech sounds. Because of the practical limitations of human psychophysics experiments, the subjective comparison of Conv-TasNet is restricted to the ideal ratio mask (IRM) which has the highest PESQ score among the three ideal masks (table 2.7). 25 two-speaker mixture sounds as well as their separation output were randomly selected from the two-speaker test set (WSJ0-2mix). To avoid a possible selection bias, the average PESQ scores for the IRM and Conv-TasNet separated sounds for the selected 25 samples were ensured to equal to the average PESQ scores over the entire test set (comparison of tables 2.7 and 2.8). The length of each utterance was constrained to be within 0.5 standard deviation of the mean of the entire test set. The subjects were asked to rate the quality of the clean utterances, the IRM-separated utterances, and the Conv-TasNet separated utterances on the scale of 1 to 5 (1: bad, 2: poor, 3: fair, 4: good, 5: excellent). A clean utterance was first given as the reference for the highest possible score (i.e. 5). Then the clean, IRM, and Conv-TasNet samples were presented to the subjects in random order. The mean opinion score (MOS) of each of the 25 utterances was then averaged over the 40 subjects.

Figure 2.4 and table 2.8 show the result of the human subjective quality test, where the MOS for Conv-TasNet is significantly higher than the MOS for the IRM ($p < 1e - 16$, t-test). In addition, the superior subjective quality of Conv-TasNet over IRM is consistent across most of the 25 test utterances as shown in figure 2.4 (C). This observation shows that PESQ consistently underestimates MOS for Conv-TasNet separated utterances, which may be due to the dependence of PESQ on the magnitude spectrogram of speech [16] which could produce lower scores for time-domain approaches.

The fourth experiment is on the sensitivity of LSTM-TasNet and Conv-TasNet on the mixture

Table 2.7: PESQ scores for the ideal T-F masks and Conv-TasNet on the entire WSJ0-2mix and WSJ0-3mix test sets.

Dataset	PESQ			
	IRM	IBM	WFM	Conv-TasNet
WSJ0-2mix	**3.74**	3.33	3.70	3.24
WSJ0-3mix	**3.52**	2.91	3.45	2.61

Table 2.8: Mean opinion score (MOS, N=40) and PESQ for the 25 random selected utterances from the WSJ0-2mix test set.

Method	MOS	PESQ
Conv-TasNet-gLN	**4.03**	3.22
IRM	3.51	**3.74**
Clean	4.23	4.5

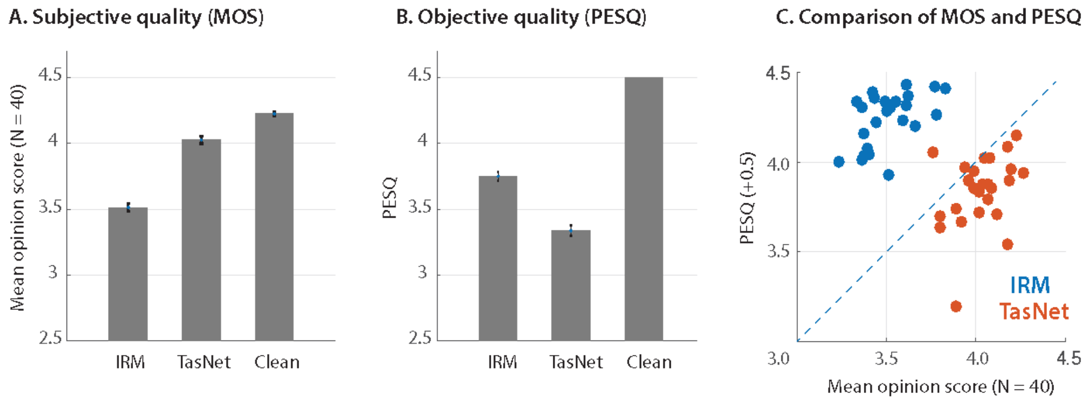

Figure 2.4: Subjective and objective quality evaluation of separated utterances in WSJ0-2mix. (A): The mean opinion scores (MOS, N = 40) for IRM, Conv-TasNet and the clean utterance. Conv-TasNet significantly outperforms IRM ($p < 1e - 16$, t-test). (B): PESQ scores are higher for IRM compared to the Conv-TasNet ($p < 1e - 16$, t-test). Error bars indicate standard error (STE) (C): MOS versus PESQ for individual utterances. Each dot denotes one mixture utterance, separated using the IRM (blue) or Conv-TasNet (red). The subjective ratings of almost all utterances for Conv-TasNet are higher than their corresponding PESQ scores.

starting point. Unlike language processing tasks where sentences have determined starting words, it is difficult to define a general starting sample or frame for speech separation and enhancement tasks. A robust audio processing system should therefore be insensitive to the starting point of the mixture. However, it has been empirically found that the performance of the causal LSTM-TasNet is very sensitive to the exact starting point of the mixture, which means that shifting the input mixture by several samples may adversely affect the separation accuracy. Here, a systematic examination on the robustness of LSTM-TasNet and causal Conv-TasNet to the starting point of the mixture is done by evaluating the separation performance for each mixture in the WSJ0-2mix test set with different sample shifts of the input. A shift of s samples corresponds to starting the separation at sample s instead of the first sample. Figure 2.5 (A) shows the performance of both systems on the same example mixture with different values of input shift. Unlike LSTM-TasNet, the causal Conv-TasNet performs consistently well for all shift values of the input mixture. Moreover, the overall robustness for the entire test set are measured by the standard deviation of SDRi in each mixture with shifted mixture inputs similar to figure 2.5 (A). The box plots of all the mixtures in the WSJ0-2mix test set in figure 2.5 (B) show that causal Conv-TasNet performs consistently better across the entire test set, which confirms the robustness of Conv-TasNet to variations in the starting point of the mixture. One explanation for this inconsistency may be due to the sequential processing constraint in LSTM-TasNet which means that failures in previous frames can accumulate and affect the separation performance in all following frames, while the decoupled processing of consecutive frames in Conv-TasNet alleviates the effect of occasional error.

Finally, a visualization can be made on all the intermediate outputs as well as the linear encoder and decoder weights in Conv-TasNet. Figure 2.6 visualizes all the internal variables of Conv-TasNet for one example mixture sound with two overlapping speakers (denoted by red and blue). The encoder and decoder basis functions are sorted by the similarity of the Euclidean distance of the basis functions found using the unweighted pair group method with arithmetic mean (UPGMA) method [1]. The basis functions show a diversity of frequency and phase tuning. The representation of the encoder is colored according to the power of each speaker at the correspond-

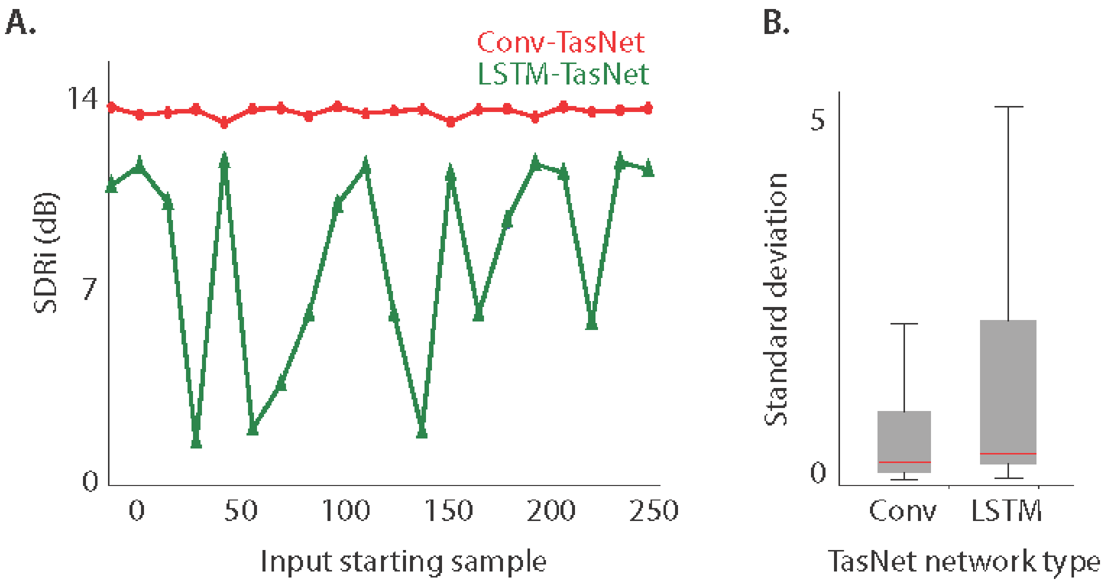

Figure 2.5: (A): SDRi of an example mixture separated using LSTM-TasNet and causal Conv-TasNet as a function of the starting point in the mixture. The performance of Conv-TasNet is considerably more consistent and insensitive to the start point. (B): Standard deviation of SDRi across all the mixtures in the WSJ0-2mix test set with varying starting points.

ing basis output at each time point, demonstrating the sparsity of the encoder representation. As can be seen in figure 2.6, the estimated masks for the two speakers highly resemble their encoder representations, which allows for the suppression of the encoder outputs that correspond to the interfering speaker and the extraction of the target speaker in each mask. The separated waveforms for the two speakers are estimated by the linear decoder, whose basis functions are shown in figure 2.6. The separated waveforms are shown on the right.

To better understand the properties of the basis functions, the frequency responses of the filters are shown in figure 2.7 for the best noncausal Conv-TasNet, sorted in the same way as figure 2.6. The magnitudes of the FFTs for each filter are also shown in the same order. As seen in the figure, the majority of the filters are tuned to lower frequencies. In addition, it shows that filters with the same frequency tuning express various phase values for that frequency. This observation can be seen by the circular shift of the low-frequency basis functions. This result suggests an important role for low-frequency features of speech such as pitch as well as explicit encoding of the phase information to achieve superior speech separation performance.

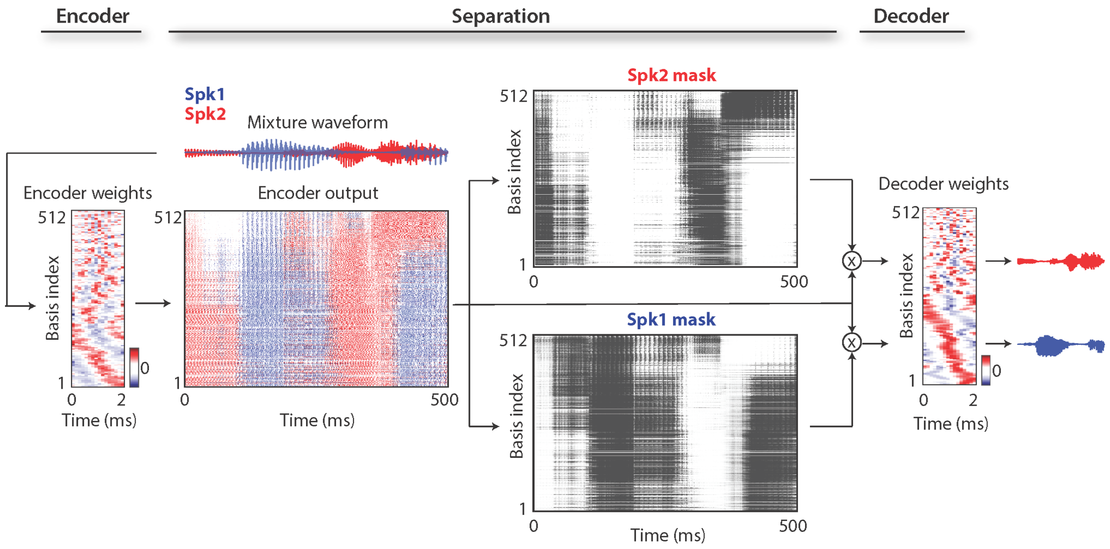

Figure 2.6: Visualization of the encoder and decoder basis functions, encoder representation, and source masks for a sample 2-speaker mixture. The speakers are shown in red and blue. The encoder representation is colored according to the power of each speaker at each basis function and point in time. The basis functions are sorted according to their Euclidean similarity and show diversity in frequency and phase tuning.

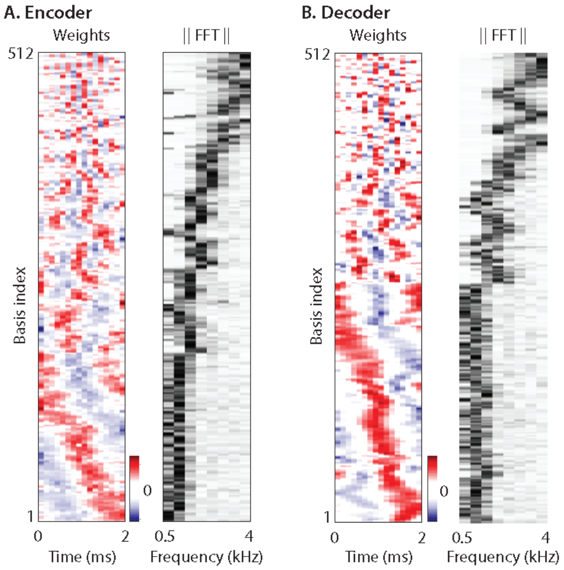

Figure 2.7: Visualization of encoder and decoder basis functions and the magnitudes of their FFTs. The basis functions are sorted based on their pairwise Euclidean similarity.

2.3 DPRNN-TasNet: Stronger Long Sequence Modeling Ability

Conv-TasNet showed that improved separation performance can be achieved by using smaller window size L. However, a smaller window comes at the cost of a significantly longer mixture hidden representation [234], [243]. This poses an additional challenge as the sequential modeling networks in LSTM-TasNet and Conv-TasNet might both have difficulties on learning such long-term temporal dependency [196]. Moreover, unlike RNNs that have dynamic receptive fields, TCNs with fixed receptive fields that are smaller than the sequence length are not able to fully utilize the sequence-level dependency [179].

Dual-path RNN (DPRNN) is introduced here to replace TCN and tackle the aforementioned issue in long sequence modeling. DPRNN organizes any kinds of RNN layers to model long sequential inputs in a very simple way. The intuition is to split the input sequence into shorter chunks and interleave two RNNs, an *intra-chunk* RNN and an *inter-chunk* RNN, for local and global modeling, respectively. In a DPRNN block, the intra-chunk RNN first processes the local chunks independently, and then the inter-chunk RNN aggregates the information from all the chunks to perform utterance-level processing. For a sequential input of length $\hat{T}$, DPRNN with chunk size K and chunk hop size P contains S chunks, where K and S corresponds to the input lengths for the inter- and intra-chunk RNNs, respectively. When $K \approx S$, the two RNNs have a sublinear input length ($O(\sqrt{\hat{T}})$) as opposed to the original input length ($O(\hat{T})$), which greatly decreases the optimization difficulty that arises when $\hat{T}$ is extremely large.

2.3.1 Modifications upon Conv-TasNet

The only difference between DPRNN-TasNet and Conv-TasNet is the use of DPRNN instead of TCN. A DPRNN consists of three stages: *segmentation*, *block processing*, and *overlap-add*. The segmentation stage splits a sequential input into overlapped chunks and concatenates all the chunks into a 3-D tensor. The tensor is then passed to stacked DPRNN blocks to iteratively apply local (intra-chunk) and global (inter-chunk) modeling in an alternate fashion. The output from the last layer is transformed back to a sequential output with overlap-add method. Figure 2.8 shows the flowchart of a DPRNN block.

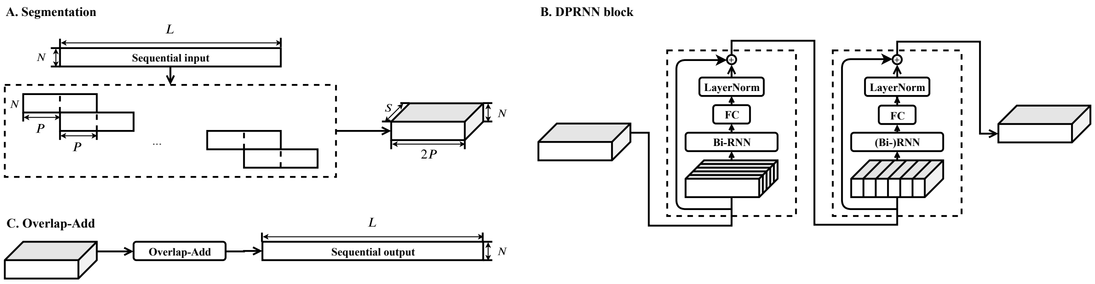

Figure 2.8: System flowchart of dual-path RNN (DPRNN). (A) The segmentation stage splits a sequential input into chunks with or without overlaps and concatenates them to form a 3-D tensor. In the implementation, the overlap ratio is set to 50%. (B) Each DPRNN block consists of two RNNs that have recurrent connections in different dimensions. The *intra-chunk* bi-directional RNN is first applied to individual chunks in parallel to process local information. The *inter-chunk* RNN is then applied across the chunks to capture global dependency. Multiple blocks can be stacked to increase the total depth of the network. (C) The 3-D output of the last DPRNN block is converted back to a sequential output by performing overlap-add on the chunks.

For a sequential input $\mathbf{W} \in \mathbb{R}^{N \times \hat{T}}$ where N is the feature dimension and $\hat{T}$ is the number of time steps, the segmentation stage splits $\mathbf{W}$ into chunks of length K and hop size P. The first and last chunks are zero-padded so that every sample in $\mathbf{W}$ appears and only appears in K/P chunks, generating S equal size chunks $\mathbf{D}_s \in \mathbb{R}^{N \times K}$, $s = 1, \ldots, S$. All chunks are then concatenated together to form a 3-D tensor $\mathbf{T} = [\mathbf{D}_1, \ldots, \mathbf{D}_S] \in \mathbb{R}^{N \times K \times S}$.

The segmentation output $\mathbf{T}$ is then passed to the stack of B DPRNN blocks. Each block transforms an input 3-D tensor into another tensor with the same shape. Denote the input tensor for block $b = 1, \ldots, B$ as $\mathbf{T}_b \in \mathbb{R}^{N \times K \times S}$, where $\mathbf{T}_1 = \mathbf{T}$. Each block contains two sub-modules corresponding to intra- and inter-chunk processing, respectively. The intra-chunk RNN is always bi-directional and is applied to the second dimension of $\mathbf{T}_b$, i.e., within each of the S blocks:

$$\mathbf{U}_b = [f_b(\mathbf{T}_b[:, :, i]),\ i = 1, \ldots, S] \tag{2.18}$$

where $\mathbf{U}_b \in \mathbb{R}^{H \times K \times S}$ is the output of the RNN, $f_b(\cdot)$ is the mapping function defined by the RNN, and $\mathbf{T}_b[:, :, i] \in \mathbb{R}^{N \times K}$ is the sequence defined by chunk i. A linear fully-connected (FC) layer is then applied to transform the feature dimension of $\mathbf{U}_b$ back to that of $\mathbf{T}_b$

$$\hat{\mathbf{U}}_b = [\mathbf{G}\mathbf{U}_b[:,:,i] + \mathbf{m},\, i = 1, \ldots, S] \tag{2.19}$$

where $\hat{\mathbf{U}} \in \mathbb{R}^{N \times K \times S}$ is the transformed feature, $\mathbf{G} \in \mathbb{R}^{N \times H}$ and $\mathbf{m} \in \mathbb{R}^{N \times 1}$ are the weight and bias of the FC layer, respectively, and $\mathbf{U}_b[:,:,i] \in \mathbb{R}^{H \times K}$ represents chunk i in $\mathbf{U}_b$. Layer normalization (LN) [114] is then applied to $\hat{\mathbf{U}}$, which is empirically found to be important for the model to have a good generalization ability:

$$LN(\hat{\mathbf{U}}_b) = \frac{\hat{\mathbf{U}}_b - \mu(\hat{\mathbf{U}}_b)}{\sqrt{\sigma(\hat{\mathbf{U}}_b) + \epsilon}} \odot \mathbf{z} + \mathbf{r} \tag{2.20}$$

$$\tag{2.21}$$

where $\mathbf{z}, \mathbf{r} \in \mathbb{R}^{N \times 1}$ are the rescaling factors, ϵ is a small positive number for numerical stability, and $\odot$ denotes the Hadamard product. $\mu(\cdot)$ and $\sigma(\cdot)$ are the mean and variance of the 3-D tensor defined as

$$\mu(\hat{\mathbf{U}}_b) = \frac{1}{NKS} \sum_{i=1}^{N} \sum_{j=1}^{K} \sum_{s=1}^{S} \hat{\mathbf{U}}_b[i,j,s] \tag{2.22}$$

$$\sigma(\hat{\mathbf{U}}_b) = \frac{1}{NKS} \sum_{i=1}^{N} \sum_{j=1}^{K} \sum_{s=1}^{S} (\hat{\mathbf{U}}_b[i,j,s] - \mu(\hat{\mathbf{U}}_b))^2 \tag{2.23}$$

A residual connection is then added between the output of LN operation and the input $\mathbf{T}_b$:

$$\hat{\mathbf{T}}_b = \mathbf{T}_b + LN(\hat{\mathbf{U}}_b) \tag{2.24}$$

$\hat{\mathbf{T}}_b$ is then served as the input to the inter-chunk RNN sub-module, where the RNN is applied to the last dimension, i.e. the aligned K time steps in each of the S blocks:

$$\mathbf{V}_b = [h_b(\hat{\mathbf{T}}_b[:,i,:]),\, i = 1, \ldots, K] \tag{2.25}$$

where $\mathbf{V}_b \in \mathbb{R}^{H \times K \times S}$ is the output of RNN, $h_b(\cdot)$ is the mapping function defined by the RNN, and $\hat{\mathbf{T}}_b[:, i, :] \in \mathbb{R}^{N \times S}$ is the sequence defined by the i-th time step in all S chunks. As the intra-chunk RNN is bi-directional, each time step in $\hat{\mathbf{T}}_b$ contains the entire information of the chunk it belongs to, which allows the inter-chunk RNN to perform fully sequence-level modeling. As with the intra-chunk RNN, a linear FC layer and the LN operation are applied on top of $\mathbf{V}_b$. A residual connection is also added between the output and $\hat{\mathbf{T}}_b$ to form the output for DPRNN block b. For $b < B$, the output is served as the input to the next block $\mathbf{T}_{b+1}$.

Denote the output of the last DPRNN block as $\mathbf{T}_{B+1} \in \mathbb{R}^{N \times K \times S}$. To transform it back to a sequence, the overlap-add method is applied to the S chunks to form output $\mathbf{Q} \in \mathbb{R}^{N \times \hat{T}}$.

Simple analysis on the complexity of DPRNN can be made. Consider the sum of the input sequence lengths for the intra- and inter-chunk RNNs in a single block denoted by $K+S$ where the hop size is set to be 50% (i.e. $P = K/2$) as in Figure 2.8. It is simple to see that $S = \lceil 2\hat{T}/K \rceil + 1$ where $\lceil \cdot \rceil$ is the ceiling function. To achieve minimum total input length $K+S = K+\lceil 2\hat{T}/K \rceil+1$, K should be selected such that $K \approx \sqrt{2\hat{T}}$, and then S also satisfies $S \approx \sqrt{2\hat{T}} \approx K$. This gives a sublinear input length ($O(\sqrt{L})$) rather than the original linear input length ($O(\hat{T})$).

Compared with other approaches for arranging local and global RNN layers, or more general the hierarchical RNNs that perform sequence modeling in multiple time scales [108], [116], [129], [138], [145], [177], the stacked DPRNN blocks *iteratively and alternately* perform the intra- and inter-chunk operations, which can be treated as an interleaved processing between local and global inputs. Moreover, the first RNN layer in most hierarchical RNNs still receives the entire input sequence, while in stacked DPRNN each intra- or inter-chunk RNN receives the same sublinear input size across all blocks. Compared with CNN-based architectures such as TCNs that only perform local modeling due to the fixed receptive fields [239], [243], [315], DPRNN is able to fully utilize global information via the inter-chunk RNNs.

For tasks that require online processing, the inter-chunk RNN can be made uni-directional, scanning from the first up to the current chunks. The later chunks can still utilize the information from all previous chunks, and the minimal system latency is thus defined by the chunk size K.

This is unlike standard CNN-based models that can only perform local processing due to the fixed receptive field or conventional RNN-based models that perform frame-level instead of chunk-level modeling.

2.3.2 Experiment Configurations and Results

DPRNN-TasNet is again evaluated on the benchmark WSJ0-2mix dataset with the identical configuration with Conv-TasNet. The same encoder and decoder design as in [243] is used, where the number of basis kernels N is set to be 64. As for the separator, the proposed deep DPRNN is compared with the optimally configured TCN in the best Conv-TasNet model, and 6 DPRNN blocks using BLSTM [11] as the intra- and inter-chunk RNNs with 128 hidden units in each direction are applied for all experiments. The chunk size K for DPRNN is defined empirically according to the length of the front-end representation such that $K \approx \sqrt{2\hat{T}}$ in the training set.

The first experiment compares the performance of TCN and different configurations of DPRNN and the results are shown in table 2.9. Simply replacing TCN by DPRNN improves the separation performance by 4.6% with a 49% smaller model size, which proves the superiority of the proposed local-global modeling to the previous CNN-based local-only modeling. Moreover, the performance can be consistently improved by further decreasing the window length L (and the hop size as a consequence) in the encoder and decoder. The best performance is obtained when the filter length is 2 samples with an encoder output of more than 30000 frames. This can be extremely hard or even impossible for standard RNNs or CNNs to model, while with the proposed DPRNN the use of such a short window size becomes possible and achieves the best performance.

Table 2.10 compares the DPRNN-TasNet with other previous systems on WSJ0-2mix. With 2-sample window size, DPRNN-TasNet achieves a new record on SI-SDRi with a 20 times smaller model than FurcaNeXt [315], the previous state-of-the-art system. The small model size and the superior performance of DPRNN-TasNet indicate that speech separation on WSJ0-2mix dataset can be solved without using enormous or complex models, revealing the need for using more challenging and realistic datasets in future research.

Table 2.9: Comparison of Conv-TasNet and different configurations of DPRNN-TasNet. SI-SDRi and SDRi are reported on decibel scale.

Separator network	Size	L	K	SI-SDRi	SDRi
TCN	5.1M	16	–	15.2	15.5
DPRNN	**2.6M**	16	100	16.0	16.2
		8	150	17.0	17.3
		4	200	17.9	18.1
		2	250	**18.8**	**19.0**

Table 2.10: Comparison with other methods on WSJ0-2mix. SI-SDRi and SDRi are reported on decibel scale.

Method	Size	SI-SDRi	SDRi
DPCL++ [123]	13.6M	10.8	–
uPIT-BLSTM-ST [148]	92.7M	–	10.0
ADANet [198]	9.1M	10.4	10.8
WA-MISI-5 [220]	32.9M	12.6	13.1
Conv-TasNet-gLN [243]	5.1M	15.3	15.6
Sign Prediction Net [255]	55.2M	15.3	15.6
Deep CASA [239]	12.8M	17.7	18.0
FurcaNeXt [315]	51.4M	–	18.4
DPRNN-TasNet	**2.6M**	**18.8**	**19.0**

Beyond evaluation metrics on signal quality, the effect of speech separation on the speech recognition systems is also evaluated here. A conventional hybrid speech recognition system trained only on single-speaker data is used as the ASR backend, which is trained on large-scale single-speaker noisy reverberant speech collected from various sources [260]. Table 2.11 compares Conv-TasNet and DPRNN-TasNet models with a 2-ms window (32 samples with 16 kHz sample rate). The results show that DPRNN-TasNet significantly outperforms Conv-TasNet in both SI-SDRi and WER, proving the superiority of DPRNN even under challenging noisy and reverberant conditions. This further indicates that DPRNN can replace conventional sequential modeling modules across a range of tasks and scenarios.

2.4 Discussions

The TasNet series of networks provide a standard pipeline for time-domain source separation systems. The encoder-separator-decoder design matches both the conventional frequency-domain

Table 2.11: SI-SDRi and WER results for noisy reverberant separation and recognition task. Window size is set to 32 samples for both models, and the chunk size is set to 100 frames for DPRNN-TasNet. WER is calculated for both separated speakers.

Separator network	Size	SI-SDRi	WER
TCN	5.1M	7.6	28.7
DPRNN	**2.6M**	**8.4**	**25.9%**
Noise-free reverberant speech	–	–	9.1%

systems and the newly proposed time-domain systems, where the difference mainly lies on the operation selected in the encoder and decoder. Frequency-domain systems can also be trained with time-domain training objectives to form an end-to-end pipeline by treating STFT and its inverse as encoder and decoder and backpropagating together with the separator.

TasNet, as well as its extensions, can be applied to the separation of a wide range of nonspeech signals. For example, TasNet has been applied to the separation of vocal and instrumental tracks, seismic signals [297], electrocardiograms signals, and environmental sounds. The successful applications of TasNet on these topics show that advances in speech separation models have great potential to reform the development of source separation systems in other domains and eventually towards a universal source separation system.

Chapter 3: Multi-channel System: Filter-and-sum Network

In this chapter I will introduce a time-domain multi-channel system, the filter-and-sum network (FaSNet), for multi-channel source separation. The concept of *neural beamformers* has been discussed and reviewed in Chapter 1.2, where a neural network is used to enhance the spatial filtering process or even directly learn the spatial filters. The intuition of FaSNet is to replace the frequency-domain spatial filtering process with a time-domain process, where the time-domain spatial filters are directly learned by a neural network. However, there are two main differences compared with the frequency-domain beamformers: first, FaSNet performs adaptive filter-and-sum beamforming at frame-level, while conventional frequency-domain neural beamformers perform utterance-level beamforming; second, FaSNet moves all the operations to time domain.

According to how the filter-and-sum operation is defined and how the filters are estimated, three versions of FaSNet have been proposed: the *two-stage FaSNet* [241] was the first version of FaSNet that performed a two-stage spatial filtering process in time domani, the *TAC-FaSNet* [286] was the second version that achieved full invariance to microphone array configurations, which was specially designed for ad-hoc array applications; the *iFaSNet* [289] was the third version of FaSNet that defined the filter-and-sum operation in a hidden representation space instead of the waveforms with improved cross-channel feature extraction.

3.1 Two-stage FaSNet: Time-domain Adaptive Beamforming

Prior to the two-stage FaSNet, all neural beamformers were applied in frequency domain with an explicit formulation of a selected beamformer, e.g., MVDR or GEV beamformer. The two-stage FaSNet performs end-to-end time-domain adaptive beamforming with two stages: the first stage selects a reference microphone and estimates its beamforming filters for all the target sources, and the second stage utilizes the outputs from the first stage to estimate the beamforming filters for the remaining channels. The outputs from the first and second stages are summed to generate the final separation outputs. Intuitively, the first stage in the two-stage FaSNet can be treated as a pre-separation single-channel separation process with additional cross-channel features, and the second stage can be viewed as a target speaker extraction process with each of the separated outputs in the first stage.

3.1.1 System Pipeline

The problem of frame-level time-domain filter-and-sum beamforming is defined as estimating a set of time-domain filters for a microphone array of $N \geq 2$ microphones, such that the summation of the filtered signals of all microphones provides the best estimation of a signal of interest in a selected reference microphone. The signals $\mathbf{x}^i$ are first split at each microphone into frames of L samples with a hop size of $H \in [0, L-1]$ samples

$$\mathbf{x}_t^i = \mathbf{x}^i[tH : tH + L - 1], \quad t \in \mathbb{Z}, \quad i = 1, \ldots, N \tag{3.1}$$

where t is the frame index, i is the index of the microphone and the operation $\mathbf{x}[a : b]$ selects the values of vector $\mathbf{x}$ from index a to index b. To account for the time-difference of arrival (TDOA) of the signal of interest at different microphones, the filter-and-sum operation is applied on a context window around frame t for each microphone to generate the beamformed output at frame t

$$\hat{\mathbf{y}}_t = \sum_{i=1}^{N} \mathbf{h}_t^i \circledast \hat{\mathbf{x}}_t^i \tag{3.2}$$

where $\hat{\mathbf{y}}_t \in \mathbb{R}^{1 \times L}$ is the beamformed signal at frame t, $\hat{\mathbf{x}}_t^i = \mathbf{x}^i[tH - W : tH + 2W - 1] \in \mathbb{R}^{1 \times (L+2W)}$ is the context window around $\mathbf{x}_t$ for microphone i, $\mathbf{h}_t^i \in \mathbb{R}^{1 \times (2W+1)}$ is the beamforming filter to be learned for microphone i, and $\circledast$ represents the convolution operation. For frames where $tH < W$ or $tH + 2W > l$ where l is the total length of the signal, zero is padded to the context windows. The use of context window $\hat{\mathbf{x}}_t^i$ is to make sure the model can capture cross-microphone delays of $\pm W$ samples, since the directions of the sources are always unknown. As shown in [125], the use of the context window incorporates the estimation of cross-microphone delay into the learning process of $\mathbf{h}_t^i$. The problem of filter-and-sum beamforming thus becomes estimating $\mathbf{h}_t^i$ given the observations of $\mathbf{x}^i$. For simplicity, the frame index t is dropped in the following discussions where there is no ambiguity.

The first stage is to calculate the beamforming filter for the reference microphone which is randomly selected from the array. Motivated by the GCC-PHAT feature [2], [10] in other frequency-domain beamformers and tasks such as DOA and TDOA estimation, a frame-level normalized cross-correlation (NCC) is calculated as the inter-channel feature. To be specific, let $\hat{\mathbf{x}}^1 \in \mathbb{R}^{1\times(L+2W)}$ be the context window of the signal in the reference microphone, and $\mathbf{x}^i \in \mathbb{R}^{1\times L}, i = 2, \ldots, N$ be the corresponding center frame of all the other microphones with same index, then the NCC feature, which is defined as the cosine similarity here, is calculated between $\hat{\mathbf{x}}^1$ and $\mathbf{x}^i$:

$$\begin{cases} \hat{\mathbf{x}}_j^1 = \hat{\mathbf{x}}^1[j : j+L-1] \\ f_j^i = \frac{\hat{\mathbf{x}}_j^1(\mathbf{x}^i)^T}{\left\|\hat{\mathbf{x}}_j^1\right\|_2 \|\mathbf{x}^i\|_2} \end{cases}, \quad j = 1, \ldots, 2W+1 \tag{3.3}$$

where $\mathbf{f}^i \in \mathbb{R}^{1\times(2W+1)}$ is the cosine similarity between reference microphone and microphone i. The NCC feature contains both the TDOA information and the content-dependent information of the signal of interest in the reference microphone and the other microphones. In order to combine the $N-1$ such features $\mathbf{f}^i, i = 2, \ldots, N$ for all non-reference microphones in a permutation-free manner (i.e. independent from microphone indexes), a mean-pooling operation is applied:

$$\bar{\mathbf{f}}^i = \frac{1}{N-1}\sum_{i=2}^{N} \mathbf{f}^i \tag{3.4}$$

For channel-specific feature, a linear layer is applied on $\mathbf{x}^1 \in \mathbb{R}^{1\times L}$, the center frame of $\hat{\mathbf{x}}^1$, to create a K-dimensional embedding $\mathbf{R}^1 \in \mathbb{R}^{1\times K}$

$$\mathbf{R}^1 = \mathbf{x}^1\mathbf{U} \tag{3.5}$$

where $\mathbf{U} \in \mathbb{R}^{L\times K}$ is the weight matrix. $\mathbf{R}^1$ is then concatenated with $\bar{\mathbf{f}}^i$ and passed to a separation module to generate C beamforming filters $\mathbf{h}_c^1 \in \mathbb{R}^{1\times(2W+1)}$, $c = 1, \dots, C$ where C is the number of sources of interest:

$$\{\mathbf{h}_c^1\}_{c=1}^C = \mathcal{H}_1\big([\mathbf{R}^1, \bar{\mathbf{f}}]\big) \tag{3.6}$$

where $\mathcal{H}_1(\cdot)$ is the mapping function defined by the separation module. $\mathbf{h}_c^1$ is then convolved with $\hat{\mathbf{x}}^1$ to generate the beamformed output of source c, $\hat{\mathbf{y}}_c^1 \in \mathbb{R}^{1\times L}$, for the reference microphone:

$$\hat{\mathbf{y}}_c^1 = \hat{\mathbf{x}}^1 \circledast \mathbf{h}_c^1. \tag{3.7}$$

The second stage is to estimate the beamforming filters $\mathbf{h}_c^i, i = 2, \dots, N$ for all remaining microphones. Using the output of each estimated sources of interest from the first stage $\hat{\mathbf{y}}_c^1$ as the cue, a similar procedure as above is applied to all the remaining microphones. For microphone i with context window $\hat{\mathbf{x}}^i \in \mathbb{R}^{1\times(L+2W)}$, the NCC feature is calculated between it and $\hat{\mathbf{y}}_c^1$:

$$\begin{cases} \hat{\mathbf{x}}_j^i = \hat{\mathbf{x}}^i[j : j+L-1] \\ g_{c,j}^i = \frac{\hat{\mathbf{x}}_j^i(\hat{\mathbf{y}}_c^1)^T}{\left\|\hat{\mathbf{x}}_j^i\right\|_2 \left\|\hat{\mathbf{y}}_c^1\right\|_2} \end{cases}, \quad j = 1, \dots, 2W+1 \tag{3.8}$$

An filter extraction module with its corresponding mapping function $\mathcal{H}_2(\cdot)$ is then used to generate $\mathbf{h}_c^i$ given $\mathbf{g}_c^i \in \mathbb{R}^{1\times(2W+1)}$ and the linear transformation $\mathbf{R}^i = \mathbf{x}^i\mathbf{U}$:

$$\mathbf{h}_c^i = \mathcal{H}_2\big([\mathbf{R}^i, \mathbf{g}_c^i]\big) \tag{3.9}$$

Note that all remaining microphones share the same extraction module for each of the target sources. The filters $\mathbf{h}_c^i$ are then convolved with $\hat{\mathbf{x}}^i$ and summed up to $\hat{\mathbf{y}}_c^1$ to generate the final beamformed output of source c

$$\hat{\mathbf{y}}_c = \hat{\mathbf{y}}_c^1 + \sum_{i=2}^{N} \hat{\mathbf{x}}^i \circledast \mathbf{h}_c^i \tag{3.10}$$

Finally, all segments in $\hat{\mathbf{y}}_c$ are transformed back to the full utterance $\mathbf{y}_c^* \in \mathbb{R}^{1 \times L}$ through the overlap-and-add operation.

The output of the two-stage FaSNet can also be passed to any single-channel enhancement system for further performance improvement. As FaSNet directly generates waveforms, the tandem system can still be trained end-to-end for either time-domain or frequency-domain objectives.

Similar to the TasNet models, the training objective of FaSNet can still be the negative SI-SDR score under the PIT framework. For tasks where frequency-domain output is favored (e.g., ASR tasks), mel-spectrogram with scale-invariant MSE (SI-MSE) loss is used as the training objective:

$$\begin{cases} \mathbf{Y}_c = \left| \text{STFT}\left(\dfrac{\mathbf{y}_c}{\|\mathbf{y}_c\|_2} \right) \right| \\ \mathbf{Y}_c^* = \left| \text{STFT}\left(\dfrac{\mathbf{y}_c^*}{\|\mathbf{y}_c^*\|_2} \right) \right| \end{cases} \tag{3.11}$$

$$\mathcal{L}_{\text{SI-MSE}} = \frac{1}{C} \sum_{c=1}^{C} ||\mathbf{Y}_c \mathbf{M} - \mathbf{Y}_c^* \mathbf{M}||_2^2 \tag{3.12}$$

where $\mathbf{Y}_c, \mathbf{Y}_c^* \in \mathbb{R}^{T \times F}$ are the magnitude spectrograms of the target and estimated signals respectively, and $\mathbf{M} \in \mathbb{R}^{F \times D}$ is the mel-filterbank.

3.1.2 Design of Filter Separation and Extraction Modules

The filter separation module in the first stage and the filter extraction module in the second stage are both TCN models proposed in the Conv-TasNet model in Chapter 2.2.1. The main difference with the TCN applied for Conv-TasNet is the design of the output layer. Suppose that $\{\mathbf{p}_c^1\}_{c=1}^C \in \mathbb{R}^{1 \times K}$ denote the outputs of the last TCN block at the first stage and serve as the input to the output layer, then the time-domain filters $\{\mathbf{h}_c^1\}_{c=1}^C$ are obtained by:

$$\mathbf{h}_c^1 = tanh(\mathbf{p}_c^1\mathbf{W}^1 + \mathbf{b}^1) \odot \sigma(\mathbf{p}_c^1\mathbf{V}^1 + \mathbf{q}^1) \tag{3.13}$$

where $\mathbf{W}^1, \mathbf{V}^1 \in \mathbb{R}^{K\times(2L+1)}$ and $\mathbf{b}^1, \mathbf{q}^1 \in \mathbb{R}^{1\times(2L+1)}$ are weight and bias parameters of the output layer, respectively, $tanh(\cdot)$ and $\sigma(\cdot)$ denote the hyperbolic tangent and Sigmoid functions respectively, and $\odot$ represents the Hadamard product. In other words, the output layer is a gated layer consisting of two heads to constrain the dynamic range of the estimated filters to be between -1 and 1. The design at the second stage is identical to the first stage. Figure 3.1 shows the full diagram of the system.

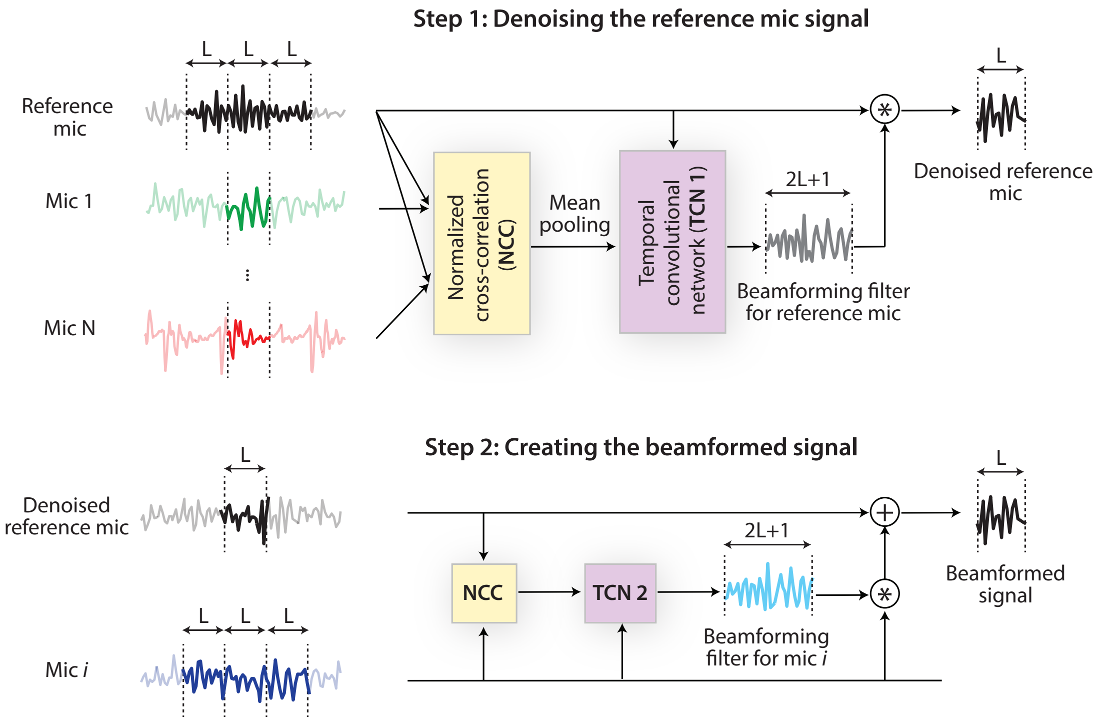
Step 1: Denoising the reference mic signal
L
L
L
Reference mic
Mic 1
⋮
Mic N
Normalized cross-correlation (NCC)
Mean pooling
Temporal convolutional network (TCN 1)
2L+1
Beamforming filter for reference mic
L
Denoised reference mic
Step 2: Creating the beamformed signal
L
Denoised reference mic
L
L
L
Mic i
NCC
TCN 2
2L+1
Beamforming filter for mic i
L
Beamformed signal

Figure 3.1: System flowchart for the two-stage FaSNet system. The first stage estimates the frame-level beamforming filters for the reference microphone based on the normalized correlation correlation coefficient (NCC) feature, and the second stage uses the cleaned reference microphone signal to estimate the beamforming filters for all remaining microphones. Cosine similarity is used as the NCC feature.

3.1.3 Experiment Configurations and Results

The evaluation of the two-stage FaSNet is applied on three tasks:

1. **Echoic noisy speech enhancement (ESE)**: Speech denoising and dereverberation are jointly performed in an echoic environment;
2. **Echoic noisy speech separation (ESS)**: The direct path of two speakers are separated in a noisy, echoic environment;
3. **Multichannel noisy ASR**: The 3rd CHiME challenge dataset [95] is selected for ASR task.

The direct-path speech signals for all sources of interest are always used as the target, which means that the system attempts to perform joint denoising/separation and dereverberation.

For ESE and ESS tasks, simulated datasets are generated from a circular omni-directional microphone array with a maximum of 4 microphones evenly distributed. The diameter of the array is fixed to 10 cm. The positions of the sources (speakers and the noise) and the center of the microphone array are randomly sampled, with the constraint that all sources should be at least 0.5 m away from the room walls. The height for all sources is fixed to 1 m. The room impluse response (RIR) filters are then simulated with the image method [3], and specifically with the gpuRIR toolbox [270]. The length and the width of the rooms are randomly sampled within the range $[3, 8]$ m with a fixed height of 3 m. The utterances in the datasets are sampled from the TIMIT dataset [8]. Each speaker's utterances are splitted into 7 training, 2 validation and 1 test samples, and then the training, validation and test sets are generated within the corresponding categories to include 20000, 5000 and 3000 rooms respectively. Each room contains two speakers and one noise source, within which the noise is randomly sampled from first 80 samples in the 100 Nonspeech Corpus [334] for training and validation sets and all 100 samples for the test set. For ESE, the relative SNR between the speaker and the noise is randomly sampled between $[-5, 15]$ dB. In ESS, the relative SNR between the two speakers is randomly sampled between $[-5, 5]$ dB and the noise is randomly sampled between $[-5, 15]$ dB with respect to the low energy speaker.

Table 3.1 shows the symbols for the hyperparameters in the two-stage FaSNet. Each TCN has an identical design to [201] and contains R repeats of the 1-D convolutional blocks with P blocks in each repeat, where $R = 2$ and $P = 5$ are used in all experiments. The size of the 1-D convolutional kernel in each 1-D convolutional block is 3, and the input and hidden channels in each block are set to 64 and 320, respectively. The embedding dimension K is set to 64. The number of parameters in each TCN is thus 0.76M. For tandem systems with a single-channel system for post-enhancement, the Conv-TasNet configuration [201] is adopted but the masking layer is modified into a direct regression layer. The model size of the single-output Conv-TasNet is 1.9M. The window size L and context size W are identical in all experiments.

Table 3.1: Hyperparameters in two-stage FaSNet.

Symbol	Description
L	Window size (in samples)
P	Number of convolutional blocks in each repeat in TCN
R	Number of repeats in TCN
K	Dimension of embeddings as well as the output of TCN

In the ASR and ESE tasks, each TCN estimates one beamforming filter at each frame, while in the ESS task, each TCN estimates two beamforming filters corresponding to the two speakers.

In order to show the advantages and performance of the two-stage FaSNet, the model is compared against a variety of classical beamformers. Both beamformers in the time- and frequency-domain are considered. The comparison on the time-domain beamformers is carried out since it represents a fairer comparison to FaSNet which is also based on the time domain. This comparison is extended to more traditional and more robust frequency-domain beamformers which are vastly used in practice. Four classes of beamformers are considered in the comparison. The first class is time-domain (TD) beamformers and comprises time-domain multi-channel Wiener filter (TD-MWF) and time-domain minimum variance distortionless response (TD-MVDR) beamformers [67]. The second class is frequency-domain (FD) beamformers and considers the speech distortion weigted MWF (SDW-MWF) and FD-MVDR beamformers [52]. For both of these classes the eigen-decomposition method is used in order to estimate the steering vector [57] from the estimated spatial covariance matrices. The third class comprises mask-based (MB) beamformers, specifically mask-based MVDR [118] and generalized eigenvalue (GEV) [100] beamformers. Both these mask-based beamformers use the ideal binary masks (IBM) to estimate the beamforming filters. In the interest of space, the exact formulation of each of the beamformers is omitted, and the interested reader can refer to the original formulations in table 3.2 and the open source implementation[1].

The benchmark results of the aforementioned beamformers are obtained on both ESE and ESS tasks and evaluated with signal quality measurement (i.e. SI-SDR). Both time- and frequency-domain beamformers use the full utterance to estimate the spatial covariance and consequently calculate the steering vector. Similarly, MB beamformers use the oracle IBMs on the full utterance to calculate the spatial covariance matrices. Table 3.2 provides the SI-SDRi scores of all described conventional beamformers. Among the time-domain beamformers, TD-MVDR shows better performance in the ESS task while TD-MWF is better in the ESE task. Even though the differences are minimal, the statement in [67] can be validated that for speech enhancement in time domain, MVDR is typically better than MWF. Among the frequency-domain beamformers, the SDW-MWF beamformer is significantly better than MVDR, given the fact that by design SDW-MWF also leads to better dereverberation. For MB beamformers, MB-MVDR shows significantly better performance than MB-GEV. This confirms the observation in [100] that GEV suffers from phase adjustment problems which can significantly decrease signal quality. The overall performance of frequency-domain beamformers is significantly better than time-domain beamformers especially with an increasing number of microphones [78].

As the two-stage FaSNet has a fixed receptive field defined by the TCNs, another experiment is also designed, where the spatial covariances and masks are estimated based on short segments of length $s \in \{100, 250, 500\}$ ms with two possible ways for the estimation: the spatial covariance is calculated over time for every non-overlapping segment, or only estimated once based on a segment randomly selected within the utterance. Empirically the two ways lead to results lacking significant

[1] `https://pypi.org/project/beamformers/`

differences, so only the results from the former configuration is reported here. Table 3.3 shows the comparison of the best performing oracle beamformers in table 3.2 with different segment sizes. For the widely-used MB-MVDR, a large enough receptive field is crucial for a reasonable performance which makes it harder to apply in rapid changing conditions.

Table 3.2: Performance of oracle beamformers. SI-SDRi is reported on decibel scale. CC: close-condition (development) set. OC: open-condition (evaluation) set.

Method	# of mics	SI-SDRi			
		ESE		ESS	
		CC	OC	CC	OC
TD-MVDR [67]	2	2.1	2.6	3.2	3.4
	3	2.5	2.9	4.2	4.3
	4	**2.8**	**3.2**	3.9	4.3
TD-MWF [67]	2	1.6	1.8	3.1	3.2
	3	2.1	2.5	3.9	4.2
	4	2.5	2.7	**4.4**	**4.5**
FD-MVDR [52]	2	2.1	2.0	2.1	2.1
	3	3.2	3.0	3.5	3.5
	4	4.1	3.9	4.6	4.5
FD-SDW-MWF [52]	2	3.7	3.6	3.3	3.1
	3	6.4	6.2	5.9	5.9
	4	**8.1**	**7.9**	**7.6**	**7.5**
MB-MVDR [118]	2	3.9	3.8	4.1	3.3
	3	5.8	5.7	6.2	5.1
	4	**6.7**	**6.6**	**7.5**	**6.3**
MB-GEV [100]	2	-4.8	-5.7	-4.1	-3.6
	3	0.8	0.9	1.1	0.6
	4	2.5	2.5	2.9	2.3

Table 3.3: Performance of oracle beamformers with different segment sizes for spatial covariance estimation. SI-SDRi is reported on decibel scale only on the OC set.

Method	Segment size (ms)	# of mics	SI-SDRi	
			ESE	ESS
FD-SDW-MWF [52]	100	4	4.5	4.0
	250	4	5.7	5.3
	500	4	**6.5**	**6.1**
MB-MVDR [118]	100	4	-0.3	-1.2
	250	4	3.0	2.7
	500	4	4.7	4.6

The first experiment on the two-stage FaSNet is on the investigation of the effect of window size

L. Table 3.4 shows how different frame sizes affect the system performance. It can be observed that a longer window size leads to constantly better performance, which is expected as higher frequency resolution can be achieved. As the system latency of the two-stage FaSNet is $2L$, tradeoff between performance and window size needs to be considered for applications that strictly require low-latency processing. Here the best performing system, i.e. $L = 16$, is selected for all following experiments.

Table 3.4: Dependence of SI-SDRi on frame size for a 2-ch two-stage FaSNet in the ESE task.

	L			
	2	4	8	16
CC	1.6	2.4	3.3	**4.0**
OC	1.4	2.2	3.0	**3.7**

The second experiment compares the two-stage FaSNet with Conv-TasNet [201], the single-channel separation model, as they share a same design on the separation modules. Table 3.5 provides the comparison across different number of microphones and causality settings. It can be observed that in a noncausal setting, the two-stage FaSNet achieves on par performance with the single-channel Conv-TasNet baseline of 4 microphones, while in a causal setting, it outperforms Conv-TasNet even with only 2 microphones. Moreover, adding a post single-channel enhancement network constantly improves the performance across almost all configurations on both tasks. The 4-channel tandem system is able to achieve on par performance with an MB-MVDR system with oracle IBM, and is significantly better than the segment-level oracle MB-MVDR. This shows that when comparing with frequency-domain beamformers which highly rely on a long segment for robust spatial covariance estimation, the two-stage FaSNet has better potential for low-latency processing on much shorter segments.

The third experiment evaluates the two-stage FaSNet on CHiME-3 dataset to investigate its potential as the front-end for speech recognition systems. Table 3.6 shows the performance of the two-stage FaSNet with respect to signal quality measure. Two different training targets, the reverberant clean signal or the original clean signal, are applied during training. Note that the original clean source has an unknown shift with the oracle direct path signal in the reference microphone,

Table 3.5: Performance of two-stage FaSNet and tandem system in both ESE and ESS tasks.

Method	Size	Causal	# of mics	SI-SDRi			
				ESE		ESS	
				CC	OC	CC	OC
Conv-TasNet	1.9M	×	1	5.3	5.0	4.1	4.1
		✓		3.5	3.3	2.7	2.6
FaSNet	1.5M	×	2	4.0	3.7	3.7	3.6
			3	4.4	4.1	4.0	3.9
			4	**5.3**	**5.0**	**4.7**	**4.6**
		✓	2	3.8	3.5	3.2	3.1
			3	4.1	3.8	3.5	3.4
			4	**4.5**	**4.3**	**3.9**	**3.8**
Tandem	3.4M	×	2	5.8	5.5	4.5	4.4
			3	5.4	5.0	5.5	5.5
			4	**6.7**	**6.4**	**6.2**	**6.1**
		✓	2	4.8	4.5	3.9	3.8
			3	**5.3**	**5.0**	4.1	4.0
			4	4.7	4.4	**4.5**	**4.4**

so here a *shift invariant training (SIT)* strategy is applied, where the maximum SI-SNR between the system output and the original clean signal with ±2 ms of shift is seleted for backpropagation. The results show that the two-stage FaSNet is significantly better than the Conv-TasNet baseline with both targets, further proving its effectiveness on real-world recordings. Table 3.7 compares the word error rate (WER) of the two-stage FaSNet and the official CHiME-3 baseline system on the recognition task. The officially provided DNN baseline recognizer is used as the backend ASR system, although more advanced systems with fully end-to-end training may further boost the performance. The table shows that when training with the original clean source as target and SI-SNR as objective, the two-stage FaSNet is able to achieve 9.3% relative WER reduction (RWERR) compared with the MVDR baseline, and when training with the mel-spectrogram of the original clean signal as target with SI-MSE as objective, the two-stage FaSNet achieves a 14.3% RWERR. This result proves that when training with a frequency-domain objective that favors ASR backends, two-stage FaSNet can also serve as an effective ASR front-end.

Finally, to better understand the beampatterns of the estimated time-domain filters, figure 3.2 visualizes them for two example utterances in the ESS task. The figure shows the beampatterns

Table 3.6: Performance of two-stage FaSNet on CHiME-3 evaluation dataset. SI-SDRi is reported on decibel scale.

Target	Method	Causal	SI-SDRi
Reverberant clean	Conv-TasNet	×	8.7
	FaSNet	×	**12.2**
		✓	10.6
Clean source	Conv-TasNet	×	7.5
	FaSNet	×	**11.6**
		✓	11.1

Table 3.7: Performance of two-stage FaSNet on CHiME-3 evaluation dataset of real recordings. WER is reported.

Method	Target	WER (%)
Noisy	-	32.53
Baseline	-	32.48
FaSNet	Reverberant clean	32.23
	Clean source	29.47
	Mel-spectrogram	**27.89**

estimated by the model at different frames of the utterances. The beampatterns are shown as a function of frequency and DOA. The two-stage FasNet learns specific beampatterns which are content-dependent within each utterance, where different regions have different beampatterns. Specifically, nonspeech regions receive filters with null pattern for both utterances, further proving the adaptation ability of FaSNet across the utterance.

3.2 TAC-FaSNet: Microphone-number-invariant and Geometry-independent Processing

There are two core drawbacks in the two-stage FaSNet. First, the processing in the second stage only makes use of the pairwise information of the output from the first stage and another remaining channel, which prevents the system from utilizing the information from all microphones to make a global decision during filter estimation. Second, failures in the first stage may greatly affect the performance of the second stage. To allow the model to perform a single-stage filter estimation while making use of the global information and being invariant to the microphone number and permutation configurations, the *transform-average-concatenate (TAC)* is proposed to tackle the

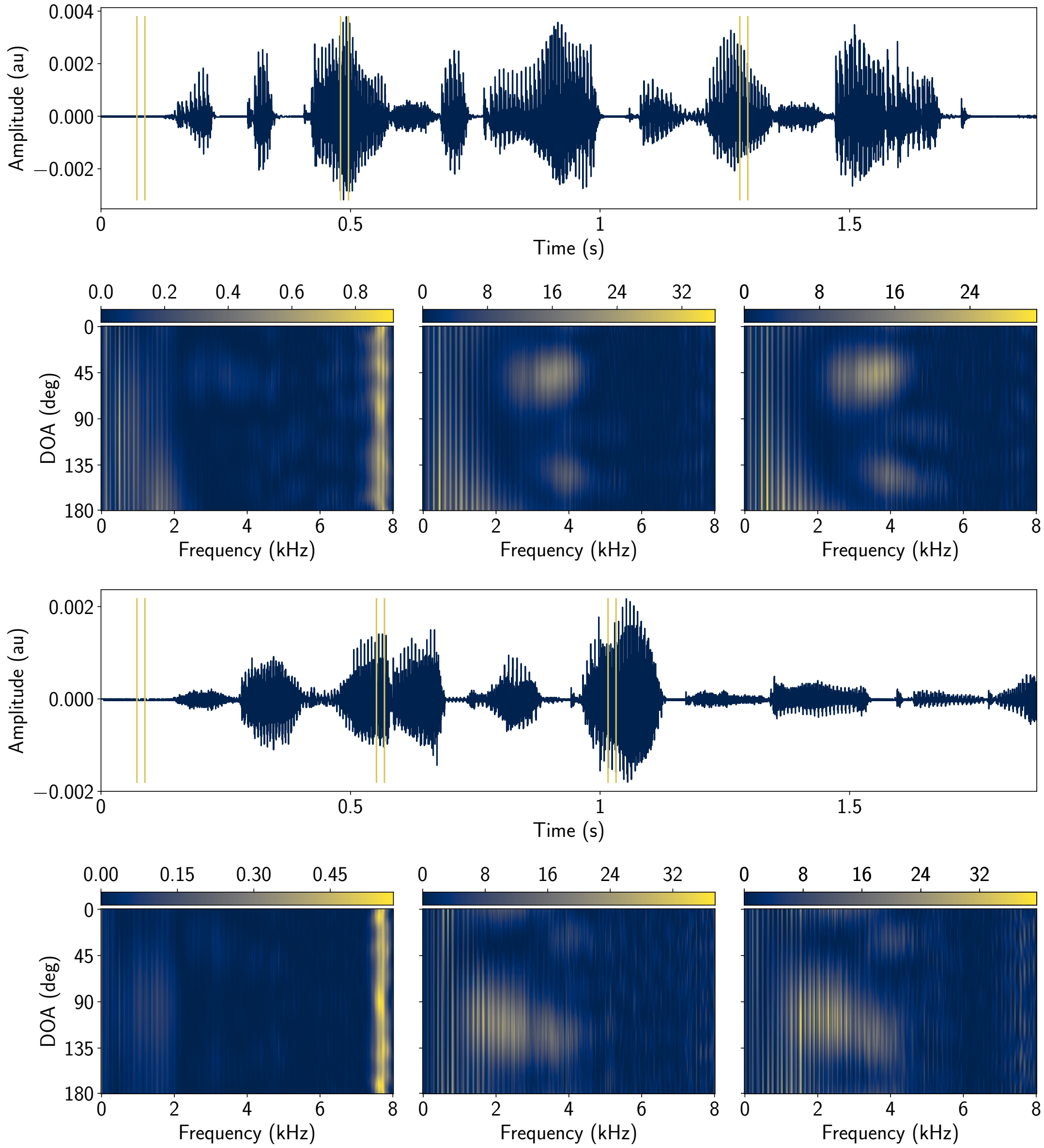

Figure 3.2: Beampattern examples for two different utterances in the ESS task.

disadvantages of the two-stage FaSNet.

A TAC module takes the feature from multiple channels as input. It first *transforms* each channel's feature with a sub-module shared by all channels, and then the outputs are *averaged* as a global-pooling stage and passed to another sub-module for extra nonlinearity. The corresponding output is then *concatenated* with each of the outputs of the first transformation sub-module and passed to a third sub-module for generating channel-dependent outputs. It is easy to see that, with parameter sharing at the *transform* and *concatenate* stages and the permutation-invariant property of the *average* stage, TAC guarantees channel permutation and number invariant processing and is always able to make global decisions.

3.2.1 Modifications upon the Two-stage FaSNet

There are three differences between the TAC-FaSNet and the two-stage FaSNet. First, the TAC module is introduced and applied to ensure the microphone number and geometry invariant property. Second, the two-stage design is replaced by a single-stage design to better utilize the global information. Third, the TCN separation module is replaced by DPRNN blocks for better sequential modeling ability.

To introduce the design of the TAC module, consider an N-channel microphone array with an arbitrary geometry where $N \in \{2, \ldots, N_m\}$ can vary between 2 and a pre-defined maximum number $N_m \geq 2$. Each channel is represented by a sequential feature $\mathbf{Z}_i \in \mathbb{R}^{T \times *}, i = 1, \ldots, N$ where T denotes the sequence length and $*$ denotes arbitrary feature dimensions. Only one-dimensional features, i.e. $\mathbf{Z}_i \in \mathbb{R}^{T \times K}$, are considered here for simplicity, although the proposed method can be easily extended to higher dimensions.

A TAC module first transforms each channel's feature with a shared sub-module. Although any neural network architectures can be applied, here a simple fully-connected (FC) layer with parametric rectified linear unit (PReLU) activation is applied at each time step:

$$\mathbf{f}_{i,j} = P(\mathbf{z}_{i,j}),\ j = 1, \ldots, T \tag{3.14}$$

where $\mathbf{z}_{i,j} \in \mathbb{R}^{1 \times K}$ is the j-th time step in $\mathbf{Z}_i$, $P(\cdot)$ is the mapping function defined by the FC layer, and $\mathbf{f}_{i,j} \in \mathbb{R}^{1 \times D}$ denotes the output for channel i at time step j. All features $\mathbf{f}_{i,j}, i = 1, \ldots, N$ at time step j are then averaged as a global-pooling stage, and passed to another FC layer with PReLU activation:

$$\hat{\mathbf{f}}_j = R(\frac{1}{N}\sum_{i=1}^{N}\mathbf{f}_{i,j}) \tag{3.15}$$

where $R(\cdot)$ is the mapping function defined by this FC layer and $\hat{\mathbf{f}}_j \in \mathbb{R}^{1\times D}$ is the output at time step j. $\hat{\mathbf{f}}_j$ is then concatenated with $\mathbf{f}_{i,j}$ at each channel and passed to a third FC layer with PReLU activation to generate channel-specific output $\mathbf{g}_{i,j} \in \mathbb{R}^{1\times D}$:

$$\hat{\mathbf{g}}_{i,j} = S([\mathbf{f}_{i,j}; \hat{\mathbf{f}}_j]) \tag{3.16}$$

where $S(\cdot)$ is the mapping function defined by this FC layer and $[x; y]$ denotes the concatenation operation of vector x and y. A residual connection is then added between the original input $\mathbf{z}_{i,j}$ and $\hat{\mathbf{g}}_{i,j}$ to form the output of the TAC module:

$$\hat{\mathbf{z}}_{i,j} = \mathbf{z}_{i,j} + \hat{\mathbf{g}}_{i,j} \tag{3.17}$$

Figure 3.3 shows the flowchart of a TAC module.

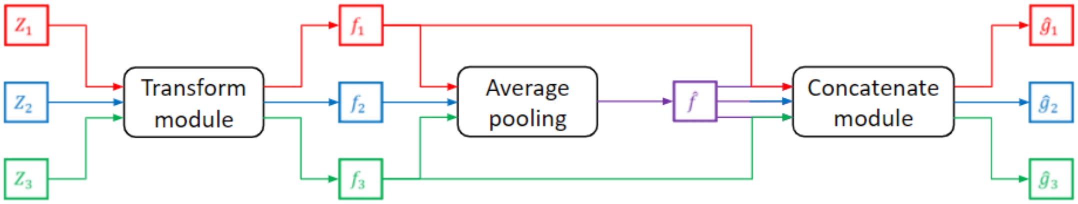

Figure 3.3: Flowchart for the TAC module. A *transform* module is shared across all the channels to transform the input at each channel via a nonlinear mapping. An *average* module applies average-pooling across the channels and applies another nonlinear mapping. A *concatenate* module concatenates the outputs from the *transform* and *average* stages and generates channel-dependent outputs.

TAC is closely related to the recent progress in permutation invariant functions and functions defined on sets [174]. Permutation invariant neural architectures have been widely investigated in problems such as relational reasoning [162], point-cloud analysis [195] and graph neural networks [223]. The *transform* and *average* stages correspond to the general idea of parameter-sharing and pooling in a family of permutation invariant functions [174], while the *concatenate* stage is applied as in the problem setting of beamforming, the dimension of outputs should match that of the inputs. The *concatenate* stage also allows the usage of residual connections, which enables the TAC module to be inserted into any deep architectures without increasing the optimization difficulty.

The most straightforward way to apply TAC in FaSNet is to replace the pairwise filter estimation in the second stage to a global operation, allowing the filters for each of the C sources to be jointly estimated across all remaining microphones. Figure 3.4 (A) and (B) compare the flowcharts of the original and modified two-stage FaSNet models. However, the pre-separation results at the reference microphone still cannot benefit from the TAC operation with the two-stage design. A single-stage architecture can thus be proposed where the filters for all channels are jointly estimated. Figure 3.4 (C) and (D) show the single-stage FaSNet models without and with TAC, respectively. For single-stage models, the NCC feature for each channel is directly used without a cross-channel mean-pooling operation. Moreover, as shown in figure 3.4, the original TCN modules are replaced with the DPRNN modules.

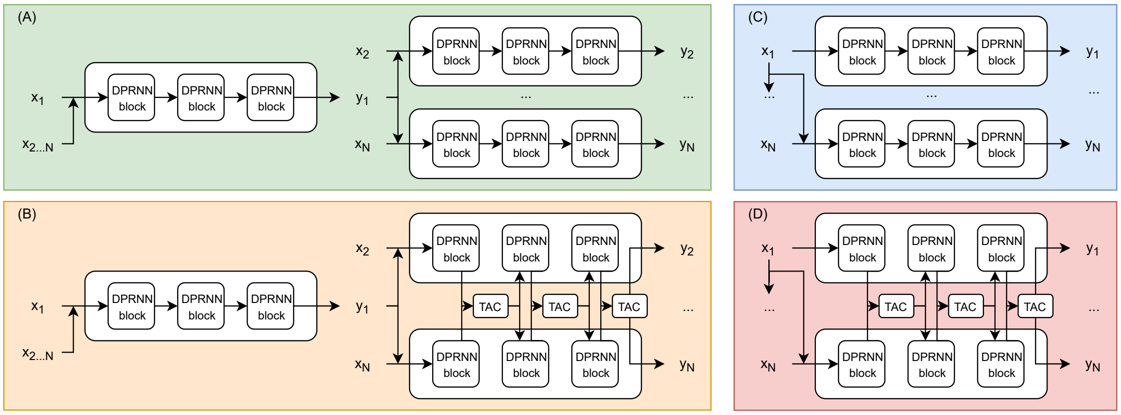

Figure 3.4: Flowcharts of variants of FaSNet models. Only one output is illustrated for the sake of simplicity. (A) The original two-stage FaSNet. (B) The two-stage FaSNet with TAC applied to every processing block in the second stage. (C) The single-stage FaSNet. (D) The single-stage FaSNet with TAC applied to every processing block.

3.2.2 Experiment Configurations and Results

The two-stage FaSNet baseline and the TAC-FaSNet are evaluated on the task of multi-channel two-speaker noisy speech separation with both ad-hoc and fixed geometry microphone arrays. A multi-channel noisy reverberant dataset with 20000, 5000 and 3000 4-second long utterances is simulated from the Librispeech dataset [109]. Two speakers and one nonspeech noise are randomly selected from the 100-hour Librispeech dataset and the 100 Nonspeech Corpus [334], respectively. An overlap ratio between the two speakers is uniformly sampled between 0% and 100% such that the average overlap ratio across the dataset is 50%. The two speech signals are then shifted accordingly and rescaled to a random relative SNR between 0 and 5 dB. The noise is repeated if its length is smaller than 4 seconds, and the relative SNR between the power of the sum of the two clean speech signals and the noise is randomly sampled between 10 and 20 dB. The transformed signals are then convolved with RIRs generated by the image method [3] using the gpuRIR toolbox [270]. The length and width of the room are randomly sampled between 3 and 10 meters, and the height is randomly sampled between 2.5 and 4 meters. The reverberation time (T60) is randomly sampled between 0.1 and 0.5 seconds. The echoic signals are summed to create the mixture for each microphone. All microphone, speaker and noise locations in the ad-hoc array dataset are randomly sampled to be at least 0.5 m away from the room walls. In the fixed geometry array dataset, the microphone center is first sampled and then 6 microphones are evenly distributed around a circle with diameter of 10 cm. The speaker locations are then sampled such that the average speaker angle with respect to the microphone center is uniformly distributed between 0 and 180 degrees. The noise location is sampled without further constraints. The ad-hoc array dataset contains utterances with 2 to 6 microphones, where the number of utterances for each microphone configuration is set equal.

Single-channel baseline is also added here for a more comprehensive comparison. The first stage in the two-stage FaSNet is used as a modification to the TasNet model, where the separation is done by estimating filters for each context frame in the mixture instead of masking matrices on a generated front-end. This model is referred to as *TasNet-filter*. For adding NCC features to the single-channel baseline, three strategies are applied: (1) no NCC feature (pure single-channel processing), (2) concatenate the mean-pooled NCC features (i.e. first stage in FaSNet), and (3) concatenate all NCC features according to microphone indexes (similar to [231], only applicable in fixed geometry array). For multi-channel models, the four aforementioned variants of FaSNets are compared with a similar model size and complexity. The training target is always the reverberant clean speech signals, which is different from the configuration in the two-stage FaSNet where the direct path signal is used as the target. Moreover, the effect of the window size L is also examined, while the context size W is always set to 16 ms (i.e. 256 samples at 16k Hz sample rate). The details about the dataset generation as well as model configurations is available online[2].

Table 3.8 shows the experiment results on the ad-hoc array configuration. Only the results on 2, 4 and 6 microphones are reported due to the space limit. For the TasNet-based models, minor performance improvement can be achieved with the averaged NCC features, however increasing the number of microphones does not necessarily improves the performance. For the original two-stage FaSNet models, the performance is worse than TasNet with NCC feature even with TAC applied at the second stage. As TasNet with averaged NCC feature is equivalent to the first stage in the two-stage FaSNet, this observation indicates that the two-stage design cannot perform reliable beamforming at the second stage in the ad-hoc array configuration. On the other hand, single-stage FaSNet without TAC already outperforms both TasNet-based and two-stage FaSNet models, showing that the pre-separation stage is unnecessary in this configuration. Adding TAC to the single-stage FaSNet further improves the performance in all conditions and microphone numbers, and guarantees that more microphones will not make the performance worse. The improvement in conditions where the overlap ratio is high is rather significant. This shows that adding TAC modules enables the model to estimate much better filters by using all available information.

Although TAC is designed for the ad-hoc array configuration where the permutation and the number of microphones are unknown, experiments in a fixed geometry array configuration are also conducted to investigate whether improvements can also be achieved. Table 3.9 shows the

[2] `https://github.com/yluo42/TAC`

Table 3.8: Experiment results on ad-hoc array with various numbers of microphones. SI-SDRi is reported on decibel scale.

Model	Size	# of mics	Overlap ratio				Average
			<25%	25-50%	50-75%	>75%	
TasNet-filter	2.9M	2 / 4 / 6	12.5 / 12.2 / 12.3	8.9 / 8.6 / 9.0	6.4 / 6.2 / 6.1	3.9 / 3.6 / 3.8	7.8 / 7.8 / 8.0
+NCC ave.	2.9M		13.1 / 13.0 / 13.2	8.8 / 8.8 / 8.9	6.4 / 6.1 / 6.2	3.2 / 3.6 / 3.6	7.7 / 8.0 / 8.2
+NCC ave.+4ms	2.9M		13.2 / 13.3 / 13.6	9.5 / 9.3 / 9.7	7.0 / 6.6 / 7.1	4.6 / 4.4 / 4.7	8.4 / 8.5 / 9.0
FaSNet	3.0M		11.0 / 11.5 / 11.5	7.0 / 7.9 / 8.1	4.5 / 5.2 / 5.4	2.0 / 2.6 / 3.0	5.9 / 6.9 / 7.3
+TAC	3.0M		11.3 / 11.8 / 11.7	7.2 / 7.8 / 8.5	5.1 / 5.4 / 5.5	1.9 / 2.3 / 3.0	6.2 / 7.0 / 7.4
+joint	2.9M		14.4 / 13.7 / 14.1	10.2 / 9.8 / 10.4	7.5 / 7.2 / 7.7	4.6 / 4.5 / 4.7	9.0 / 8.9 / 9.5
+TAC+joint	2.9M		**15.2 / 16.1** / 16.1	**10.9** / 11.6 / 12.2	**8.6** / 9.5 / **9.8**	5.5 / 7.2 / 7.6	9.8 / 11.2 / 11.7
+TAC+joint+4ms	2.9M		15.1 / 16.0 / **16.2**	10.8 / **12.0 / 12.5**	**8.6 / 9.6 / 9.8**	**6.2 / 7.8 / 8.3**	**10.0 / 11.5 / 12.0**

experiment results with the 6-mic circular array described earlier. It can be observed that TasNet with all NCC features concatenated leads to even worse performance than the pure single-channel model, indicating that the properness of feature concatenation in such frameworks might need to be reconsidered. The two-stage FasNet has already obtained significantly better performance than all TasNet-based models, while the TAC-FaSNet still greatly outperforms the two-stage FaSNet across all conditions, showing that TAC is also helpful for fixed geometry arrays. A possible explanation for this is that TAC is able to learn geometry-dependent information even without explicit geometry-related features.

Table 3.9: Experiment results on 6-mic fixed geometry (circular) array. SI-SDRi is reported on decibel scale.

Model	Size	Speaker angle				Overlap ratio				Average
		<15°	15-45°	45-90°	>90°	<25%	25-50%	50-75%	>75%	
TasNet-filter	2.9M	7.6	7.9	8.2	8.3	12.8	9.1	6.4	3.7	8.0
+NCC concat.	3.1M	6.6	6.8	7.0	7.1	11.2	8.6	5.2	2.6	6.9
+NCC ave.	2.9M	8.2	8.6	8.9	8.9	13.3	9.9	7.1	4.4	8.7
+NCC ave.+4ms	2.9M	8.5	8.8	9.1	9.3	13.6	10.0	7.3	4.8	8.9
FaSNet	3.0M	8.5	9.6	10.7	11.4	14.1	11.1	8.7	6.3	10.0
+TAC+joint	2.9M	9.0	10.8	12.3	13.1	15.5	12.2	9.9	7.6	11.3
+TAC+joint+4ms	2.9M	**9.1**	**11.1**	**12.6**	**13.4**	**15.6**	**12.4**	**10.1**	**8.0**	**11.5**

Smaller center window size L in the two-stage FaSNet led to significantly worse performance due to the lack of frequency resolution (table 3.4). However, the results here show that the worse performance was actually due to the lack of global processing in filter estimation. In the last row of both tables better or on par performance for TAC-FaSNet with 4 ms window can be observed. This strengthens the argument and further proves the effectiveness of TAC across various model configurations.

3.3 iFaSNet: Implicit Filter-and-sum with Improved Feature Extraction

Both two-stage FaSNet and TAC-FaSNet are based on the problem formulation of an explicit filter-and-sum operation on the mixture waveforms. However, conventional time-domain filter-and-sum beamformers have shown to be less effective than frequency-domain filter-and-sum beamformers. Motivated by the TasNet framework where the masking in the frequency domain is replaced by the masking in a learnable hidden representation, it is thus natural to consider the filter-and-sum operation in a learnable representation rather than the waveform domain. Implicit FaSNet (iFaSNet) marks an attempt to perform implicit filter-and-sum with improved cross-channel feature extraction.

3.3.1 Modifications upon the TAC-FaSNet

iFaSNet contains four main modifications compared with the TAC-TasNet. First, the original multi-input-multi-output (MIMO) formulation is compared with the multi-input-single-output (MISO) formulation, where the filter is only estimated for the reference channel instead of all the channels. Second, the filter estimation in a learnable latent space is investigated upon the original waveform-domain. Third, better cross-channel features that are more suitable for the MISO and latent-space filtering design are explored. Fourth, a context-aware processing is proposed to further improve the model performance.

The training target for the standard FaSNet is typically the reverberant clean signals. In the problem configuration where the time-domain filter-and-sum operation is applied, it implies that the beamforming filters should not only enhance the signal coming from a certain direction, but also reconstruct all the reverberation components. However, as reverberation may come from all possible directions, the ideal beampattern of such beamforming filters might be hard or even impossible to define. Although FaSNet applies frame-level beamforming where infinite optimal frame-level filters may exist since the linear equation in equation (3.2) is underdetermined (L equations and $M \times (1 + 2W)$ unknowns), finding such reverberation-preserving filters for all channels

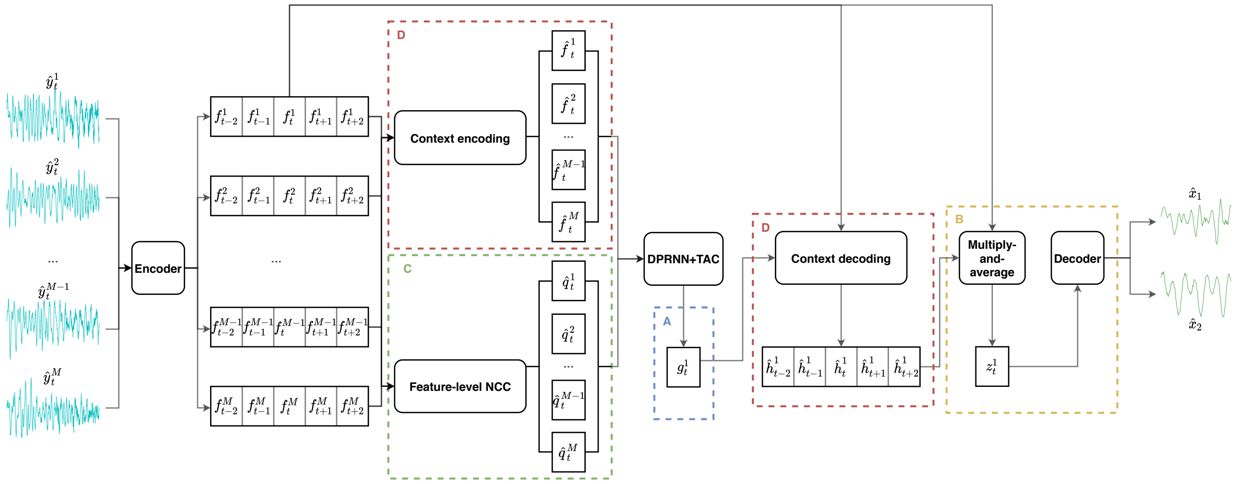
$\hat{y}_t^1$
$\hat{y}_t^2$
...
$\hat{y}_t^{M-1}$
$\hat{y}_t^M$
Encoder
f_{t-2}^1 f_{t-1}^1 f_t^1 f_{t+1}^1 f_{t+2}^1
f_{t-2}^2 f_{t-1}^2 f_t^2 f_{t+1}^2 f_{t+2}^2
...
f_{t-2}^{M-1} f_{t-1}^{M-1} f_t^{M-1} f_{t+1}^{M-1} f_{t+2}^{M-1}
f_{t-2}^M f_{t-1}^M f_t^M f_{t+1}^M f_{t+2}^M
D
Context encoding
$\hat{f}_t^1$
$\hat{f}_t^2$
...
$\hat{f}_t^{M-1}$
$\hat{f}_t^M$
C
Feature-level NCC
$\hat{q}_t^1$
$\hat{q}_t^2$
...
$\hat{q}_t^{M-1}$
$\hat{q}_t^M$
DPRNN+TAC
A
g_t^1
D
Context decoding
$\hat{h}_{t-2}^1$ $\hat{h}_{t-1}^1$ $\hat{h}_t^1$ $\hat{h}_{t+1}^1$ $\hat{h}_{t+2}^1$
B
Multiply-and-average
z_t^1
Decoder
$\hat{x}_1$
$\hat{x}_2$

Figure 3.5: Flowchart for the iFaSNet architecture. The modifications to the TAC-FaSNet are highlighted, which include (A) the use of MISO design instead of the original MIMO design, (B) the use of implicit filtering in the latent space instead of the original explicit filtering on the waveforms, (C) the use of feature-level NCC feature for cross-channel information instead of the original sample-level NCC feature, and (D) the use of context-aware filtering instead of the original context-independent filtering.

may still be unnecessary. It is natural to consider an alternative problem formulation rather than the standard filter-and-sum formulation. Since the standard FaSNet estimates a set of filters for each of the channels and can be viewed as a multi-input-multi-output (MIMO) system, a simple way to bypass the issue of bad beampatterns is to change it into a multi-input-single-output (MISO) system where only the filter for the reference channel is estimated. The features from all the other channels are thus viewed as additional information to assist the separation on a (randomly) selected reference channel. This reformulates the multi-channel separation problem back to the single-channel separation problem, while the input to the model still contains the mixtures from all channels. Figure 3.5 (A) shows the MISO module.

Most existing neural beamformers are mainly designed in the frequency domain due to the fact that oracle frequency-domain beamformers typically have better performance than those in time domain. As frequency-domain beamformers are typically formulated as a multiplication operation on the spectrums, a similar operation can be defined in time-domain systems as a multiplication operation on learnable features. Note that recent single-channel speech separation systems have widely applied a set of learnable encoder and decoder to replace the short-time Fourier transform

(STFT) and estimated a multiplicative mask on the encoder outputs to match the formulation in time-frequency masking systems. The formulation of implicit filtering can thus be connected to the masking operation in such systems.

The extraction of the channel-wise features in the standard FaSNet is calculated on the context of input mixture frame $\hat{\mathbf{x}}^i$ with a corresponding hop size (which is empirically set to $L/2$), which results in a sequence of encoder outputs $[\mathbf{f}^i_{t-C}, \ldots, \mathbf{f}^i_t, \ldots, \mathbf{f}^i_{t+C}] \in \mathbb{R}^{(1+2C)\times N}$ where t denotes the frame index and C denotes the context size. The estimated filter with shape $\mathbb{R}^{1\times N}$ is only applied to $\mathbf{f}^i_t$, while all encoder outputs of the context are used as the input the filter estimation modules. A decoder with its weight $\mathbf{P} \in \mathbb{R}^{N\times L}$ is applied to transform the filtered feature back to waveforms. Figure 3.5 (B) shows the newly-added decoder module.

The cross-channel feature in standard FaSNet is calculated by time-domain normalized cross correlation (tNCC) defined in equation (3.8). The rationale behind tNCC is to capture both the delay information across channels and the source-dependent information for different targets. However, whether tNCC is still a good feature in the implicit filtering formulation is unknown. Since implicit filtering operates in the feature space and does not explicitly requires the information of sample-level delay, it is necessary to modify tNCC such that it better explores the cross-channel information in the feature level. Here the tNCC is modified to a feature-level NCC (fNCC) feature. Denote the context feature $[\mathbf{f}^i_{t-C}, \ldots, \mathbf{f}^i_t, \ldots, \mathbf{f}^i_{t+C}]$ as $\mathbf{F}^i_t$, fNCC calculates the cosine similarity between the contextual feature in the reference channel $\mathbf{F}^1_t$ and the contextual feature in all channels $\{\mathbf{F}^i_t\}^M_{i=1}$:

$$\hat{\mathbf{q}}^i_t = \bar{\mathbf{F}}^1_t \bar{\mathbf{F}}^{iT}_t \tag{3.18}$$

where $\bar{\mathbf{F}}^i_t$ denotes the column-normalized feature of $\mathbf{F}^i_t$ where each column has a unit length, and $\hat{\mathbf{q}}^i_t \in \mathbb{R}^{(1+2C)\times(1+2C)}$ denotes the fNCC feature at time t for channel i. $\hat{\mathbf{q}}^i_t$ is then flatten to a vector of shape $1 \times (1+2C)^2$. For the default setting in FaSNet where $W = L = 16$ ms $= 256$ samples with a 50% hop size, $C = 2$ and $(1+2C)^2 = 25 \ll 1 + 2W = 513$. Figure 3.5 (C) shows the fNCC calculation module.

Utilizing context information to improve the modeling of local frame is very common in various systems [93], [173]. To make use of the contextual feature $\mathbf{F}_t^i$, a straightforward way is to concatenate all of them and pass to the filter estimation module. However, here a context encoder and decoder are proposed to perform both dimension reduction on the features. A context encoder is applied to $[\mathbf{f}_{t-C}^i, \ldots, \mathbf{f}_t^i, \ldots, \mathbf{f}_{t+C}^i]$ to model the intra-context dependencies, and the output is averaged across time to squeeze into a single feature vector $\hat{\mathbf{f}}_t^i \in \mathbb{R}^{1\times N}$. $\hat{\mathbf{f}}_t^i$ together with the fNCC feature $\hat{\mathbf{q}}_t^i$ are concatenated and used as the input to the filter estimation modules. The output of the MISO filter estimation modules $\mathbf{g}_t^1 \in \mathbb{R}^{1\times N}$ is then concatenated to each feature in the contextual encoder outputs and passed to a context decoder to generate a set of contextual filters $[\hat{\mathbf{h}}_{t-C}^1, \ldots, \hat{\mathbf{h}}_t^1, \ldots, \hat{\mathbf{h}}_{t+C}^1] \in \mathbb{R}^{(1+2C)\times N}$. The filters are then applied to the contextual encoder outputs to form an implicit, intra-context "filter-and-sum" operation:

$$\mathbf{z}_t^1 = \frac{1}{1+2C}\sum_{j=0}^{2C} \mathbf{f}_{t-C+j}^1 \odot \hat{\mathbf{h}}_{t-C+j}^1 \tag{3.19}$$

where $\odot$ denotes the Hadamard product. Here a bidirectional LSTM (BLSTM) layer is used for both the contextual encoder and decoder. Figure 3.5 (D) shows the context encoder and decoder.

3.3.2 Experiment Configurations and Results

The evaluation of the iFaSNet model is based on the same dataset used for the TAC-FaSNet, while only the ad-hoc microphone array configuration is used for comparison. The frame size L and the context size W are both set to 16 ms (256 points), and the hop size is set to 50%. Auxiliary autoencoding training (A2T) is applied to enhance the robustness on this reverberant separation task [324], which will be introduced in Chapter 5.2.

Table 3.10 presents the ablation experiment results of the standard FaSNet with different modifications applied. It can be observed that the MISO configuration which removes the beamforming filters for all other channels except for the reference channel does not harm the overall performance,

Table 3.10: Experiment results with various model configurations. SI-SDRi is reported on decibel scale.

Model	Size	# of mics	Overlap ratio				Average
			<25%	25-50%	50-75%	>75%	
FaSNet	2.9M	2 / 4 / 6	15.0 / 15.3 / 14.8	10.7 / 11.1 / 11.6	8.6 / 9.2 / 9.3	5.4 / 7.0 / 7.0	9.7 / 10.8 / 10.9
+MISO	2.9M		14.8 / 15.5 / 15.7	10.4 / 11.3 / 11.9	8.5 / 9.0 / 9.4	5.0 / 6.8 / 7.1	9.5 / 10.8 / 11.2
+fNCC	3.0M		14.5 / 14.8 / 14.4	10.1 / 11.0 / 11.3	8.3 / 8.9 / 9.0	4.9 / 6.7 / 6.9	9.3 / 10.4 / 10.6
+MISO+fNCC	2.9M		15.0 / 15.7 / 15.7	10.6 / 11.4 / 12.2	8.4 / 9.4 / 9.6	5.3 / 7.4 / 8.0	9.7 / 11.1 / 11.6
+MISO+implicit	2.9M		14.2 / 14.9 / 15.2	9.8 / 10.9 / 11.3	7.7 / 8.1 / 8.7	4.6 / 5.7 / 6.1	8.9 / 10.0 / 10.6
+MISO+implicit+fNCC	3.0M		15.3 / 16.0 / 16.1	10.9 / 11.8 / 12.5	8.5 / 9.6 / 10.1	5.7 / 7.6 / 8.3	9.9 / 11.4 / 12.0
+MISO+implicit+fNCC+context	3.0M		**15.6 / 16.4 / 16.5**	**11.2 / 12.4 / 12.9**	**9.0 / 10.1 / 10.3**	**5.8 / 7.9 / 8.8**	**10.2 / 11.8 / 12.3**

and the performance in the 6 microphone setting is even improved. This results supports the previous discussion that jointly using explicit filter-and-sum formulation and setting reverberant clean signals as training targets might not be a proper configuration. For the role of the cross-channel features in different model settings, the results show that using fNCC together with the original MIMO configuration leads to worse performance than using the original tNCC feature, while using fNCC together with the MISO configuration can improve the separation performance in high overlapped utterances. This shows that proper cross-channel features should be selected to keep inline with the system's problem formulation in order to achieve a good performance. Applying MISO configuration together with tNCC feature and implicit filtering achieves even worse performance than the baseline FaSNet, while changing the tNCC feature to fNCC feature results in a performance boost. Since fNCC is calculated on the contextual encoder outputs and the implicit filtering configuration estimates multiplicative filters on the center frame of the contextual encoder outputs, this further verifies that matching the problem formulation with a proper cross-channel feature is crucial for a good overall performance. The last ablation experiment verifies the effectiveness of the context encoder and decoder modules. With a slightly increased model size, the intra-context filter-and-sum formulation can further improve the performance upon the implicit filtering formulation, which shows that exploring contextual information is beneficial. This can also be related to recent literature in multi-tap beamformers where the beamforming filters are estimated for a context of frames [311].

Table 3.11 compares the training and inference speed for different model configurations. When the MISO, implicit filtering, and fNCC feature are applied, the training and inference speeds are 2 times and 2.2 times faster, respectively. Adding the context encoder and decoder modules makes

Table 3.11: Training and inference speeds of different model configurations. The speeds are measured on a single NVIDIA TITAN Pascal graphic card with a batch size of 4.

Model	Training speed	Inference speed
FaSNet	268.0 ms	98.1 ms
+MISO	222.6 ms	93.2 ms
+fNCC	331.7 ms	105.7 ms
+MISO+fNCC	333.0 ms	105.8 ms
+MISO+implicit	187.9 ms	96.6 ms
+MISO+implicit+fNCC	**132.2 ms**	**44.2 ms**
+MISO+implicit+fNCC+context	156.7 ms	52.5 ms

the network slightly slower, but the training and inference speeds are still 1.7 times and 1.9 times faster than the standard FaSNet, respectively. The results show that iFaSNet does not sacrifice complexity for performance.

3.4 Discussions

The FaSNet series of work are mainly designed for the ad-hoc microphone array configuration where the microphone number and geometry information are assumed unknown. As FaSNet applies end-to-end training with a time-domain objective, the comparison between FaSNet and conventional beamformers as well as frequency-domain neural beamformers needs to consider either the signal quality or the effect on ASR performance.

In practical applications, the TAC module requires cross-channel feature synchronization in the *average* stage. While in ad-hoc microphone array this does not contain the cost of synchronization, in ad-hoc device configurations where multiple devices with varying numbers of microphones in each device, how such synchronization across devices should be performed needs further investigation.

Chapter 4: Lightweight Model Design for Speech Separation

Model size and complexity remain the biggest challenges in the deployment of speech enhancement and separation systems on low-resource devices such as earphones and hearing aids. Although methods such as compression, distillation and quantization can be applied to large models, they often come with a cost on the model performance. In this chapter I will introduce two simple yet effective methods to design ultra-lightweight low-complexity speech separation models, namely the *group communication (GroupComm)* method [288] and the *context codec* method [289], [326]. GroupComm splits a high-dimensional feature into groups of low-dimensional features and applies a module to capture the inter-group dependency. A model can then be applied to the groups in parallel with a significantly smaller width. A context codec is applied to decrease the length of a sequential feature, where a context encoder compresses the temporal context of local features into a single feature representing the global characteristics of the context, and a context decoder decompresses the transformed global features back to the context features. Combining the two methods gives the *GC3* design for general lightweight sequence modeling module design.

4.1 Related Works

Tremendous efforts have been made to propose novel model architectures and model compression techniques. Early deep neural networks used for source separation contained stacked recurrent layers such as LSTM layers with a relatively large number of hidden units [80], [123], [148], [173], [198], and the corresponding model sizes were typically over tens of millions of parameters with high model complexity. Convolutional neural networks (CNNs) have also been explored in both time-frequency domain [137], [146], [165], [204], [302], [312] and time domain [211], [214], [240], [243], [248], [305], [316], and researchers have begun to focus on decreasing the model size and complexity while maintaining or improving the performance. Moreover, the combination of recurrent and convolutional layers has also been a popular topic for real-time model design, and various convolutional recurrent networks have been proposed [155], [164], [212], [213], [224], [279]. Better layer organization within the network have also been investigated [265], [283], [287], [293], [303], which further decrease the overall model size and maintain the separation fidelity. Beyond directly designing smaller models, neural architecture search (NAS) techniques have also been utilized to automatically search for compact architectures for speech-related tasks [246], [278], teacher-student learning methods have been explored for obtaining low-latency separation models [225], quantization and binarization algorithms have been studied for low-resource separation systems [192], [235], [282], and network pruning and distillation strategies can further be applied to decrease the model size [101], [150]. However, compared with directly designing lightweight architectures, existing model compression or quantization techniques typically introduce different levels of degradation on the model performance, and the tradeoff between the complexity and performance drop needs to be carefully considered.

Splitting a high-dimensional feature into low-dimensional sub-features has also been investigated in architectures for computer vision tasks [230], [277], [314]. GroupComm shares the same principle as those designs for exploring the nonlinear dependendies at the sub-feature level. However, those designs always concatenate the group-level sub-features back to a high-dimensional feature as the input of an upcoming module, while GroupComm assumes that a small, group-shared module is adequate to preserve the model capacity given the inter-group modeling step.

Context information is widely used as auxiliary information to assist the modeling of a center frame in a sequential input. While many existing studies use a plain concatenation of context features [76], [93], [94], [173], context codec modules have also been investigated in various studies to learn a nonlinear compact representation [71], [97], [129], [131], [245]. Specifically, the iFaSNet introduced in Chapter 3.3 applied a context codec for the multichannel separation task to learn a set of context-aware filters; however, the context codec did not decrease the sequence length T but was only used to capture context-aware information. The computational cost in iFaSNet is thus even higher than that without context codec. The main role of the context codec in the GC3 framework is to decrease the computational cost in the actual sequence modeling module by decreasing the sequence length.

4.2 GC3: Group Communication with Context Codec for Ultra-lightweight Long Sequence Modeling

Group communication (GroupComm) [288] is a module motivated by subband and multiband processing models such as frequency-LSTM (F-LSTM) [107], [168], [175], [238], which can easily change a model into an ultra-lightweight counterpart. GroupComm splits a high-dimensional feature, such as a spectrum, into groups of low-dimensional features, such as subband spectra, and uses the same model across all the groups for weight sharing. Another inter-group module is applied to capture the dependencies within the groups, so that the processing of each group always depends on the global information available. Compared with conventional F-LSTM or other similar architectures that explicitly model time and frequency dependencies where the subband features are concatenated back to the fullband feature [127], [132], [222], GroupComm does not perform such concatenation but simply applies a small module to communicate across the groups. Moreover, the low-dimensional features enable the use of a smaller module, e.g., CNN or RNN layer, than the original high-dimensional feature, and together with weight sharing the total model size can be significantly reduced. A *context codec* module is applied together with GroupComm to maintain the performance while further decrease the number of MAC operations, accelerate the training speed and alleviate the memory consumption in both training and inference time. A context codec module contains a context encoder and a context decoder, where the context encoder summarizes the temporal context of local features into a single feature representing the global characteristics of the context, and a context decoding module transforms the compressed feature back to the context features. Squeezing the input contexts into higher-level representations corresponds to a nonlinear downsampling step that can significantly decrease the length of a feature sequence. Note that compared with other architectures that perform iterative downsampling and upsampling steps [211], [305], the context codec is only applied once and all remaining modeling steps are applied on the downsampled features, which enables a smaller memory footprint and faster training speed. The combination of ***G***roup***C***omm and ***C***ontext ***C***odec is called the ***GC3*** design.

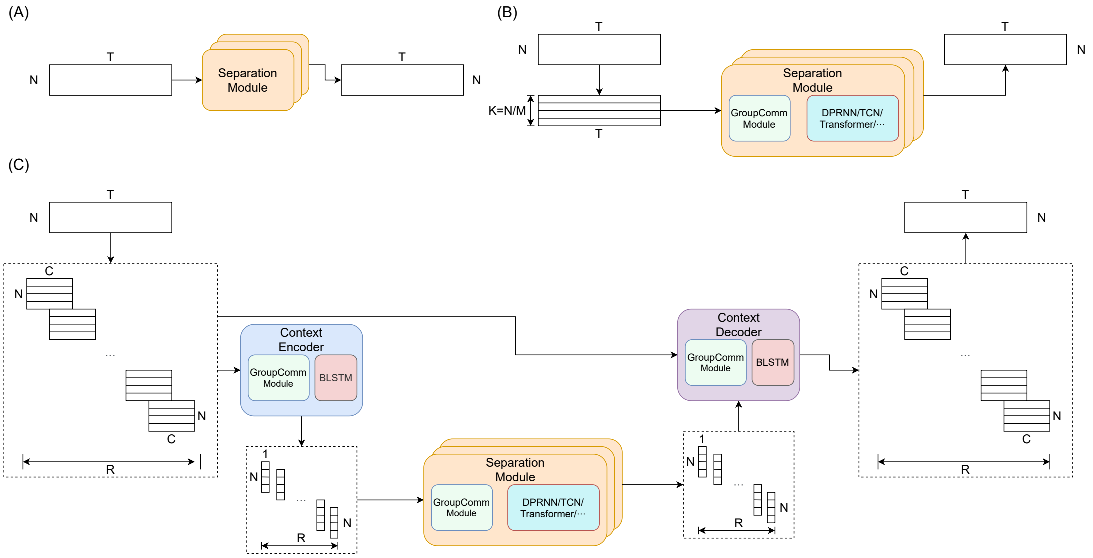

Figure 4.1: Flowcharts for (A) standard sequence processing pipeline with a large sequence modeling module; (B) GroupComm-based pipeline, where the features are split into groups with a GroupComm module for inter-group communication. A smaller module for sequence modeling is then shared by all groups; (C) GC3-based pipeline, where the sequence is first segmented into local context frames, and each context is encoded into a single feature. The sequence of summarized features is passed to a GroupComm-based module in (B). The transformed summarized features and the original local context frames are passed to a context decoding module and an overlap-add operation to generate the output with the same size as the input sequence.

4.2.1 Design of GC3 Module

Given a high-dimensional feature vector $\mathbf{h} \in \mathbb{R}^N$, $\mathbf{h}$ can be decomposed into K groups of low-dimensional feature vectors $\{\mathbf{g}^i\}_{i=1}^K$ with $\mathbf{g}^i \in \mathbb{R}^M$. $N = KM$ when there is no overlap between the groups. A group communication (GroupComm) module is applied across the group of vectors to capture the inter-group dependencies:

$$\{\hat{\mathbf{g}}^i\}_{i=1}^K = \mathcal{F}(\{\mathbf{g}^i\}_{i=1}^K) \tag{4.1}$$

where $\hat{\mathbf{g}}^i \in \mathbb{R}^P$ is the transformed feature vector for group i, and $\mathcal{F}(\cdot)$ is the mapping function defined by the module. Instead of concatenating $\{\hat{\mathbf{g}}^i\}_{i=1}^K$ back to a high-dimensional feature vector and using a large module for the processing at the next step, all $\hat{\mathbf{g}}^i$ are passed to a shared small module to save the model size and complexity. For a sequence of features $\mathbf{H} \in \mathbb{R}^{N \times T}$, it is assumed that GroupComm is applied independently at each time step. Figure 4.1 (B) presents the flowchart for the GroupComm-based pipeline. For a deep architecture for sequential modeling, a GroupComm module is added before each group-shared sequence modeling module [288].

In time-domain models such as the TasNet series introduced in Chapter 2, the length and number of the convolution kernels in the encoder play an important role in the overall performance. Table 2.4 has shown that shorter kernel length can lead to a better separation performance, and a higher overcompleteness ratio on the number of kernels can also result in a better model. Such observation makes the use of long 1-D convolution kernels less straightforward, as it may require very high-dimensional encoder outputs (i.e., large N) and further require the width of the separation module to be large to properly model them. However, shorter kernels lead to longer sequences (i.e. large T) and higher model complexity. How to decrease the sequence length while maintaining the model performance is thus an important question in such models.

A **context codec** is proposed here as a pair of encoding and decoding modules, which compress the context of feature vectors into a single summarization vector and decompress the vector back to a context, respectively. A context encoder splits $\mathbf{H}$ along the temporal dimension into blocks $\{\mathbf{D}^i\}_{i=1}^R \in \mathbb{R}^{N \times C}$, where C denotes the context size and R denotes the number of context blocks. Each $\mathbf{D}^i$ is then encoded into a single vector $\mathbf{p}^i \in \mathbb{R}^W$ by the context encoder, resulting in a sequence of vectors $\mathbf{P} \triangleq \{\mathbf{p}^i\}_{i=1}^R \in \mathbb{R}^{W \times R}$ with $R \ll T$. Any separation module can then be applied to $\mathbf{P}$ instead of $\mathbf{H}$ to save the computational cost. The transformed sequence of features are denoted as $\hat{\mathbf{P}} \in \mathbb{R}^{W \times R}$, and a context decoding module adds $\hat{\mathbf{p}}^i$ to each time step in $\mathbf{D}^i$ and applies a nonlinear transformation to generate $\hat{\mathbf{D}}^i \in \mathbb{R}^{N \times C}$ for context i. Overlap-add is then applied on $\{\hat{\mathbf{D}}^i\}_{i=1}^R$ to form the sequence of features $\hat{\mathbf{H}} \in \mathbb{R}^{N \times T}$ of the original length.

A deep residual BLSTM network is selected for both the context encoder and decoder in the configuration. The deep residual BLSTM networks contained stacked BLSTM layers, where each BLSTM layer contains a linear projected layer connected to its output to match the input and output feature dimensions. A layer normalization (LayerNorm) operator [114] is added to the transformed output, a residual connection is added between the input to the BLSTM layer and the LayerNorm-normalized output, and the feature is then served as the input for the next layer. In the context encoder, a context block $\mathbf{D}^i$ is passed to the GroupComm-equipped deep residual BLSTM network to generate a transformed sequence of features $\mathbf{Q}^i \in \mathbb{R}^{N\times C}$, and a mean-pooling operation is applied on $\mathbf{Q}^i$ across the temporal dimension to obtain $\mathbf{p}^i$. In the context decoder, $\hat{\mathbf{p}}^i$ is added to each time step in $\mathbf{D}^i$ and passed to the GroupComm-equipped deep residual BLSTM network to generate the final output $\hat{\mathbf{D}}^i$. To save the computational cost in the context codec, GroupComm is also applied to the deep residual BLSTM networks. This combination of GroupComm and context codec gives the **GC3** design, and Figure 4.1 (C) provides the flowchart for the GC3-equipped separation pipeline. Note that there is no guarantee that the context encoding and decoding modules are reconstructing the original input features as a "codec" typically does, and here, the name of codec is borrowed simply to represent the encoding and decoding properties of the two modules.

For configurations where a 50% overlap is applied between context blocks, it is easy to find that $R = 2T/C$. In network architectures where a deep module is applied for the sequence modeling part, the computational cost is $C/2$ times smaller than using the original sequence features for modeling. To save overall model complexity, C needs to be properly adjusted to balance performance and complexity, and the model architecture for the context codec needs to be properly designed so that the computational cost for encoding and decoding introduced to the entire system is not too large. Applying GroupComm to the context codec modules can achieve this goal, and such a combination is referred to as the *GC3* design. Figure 4.1 (C) provides the flowchart for the GC3-based pipeline. Similarly, a GroupComm module is added before each layer in the context codec. Note that there is no guarantee that the context encoding and decoding modules are reconstructing the original input features as a "codec" typically does, and here, the name of codec is borrowed simply to represent the encoding and decoding properties of the two modules.

4.2.2 Experiment Configurations and Results

GC3 is evaluated on the same single-channel separation task with the identical dataset described in Chapter 3.2.2. The TasNet framework is used as the backbone network design for all experiments. All models use 2 ms window size in the waveform encoder and decoder and ReLU nonlinearity as the activation function for the mask estimation layer. For GroupComm-based and GC3-based models, a GroupComm module is added before each layer in the separator, and the width of the layers is modified according to the number of groups K. The mask estimation layer in GroupComm-based and GC3-based models is shared by all the groups. The number of groups in the context codec is also set to be the same as that in the separator blocks. The notations for the hyperparameters can be found in table 4.1. The implementation of all models is available online[1].

Three model architectures are compared for the GroupComm module:

1. *BLSTM*: A standard residual BLSTM layer is applied to all the groups to model the intra-group dependencies.

2. *Transform-average-concatenate (TAC)* [286]: TAC was proposed for the multichannel speech separation task with ad-hoc microphone arrays where no microphone indexing or geometry information is known in advance. The design particularly matches the need in the GroupComm module where "group indices", i.e., the sequential order of the features in different groups, does not exist. For the group of features $\{\mathbf{g}^i\}_{i=1}^K$, a fully-connected (FC) layer with parametric rectified linear unit (PReLU) activation [99] is applied for the transformation step:

$$\mathbf{f}^i = P(\mathbf{g}^i) \tag{4.2}$$

   where $P(\cdot)$ is the mapping function defined by the first FC layer and $\mathbf{f}^i \in \mathbb{R}^D$ denotes the output for group i. All $\mathbf{f}^i$ are then averaged and passed to the second FC layer with PReLU

[1] `https://github.com/yluo42/GC3`

activation for the averaging step:

$$\hat{\mathbf{f}} = R(\frac{1}{K}\sum_{i=1}^{K}\mathbf{f}^i) \tag{4.3}$$

where $R(\cdot)$ is the mapping function defined by the second FC layer and $\hat{\mathbf{f}} \in \mathbb{R}^D$ is the output for this step. $\hat{\mathbf{f}}$ is finally concatenated with the output of the transformation step, $\mathbf{f}^i$, and passed to a third FC layer with PReLU activation to generate the final output $\hat{\mathbf{g}}^i$:

$$\hat{\mathbf{g}}^i = S([\mathbf{f}^i; \hat{\mathbf{f}}]) \tag{4.4}$$

where $S(\cdot)$ is the mapping function defined by the third FC layer and $[\mathbf{x}; \mathbf{y}]$ denotes the concatenation operation of vectors $\mathbf{x}$ and $\mathbf{y}$. A residual connection is finally added between the module input $\mathbf{g}^i$ and output $\hat{\mathbf{g}}^i$.

3. *Multi-head Self Attention (MHSA)* [166]: MHSA is widely used in various sequence modeling tasks and has already proven its effectiveness in multiple speech-related problems [166], [184], [233], [237], [252]. MHSA explicitly models the relationship between each pair of group features and thus can capture sequence-level dependencies. Following the standard definition of MHSA, the concatenation of group features $\{\mathbf{g}^i\}_{i=1}^K$ is rewritten into a matrix $\mathbf{G} \in \mathbb{R}^{K\times M}$ and apply a MHSA layer:

$$\mathrm{H}_n = \text{Softmax}(\frac{\mathbf{Q}_n\mathbf{K}_n^T}{\sqrt{d_k}})\mathbf{V}_n \tag{4.5}$$

$$\mathbf{G}'_n = [\mathrm{H}_1; \cdots; \mathrm{H}_n]\mathbf{W}^o \tag{4.6}$$

where n is the number of attention heads, $\mathbf{W}_n^q, \mathbf{W}_n^k, \mathbf{W}_n^v \in \mathbb{R}^{M\times d_k}$ are the linear transformation matrices for head n, $\mathbf{Q}_n = \mathbf{G}\mathbf{W}_n^q$, $\mathbf{K}_n = \mathbf{G}\mathbf{W}_n^k$, and $\mathbf{V}_n = \mathbf{G}\mathbf{W}_n^v$ are the linear transformations for query, key and value, respectively, $\mathrm{H}_n \in \mathbb{R}^{K\times d_k}$ is the output at head n, and $\mathbf{W}^o$ is the linear transformation matrix for the output. Both the concatenation operation and the Softmax nonlinearity are applied across the attention heads. $\mathbf{G}'$ is then passed to an FC layer with PReLU activation for further transformation, and another FC layer follows to generate the final output with the same shape as input $\mathbf{G}'' \in \mathbb{R}^{K\times M}$.

Four model architectures are also compared for the separator:

1. *Dual-path RNN (DPRNN)* [287]: The same DPRNN architeture introduced in Chapter 2.3 is directly applied.

2. *Temporal convolutional network (TCN)* [243]: The same TCN architeture introduced in Chapter 2.2 is directly applied.

3. *Sudo rm -rf* [305]: Sudo rm -rf proposed a U-net style convolutional block where multiple levels of downsampling and upsampling layers were applied to extract features at different scales. Each downsampling layer contained a depthwise separation convolution operation similar to Conv-TasNet, and each upsampling layer contained a bilinear interpolation operation.

4. *Dual-path Transformer (DPTNet)* [265]: DPTNet replaced the BLSTM layers in DPRNN with modified Transformer layers [166], where the fully connected layer in the default transformer encoder layer [166] was replaced by an LSTM layer to learn the positional information in the sequence.

Table 4.1: Hyperparameters and their notations in GC3-related architectures.

Hyperparameter	Notation
Number of groups	K
Group size	M
Number of encoder filters	N
LSTM input / hidden dimensions	H_i/H_o
Number of DPRNN blocks	L_s
Number of context codec layers	L_c
Context size (in frames)	C
DPRNN block size (in frames)	B

Table 4.2 presents the experimental results on the baseline DPRNN, GroupComm-DPRNN and GC3-DPRNN models. The separation performance and the corresponding model size and

Table 4.2: Comparison of DPRNN, GroupComm-DPRNN and GC3-DPRNN TasNet models with different hyperparameter configurations. MACs are calculated on 4-second mixtures.

Model	K	M	N	H_i / H_o	L_s	L_c	C	B	SI-SDR (dB)	Model size	MACs
DPRNN	1	128	128	64 / 128	6	–	–	100	9.0	2.6M	22.1G
GroupComm-DPRNN	2	64	128	64 / 128	4	–	–	100	9.5	2.6M (99.4%)	43.4G (196.4%)
	4	32	128	32 / 64	4				9.4	663.0K (25.3%)	22.4G (101.4%)
	8	16	128	16 / 32	4				8.9	175.5K (6.7%)	11.9G (53.8%)
	16	8	128	8 / 16	4				8.1	51.9K (2.0%)	6.6G (29.9%)
					6				**8.9**	**73.5K (2.8%)**	**9.6G (43.4%)**
		16	256	16 / 32	2				8.1	100.7K (3.8%)	12.4G (56.1%)
					4				9.7	183.9K (7.0%)	23.7G (107.2%)
	32	4	128	4 / 8	6				7.6	26.0K (1.0%)	5.7G (25.8%)
					10				**8.5**	**37.6K (1.4%)**	**9.1G (41.2%)**
		8	256	8 / 16	2				7.9	38.7K (1.5%)	7.2G (32.6%)
					4				8.6	60.3K (2.3%)	13.2G (59.7%)
GC3-DPRNN	4	32	128	32 / 64	4	1	32	24	8.9	881.5K (33.7%)	9.2G (41.6%)
							16	32	8.8		10.6G (48.0%)
							8	50	8.8		13.3G (60.2%)
							4	64	9.3		18.6G (84.2%)
	8	16	128	16 / 32	6	1	32	24	8.7	314.4K (12.0%)	5.4G (24.4%)
						2			9.3	369.9K (14.1%)	8.1G (36.7%)
	16	8	128	8 / 16	8	2			**8.9**	**124.1K (4.7%)**	**5.4G (24.4%)**
		16	256	16 / 32	6	1			9.0	322.9K (12.3%)	10.9G (49.3%)
	32	4	128	4 / 8	14	2			**8.3**	**57.1K (2.2%)**	**3.6G (16.3%)**
		8	256	8 / 16	8				9.2	132.6K (5.1%)	10.7G (48.4%)

complexity for the three types of models are reported. Model complexity is measured by the number of MAC operations (MACs), and the MACs for all models are calculated by an open-source toolbox[2]. First notice that when K is small (e.g. $K \leq 4$), the GroupComm-DPRNN models can achieve higher performance than plain DPRNN with smaller model size at the cost of an on par or higher model complexity. This is due to the extra MAC operations introduced by the GroupComm module. A larger K leads to fewer MAC operations; however, the depth of the model has to be modified accordingly to maintain the performance. Different hyperparameter settings are explored such that for each K a model with less than 5% relative performance degradation can be obtained. Among all the GroupComm-DPRNN models, the model with $K = 16$, $N = 128$ and $L_s = 6$ achieves on par performance as the standard DPRNN model with 2.8% model size and 43.4% MAC operations, and the model with $K = 32$, $N = 128$ and $L_s = 10$ only has 5% performance degradation with 1.4% model size and 41.2% MAC operations. These models show that GroupComm is effective in decreasing both the model size and complexity without sacrificing the performance. Moreover, experiments on the effect of model width in terms of N and H_i/H_o

[2] `https://github.com/Lyken17/pytorch-OpCounter`

Table 4.3: Comparison of GC3-DPRNN models with different model architectures for GroupComm.

GroupComm module	K	SI-SDR (dB)	Model size	MACs
BLSTM	16	8.9	124.1K	5.4G (24.4%)
	32	8.3	57.1K	3.6G (16.3%)
TAC	16	**9.1**	**123.8K**	**3.9G (17.6%)**
	32	**8.6**	**56.3K**	**2.6G (11.8%)**
SA	16	8.9	123.7K	4.5G (20.3%)
	32	8.2	56.5K	3.0G (13.4%)

are conducted, and it can be observed that increasing model width can significantly improve the performance with a much shallower architecture; however, the model complexity can be relatively high. For example, a performance improvement of 0.7 dB can be achieved by $K = 16$, $N = 256$ and $L_s = 4$, while its number of MAC operations is even higher than the baseline DPRNN. This indicates that when the computational cost is not a bottleneck, GroupComm can also be applied to improve the overall performance.

For the GC3-based models, the balance between model complexity and performance with different context sizes C is investigated first. A larger C leads to fewer frames for the sequence modeling module, and a smaller DPRNN block size B can be applied to save model complexity. It can be observed that models with $C = 32, 16$ and 8 have almost the same performance while differing greatly in complexity; hence, $C = 32$ is selected for all other experiments. For $K = 8$, it can be seen that increasing the number of context codec layers can improve the separation performance, implying that a strong context codec is important. The on par performance can be achieved by $K = 16$, $N = 128$, $L_s = 8$ and $L_c = 2$ with a 4.7% model size and 24.4% MAC operations, which saves 19% more MAC operations compared with the GroupComm-only model. The GC3-based model with 5% performance degradation has the configuration of $K = 32$, $N = 128$, $L_s = 14$ and $L_c = 2$, which saves 25% more MAC operations than the GroupComm-only model. Such results prove that GC3-based models are more effective than GroupComm-only models thanks to the context compression operation. Similarly, increasing the model width can also lead to better overall performance with a shallower architecture at the cost of complexity, and in such configurations it is empirically better to keep the depth of the context codec according to the results for $K = 16$.

Table 4.3 evaluates the effect of the three model architectures for GroupComm described in

Table 4.4: Effect of group overlap ratio on model complexity and separation performance in GC3-DPRNN models.

Group overlap	SI-SDR (dB)	Model size	MACs
0%	9.1	123.8K	3.9G (17.6%)
25%	9.0		4.9G (22.0%)
50%	9.4		6.9G (31.3%)

Chapter 4.2.1. For the TAC architecture, the hidden dimension for *transform* and *average* layers is set to $3H_o$. For the MHSA architecture, four attention heads with the hidden dimension d_k set to M are applied. Such configurations are applied to match the overall model sizes with a BLSTM layer. The hyperparameter configurations of the two GC3-based models marked in bold in table 4.2 with $K = 16$ and 32 are selected. The results show that although MHSA achieves on par performance as BLSTM in both configurations, TAC obtains even better performance with the fewest MAC operations. Since the number of MAC operations in TAC is fewer than those in both BLSTM and MHSA and the transformation and concatenation steps in TAC can be run in parallel across groups, TAC is used as the default module for GroupComm in all remaining experiments.

The default group segmentation configuration in all experiments above assumes no overlap between groups. However, a 50% overlap is always applied in sequence segmentation operations such as context segmentation in the context codec and block segmentation in DPRNN modules. It is thus interesting to see whether adding overlap between groups can improve the performance. Table 4.4 provides the separation performance as well as the model size and complexity for different overlap ratios between groups. It can be observed that adding a 25% percent overlap between groups increases the number of MAC operations while not leading to an better performance, but a 50% overlap between groups can improve the overall performance. Compared with the model in table 4.2 with a similar performance ($K = 8$, $N = 128$, $L_c = 2$), such a model has a smaller model size and fewer MAC operations. This shows that compared with using a smaller number of groups K, adding proper overlap between groups is a more effective method for improving the performance.

To evaluate GC3 on the four model architectures for the separator, the hyperparameters are selected so that all four models have on-par model size when no GroupComm or context codec are

Table 4.5: Comparison of DPRNN, TCN, Sudo rm -rf, and DPTNet architectures with and without GC3. The training and inference phase statistics are evaluated with a batch size of 4.

Model	SI-SDR (dB)	PESQ	STOI	Model size	MACs	Training memory (GB)	Training speed (ms)	Inference memory (GB)	Inference speed (ms)
Mixture	-0.4	1.91	0.77	–	–	–	–	–	–
DPRNN [287]	9.0	2.33	0.80	2.6M	22.1G	**3.0**	**193.4**	24.9	59.7
+ GC3	**9.1**	**2.36**	**0.82**	**123.8K (4.7%)**	**3.9G (17.6%)**	4.2	211.3	**6.3**	**57.2**
TCN [243]	7.1	2.21	0.80	2.5M	10.3G	**3.2**	254.6	14.4	53.8
+ GC3	**8.9**	**2.35**	**0.82**	**191.2K (7.6%)**	**3.4G (33.0%)**	3.8	**194.1**	**6.6**	**49.3**
Sudo rm -rf [305]	6.8	2.15	0.79	2.4M	9.5G	4.6	234.8	14.4	53.5
+ GC3	**8.7**	**2.34**	**0.81**	**60.0K (2.5%)**	**3.2G (33.7%)**	**3.7**	**200.3**	**5.3**	**47.4**
DPTNet [265]	8.1	2.20	0.79	2.8M	21.8G	**4.8**	**256.2**	21.2	78.6
+ GC3	**8.5**	**2.32**	**0.81**	**128.6K (4.6%)**	**3.9G (17.9%)**	**4.8**	272.5	**6.2**	**76.7**

applied:

1. *TCN*: TCNs with 6 convolutional blocks were selected in each TCN. The same number of TCN layers and convolutional blocks is applied for the GC3-equipped modification.

2. *Sudo rm -rf*: The default configuration of the original literature is selected, which contains 5 downsampling and upsampling layers in each U-net block. 8 blocks are used for both baseline and GC3-equipped modification.

3. *DPTNet*: The default configuration of the original literature is selected, which contains 6 Transformer layers. 8 Transformer layers is selected for the GC3-equipped DPTNet, which is similar to the configuration for GC3-DPRNN. The learning rate warm-up configuration is also set the same as the recommended configuration, where the first 4000 iterations are used for the warm-up stage.

The other hyperparameters are kept the same as the selected best GC3-DPRNN model in Table 4.3. Table 4.5 presents the separation performance as well as the model size and complexity of the four architectures with their GC3-equipped modifications. First, the plain DPRNN architecture achieves the best performance among the four architectures and is even better than the plain DPTNet, which indicates that transformer-based architectures might not be always superior than recurrent neural networks. TCN does not have satisfying performance because of the limited receptive field in the configuration (253 frames or 0.253s), as it has been shown that large receptive fields for TCN lead to better separation performance [243]. Although the selected Sudo rm

-rf configuration has a large enough receptive field to cover the entire sequential feature, it obtains an even worse separation performance with on-par model size and complexity as the TCN architecture. Although [305] reported that the Sudo rm -rf architecture achieved constantly better performance than DPRNN and TCN architectures, the results here indicates that its performance on the more challenging noisy reverberant environments needs to be revised. Moreover, although all four architectures achieve significant SI-SDR improvement with respect to the unprocessed mixture, the improvement on wideband PESQ and STOI scores are moderate. One possible reason for this phenomenon is the inconsistency between the time-domain and frequency-domain evaluation metrics [243], as all the models are trained with the time-domain objective (negative SNR) while the calculation of PESQ and STOI are both in frequency domain.

For DPRNN and DPTNet, GC3-equipped modifications can achieve a same level of separation performance with significantly smaller model sizes and number of MAC operations. For CNN-based architectures (TCN and Sudo rm -rf), GC3-equipped modifications can further achieve significantly higher SI-SDR scores. Since the context codec squeezes the long sequence by a factor of $C/2$ (16 for $C = 32$), the effective temporal receptive field of the TCN separator is significantly larger ($0.253 \times 16 = 4.05$s) and thus can better capture the temporal dependencies. Since it has also been reported in [305] that a deeper Sudo rm -rf architecture can lead to better overall separation performance, introducing GC3 to Sudo rm -rf might also be equivalent to increasing the model depth and improves the performance. More in-depth analysis on the reason behind the performance improvements in different architectures is left for future work. Nevertheless, the results prove that GC3 can be easily deployed in to various architectures and maintain its effectiveness.

Beyond the model size and number of MAC operations, the memory footprint and the training and inference speed are also important indicators for model complexity, as small models can also be slow and require enormous memory. To compare such training and inference phase statistics of different models, the batch-level training and inference phase memory footprints and running speeds are evaluated on a single NVIDIA TITAN X Pascal graphic card with a batch size of 4.

The memory footprint is calculated via an opensource toolbox [3]. It can be observed that the GC3-equipped models, e.g. DPRNN and TCN, increase the training phase memory footprint but do not affect the training speed, and an acceleration can even be observed in the GC3-equipped TCN model. The inference phase memory footprint for all four architectures with GC3 applied are significantly lower than the ones without GC3, however the inference speed are all on-par or only slightly faster than the baselines. The reason for this might be because the effective model depth for a GC3-equipped model is larger than the baseline which prevents the model from easy parallelization. The results show that although the number of intermediate outputs introduced by the deeper separation module and the GroupComm modules may increase the training phase memory footprint, GC3 can always decrease the inference phase memory footprint without sacrificing the inference speed.

4.3 Discussions

Note that the application of model binarization or quantization techniques are not jointly considered with GC3. Such techniques can significantly decrease the model storage size and MAC operations without changing the model architecture, although they typically lead to certain levels of performance degradation [250]. Applying GC3 together with such techniques may require an increase in the overall model size to achieve on par performance, and the actual model configuration may be directly related to the target platform to which the model will be deployed. Moreover, the GroupComm module can be used as a prototype module in any neural architecture search (NAS) algorithm [197] to search for better both model architecture and layer organization, balancing the model size, complexity and performance.

[3] https://github.com/Stonesjtu/pytorch_memlab

Chapter 5: Training Objectives for Speech Separation

In this chapter I will introduce two training objectives for speech separation in different conditions. Both objectives rely on *auxiliary autoencoding*, which adds an autoencoding loss to the standard training objectives, e.g., SNR and SI-SDR, to tackle certain problems in speech separation. The *auxiliary autoencoding permutation invariant training (A2PIT)* [290] was proposed for separating varying numbers of sources in the mixtures with a single network, which was based on a design principle called *do nothing is better than do wrong things*. The *auxiliary autoencoding training (A2T)* [324] was designed for improving the system robustness in reverberant environments, which put constraints on the search space of the network during optimization to find better separation results.

5.1 Related works

5.1.1 Training Methods for Separating Varying Numbers of Sources

Various methods have been proposed to tackle the problem of separating varying numbers of sources in an end-to-end model. A most simple way is to assume a maximum number of sources in a mixture, which is denoted by N, and let the model to always generate N outputs [148], [239]. For mixtures having M sources where $M < N$, $N - M$ outputs are invalid and need to be properly designed and effectively detected. The invalid outputs are typically forced to have a significantly smaller energy than the valid outputs, and a energy threshold can then be applied to filter out those outputs. Another approach first estimates the speaker embedding for each active source with an output-length-free model, e.g. a sequence-to-sequence generative model, and then performs speaker extraction based on the embeddings [249]. A third category of methods perform separation in an iterative way, where in each iteration only one target source is separated from the residual mixture [193], [210], [247], [251]. The iteration stops when there is no source left, and the stop time can be determined by either an energy threshold or another trained discriminator. It has been shown that under various circumstances, the number of sources in the mixture can be effectively estimated and the separation performance can be guaranteed. Moreover, clustering-based approaches have been extensively applied in frequency-domain separation systems, where the T-F masks are treated as the cluster assignment matrices and the number of clusters can be dynamically decided for different mixtures [121], [123], [140], [151], [218], [242].

5.1.2 Training Methods for Separation in Reverberant Environments

Both end-to-end systems and T-F domain systems for anechoic speech enhancement and separation can be directly applied in the reverberant scenarios [268]. For systems that do not attempt to perform joint enhancement/separation and dereverberation, a mapping function is typically learned between the reverberant mixture and the reverberant clean signals with either single-channel or multi-channel input [231], [241], [273], [286]. The evaluation of such systems is also done by comparing the system outputs with the reverberant clean signals. One exception is the *convolutive transfer function invariant signal-to-distortion ratio (CI-SDR)* [263], which is essentially the standard SDR metric, where the adaptive FIR filter is applied to the separation outputs before the calculation of the SI-SDR metric. Experiment results in a multi-channel separation task with MVDR beamforming showed that CI-SDR is beneficial for both signal quality measured in SDR and speech recognition measured in WER.

5.2 A2PIT: Separating Varying Numbers of Sources

There are various drawbacks in each category of the existing methods. For the fixed-output-number method, the training targets for the invalid outputs are typically low- or zero-energy signals. However, such targets cannot be jointly used with energy-invariant training objectives, such as scale-invariant signal-to-distortion ratio (SI-SDR) [236], which has proven to be a better training objective in many scenarios [284]. Moreover, the detection of invalid outputs typically relies on a pre-defined energy threshold, which may cause trouble when the mixture also has very low energy. For the speaker extraction method, the speaker embeddings are typically estimated at utterance level and require a long enough context, which makes the method hard to apply to online or causal systems. For methods that utilize additional target speaker enrollments for speaker embedding extraction, the generalization ability on unseen speakers is also limited. For the iterative method, the run-time complexity linearly increases as the number of sources increases, and stop time detection is typically performed at utterance level as well. When there is noise in the mixture, it is also unclear in which iteration should the noise be cancelled. Moreover, none of the methods has a "fault tolerance" mechanism when the estimated number of sources is different than the actual number. What should the model append to the output if it estimates fewer sources than the actual case? How should the model remove invalid outputs if it generates more? How can such decision process or control flow be effectively incorporated into the training of the model? These questions are important for a practical and robust system.

A simple training method based on the fixed-output assumption is proposed here by designing proper training targets for the invalid outputs. The fixed-output-number assumption is adopted as in real-world conversations such as meeting scenarios, the maximum number of simultaneously active speakers is almost always fewer than three [30], [259], thus a maximum number of speakers can typically be pre-assumed. Instead of using low-energy auxiliary targets for invalid outputs, the mixture itself is used as auxiliary targets to force the invalid outputs to perform autoencoding. With the permutation invariant training (PIT) framework [173] for speech separation, the training objective is referred to it as the auxiliary autoencoding permutation invariant training (A2PIT). A2PIT not only allows the model to perform valid output detection in a self-supervised way without additional modules, but also achieves "fault tolerance" by the *"do nothing is better than do wrong things"* principle. As the mixture itself can be treated as the output of a null separation model, i.e. perform no separation at all, the auxiliary targets force the model to generate outputs not worse than doing nothing. Moreover, the detection of invalid outputs in A2PIT can be done at frame-level based on the similarity between the outputs and the mixture, which makes it possible to perform single-pass separation and valid source detection in real-time.

5.2.1 Motivation and Design

There are two main issues in the energy-based method for invalid output detection. First, it cannot be jointly used with energy-invariant objective functions like SI-SDR. Second, once the detection of invalid speakers fails and the noise signals are selected as the targets, the outputs can be completely uncorrelated with any of the targets, which is unpreferred for applications that require high perceptual quality or low distortion. It is defined as the problem of lacking "fault tolerance" mechanism for unsuccessful separation.

To allow the models to use any objective functions and to have such "fault tolerance" ability, the mixture signal itself is selected as the auxiliary targets instead of random noise signals. For mixtures with N outputs and $M < N$ targets, $N - M$ mixture signals are appended to the targets and PIT is applied to find the best output permutation with respect to the targets. The A2PIT loss with the best permutation then becomes:

$$\mathcal{L}_{obj} = \mathcal{L}_{sep} + \mathcal{L}_{AE} \tag{5.1}$$

where $\mathcal{L}_{sep} \in \mathbb{R}$ is the loss for the valid outputs and $\mathcal{L}_{AE} \in \mathbb{R}$ is the auxiliary autoencoding loss for the invalid outputs with the input mixture as targets. As autoencoding is in general a much simpler task than separation, proper gradient balancing method should be applied on the two loss terms for successful training. Recall that SI-SDR is defined as:

$$\text{SI-SDR}(\mathbf{x}, \hat{\mathbf{x}}) = 10 \log_{10} \frac{||\alpha \mathbf{x}||_2^2}{||\hat{\mathbf{x}} - \alpha \mathbf{x}||_2^2} \tag{5.2}$$

where $\alpha = \hat{\mathbf{x}}\mathbf{x}^\top / \mathbf{x}\mathbf{x}^\top$ corresponds to the optimal rescaling factor towards the estimated signal. Let

$a \triangleq \mathbf{x}\mathbf{x}^\top$, $b \triangleq \hat{\mathbf{x}}\mathbf{x}^\top$ and $c \triangleq \hat{\mathbf{x}}\hat{\mathbf{x}}^\top$, the definition can be rewritten as:

$$\begin{aligned} \text{SI-SDR}(\mathbf{x}, \hat{\mathbf{x}}) &= 10 \log_{10} \left(\frac{b^2/a}{c - 2b^2/a + b^2/a} \right) \\ &= 10 \log_{10} \left(\frac{1}{ac/b^2 - 1} \right) \\ &\triangleq 10 \log_{10} \left(\frac{c(\mathbf{x}, \hat{\mathbf{x}})^2}{1 - c(\mathbf{x}, \hat{\mathbf{x}})^2} \right) \end{aligned} \tag{5.3}$$

where $c(\mathbf{x}, \hat{\mathbf{x}}) \triangleq b/\sqrt{ac} = \hat{\mathbf{x}}\mathbf{x}^\top/\sqrt{(\mathbf{x}\mathbf{x}^\top)(\hat{\mathbf{x}}\hat{\mathbf{x}}^\top)}$ is the cosine similarity between $\mathbf{x}$ and $\hat{\mathbf{x}}$. The scale-invariance behavior of SI-SDR can be easily observed by the nature of cosine similarity, and $\text{SI-SDR}(\mathbf{x}, \hat{\mathbf{x}}) \to +\infty$ as $|c(\mathbf{x}, \hat{\mathbf{x}})| \to 1$. It's easy to see that the second term in the derivative of SI-SDR with respect to the cosine similarity, $|\partial\, \text{SI-SDR}(\mathbf{x}, \hat{\mathbf{x}})/\partial\, c(\mathbf{x}, \hat{\mathbf{x}})|$, approaches infinity as $|c(\mathbf{x}, \hat{\mathbf{x}})|$ approaches 1. Using it for $\mathcal{L}_{AE}$ may let the system to easily collapse to a local minimum which have very high performance on the auxiliary autoencoding term while fail to separate the sources. Based on this concern, an α-skewed SI-SDR (α-SI-SDR) is proposed here:

$$\alpha\text{-SI-SDR}(\mathbf{x}, \hat{\mathbf{x}}) \triangleq 10 \log_{10} \left(\frac{c(\mathbf{x}, \hat{\mathbf{x}})^2}{1 + \alpha - c(\mathbf{x}, \hat{\mathbf{x}})^2} \right) \tag{5.4}$$

where the scale of the gradient with respect to the cosine similarity term is controlled by $\alpha \geq 0$, and $\alpha = 0$ corresponds to the standard SI-SDR. For multiple-speaker utterances, $\alpha = 0.3$ is empirically set for $\mathcal{L}_{AE}$ and $\alpha = 0$ is set for $\mathcal{L}_{sep}$. For single-speaker utterances, the training target for separation is equivalent (when there is no noise) or very close (when there is noise) to the input mixture. In this case, $\alpha = 0.3$ is also set for $\mathcal{L}_{sep}$.

5.2.2 Detection of Invalid Outputs

During inference phase, the detection of invalid outputs can be performed by calculating the similarity, e.g. SI-SDR score, between all outputs and the input mixture, and a threshold calculated from the training set can be used for the decision. For the "fault tolerance" mechanism, the following method is applied for selecting the valid outputs:

1. If the estimated number of outputs K is smaller than the actual number M, $M-K$ additional outputs are randomly selected from the $N-K$ remaining outputs.

2. If the estimated number of outputs K is larger than the actual number M, M outputs are randomly selected from the K outputs.

Another benefit for A2PIT is that it also allows frame-level detection of the invalid outputs for causal applications. Frame-level detection calculates accumulated similarity starting from the first frame of the outputs, and is able to dynamically change the selected valid outputs as the similarity scores become more reliable. For streaming-based applications that require a real-time playback of the separation outputs, e.g. hearable devices, the change of the output tracks can also be easily done by switching the outputs at frame-level.

5.2.3 Experiment Configurations and Results

A simulated single-channel noisy speech separation dataset with the Librispeech dataset [109] is used for the experiments. 40 hours of training data, 20 hours of validation data, and 12 hours of test data are generated from the 100-hour training set, development set, and test set, respectively. The number of speakers are evenly sampled between 1 and 4 to make sure the dataset is balanced to the varying numbers of speakers. All utterances are 6-second long with a sample rate of 16k Hz. For utterances with more than one speaker, an overlap ratio between all the speakers is uniformly sampled between 0% and 100% and the speech signals are shifted accordingly. The speech signals are then rescaled to a random absolute energy between -2.5 and 2.5 dB. A noise signal is randomly selected from the 100 Nonspeech Corpus [334], and is repeated if its length is less than 6 seconds. The noise signal is then rescaled to a random absolute energy between -20 and -10 dB. Both the clean and noisy mixtures are used to report the performance of A2PIT in the two scenarios.

The DPRNN-TasNet introduced in Chapter 2.3 is used for all experiments. The same hyper-parameter settings of 2 ms window configuration is applied with the only difference that 3 instead of 6 DPRNN blocks is applied. The total number of parameters is thus 1.3M. The baseline model uses the standard SI-SDR as the training objective, and all other models use the proposed A2PIT together with α-SI-SDR. All models are trained for a maximum of 100 epochs with the Adam optimizer [83]. The initial learning rate is $1e-3$ and is decayed by a factor of 0.98 for every two epochs. No other regularizers or training tricks are applied. The DPRNN-TasNet models trained for each of the speaker count configurations are used as the baseline models, and these results represents how well the models can achieve when the number of speakers is known and a specific model is trained on such mixtures. For separating varying numbers of sources, the DPRNN-TasNet models are trained on three configurations:

1. 2+3 speakers: the 2 and 3 speaker mixtures are used for both training and evaluation, and the number of outputs N is set to 3. This is to mimic the behavior under certain cases when the maximum number of active sources is bounded by 3 (e.g. meeting scenarios). It is denoted as the *2+3 model*.

2. 2+3+4 speakers: the 2, 3 and 4 speaker mixtures are used for both training and evaluation, and the number of outputs N is set to 4. This is to increase the difficulty of both the separation and speaker count. It is denoted as the *2+3+4 model*.

3. 1+2+3+4 speakers: all training and evaluation datasets are used. It is denoted as the *1+2+3+4 model*.

Each configuration contains both the clean and noisy scenarios, which results in a total of 6 different configurations.

Table 5.1 and 5.2 show the confusion matrices for all 6 configurations. Note that each of the speaker number has a test set of 1800 utterances. First notice that for the *2+3 model*, the prediction of speaker count can be done with a very high accuracy in both clean and noisy separation tasks. For the *2+3+4 model*, the detection of 3 speaker mixtures is worse than that of both 2 and 4 speaker mixtures, and the error mostly comes from the misclassification into 4 speaker mixtures. For the *1+2+3+4 model*, the detection of the 1 speaker mixtures almost always fail (detects no speakers in the mixture). With the autoencoding threshold, the model predicts no valid outputs for most of the times. This is somehow expected as in the clean separation task, the mixture itself is

Table 5.1: Confusion matrix for speaker counting for models trained for clean separation task.

Model	Prediction	Oracle			
		1 spk	2 spk	3 spk	4 spk
2+3 model	2 spk	–	1712	5	–
	3 spk	–	88	1795	–
2+3+4 model	2 spk	–	1718	10	0
	3 spk	–	82	1435	26
	4 spk	–	0	355	1774
1+2+3+4 model	1 spk	2	0	0	0
	2 spk	5	1746	13	2
	3 spk	0	62	1454	44
	4 spk	0	0	333	1756

Table 5.2: Confusion matrix for speaker counting for models trained for noisy separation task.

Model	Prediction	Oracle			
		1 spk	2 spk	3 spk	4 spk
2+3 model	2 spk	–	1716	26	–
	3 spk	–	83	1774	–
2+3+4 model	2 spk	–	1711	16	0
	3 spk	–	87	1530	87
	4 spk	–	1	254	1713
1+2+3+4 model	1 spk	31	4	0	0
	2 spk	5	1670	8	0
	3 spk	0	125	1485	27
	4 spk	0	0	307	1773

equivalent to the separated output, and in the noisy separation task, the separated output may still have very high similarity score with respect to the mixture because of the high SNR configuration. For tasks such as automatic speech recognition, this will not be an issue as the acoustic models are typically noise robust, while for tasks that require perceptual quality, the outputs need to be further evaluated. Beyond the 1 speaker mixtures, the accuracy for speaker counting for other cases remains high. Another interesting observation is that the models occasionally predict zero speakers (e.g. 2-speaker utterances in all models for noisy separation). This can only happen when the autoencoding SI-SDR of all outputs are larger than the pre-defined threshold. It indicates that in certain utterances the separation may completely fail and the model converges to always perform autoencoding. A better solution to this issue is left for future works.

Figure 5.1: Histograms of autoencoding SI-SDR (decibel scale) in different experiment configurations.

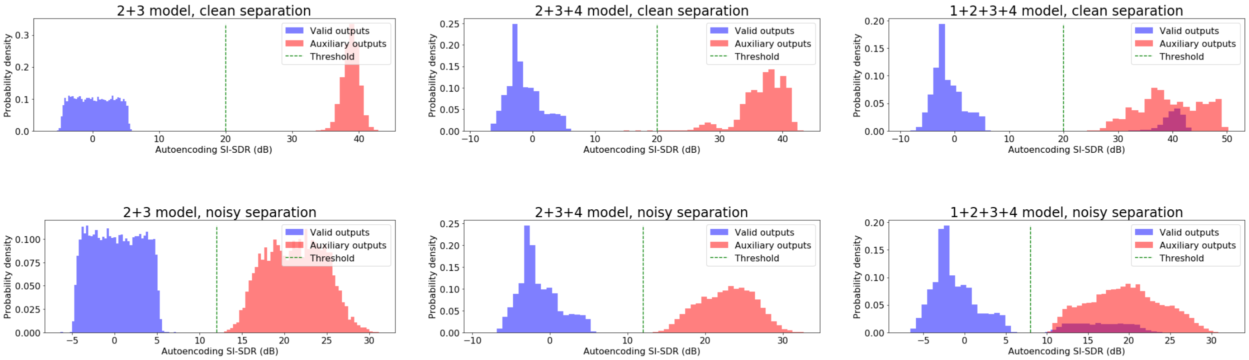

Table 5.3: Separation performance of various configurations on the clean separation task. SI-SDR is reported for one speaker utterances on decibel scale, and SI-SDRi is reported for the rest on decibel scale.

Model	Output selection	SI-SDR	SI-SDRi		
		1 spk	2 spk	3 spk	4 spk
Baseline	Oracle	**64.8**	11.5	8.0	5.7
2+3 model	Oracle	–	**12.0**	8.8	–
	Predicted	–	11.6	8.7	–
2+3+4 model	Oracle	–	11.8	**9.1**	7.1
	Predicted	–	11.7	8.1	7.1
1+2+3+4 model	Oracle	39.8	11.9	**9.1**	**7.2**
	Predicted	44.2	11.8	8.5	**7.2**

Table 5.4: Separation performance of various configurations on the noisy separation task. SI-SDRi is reported in decibel scale.

Model	Output selection	SI-SDRi			
		1 spk	2 spk	3 spk	4 spk
Baseline	Oracle	**6.9**	10.8	7.5	5.4
2+3	Oracle	–	**11.2**	8.7	–
model	Predicted	–	**11.2**	8.7	–
2+3+4	Oracle	–	11.1	**8.8**	**7.0**
model	Predicted	–	10.8	8.2	6.9
1+2+3+4	Oracle	4.8	11.1	**8.8**	6.9
model	Predicted	4.2	11.0	8.4	6.9

Table 5.3 and 5.4 provide the separation performance on the clean and noisy separation tasks, respectively. For the one speaker utterances in the clean separation task, SI-SDR instead of SI-SDRi is reported as the input is already the clean target itself. It can be observed that A2PIT can almost always improve the separation performance on all configurations with both clean and noisy data, and the gains for 3 and 4 speaker cases are significant. It can be concluded from the results that A2PIT is able to achieve on par or better overall separation performance on both clean and noisy separation tasks. Even with predicted output selection, the fault tolerance ability introduced by A2PIT allows the model to control the performance degradation. These results confirms the effectiveness of A2PIT.

5.3 A2T: Distortion-controlled Separation in Noisy Reverberant Environments

Using the reverberant clean signal as both the training and evaluation targets introduces new challenges to the current training and evaluation configurations. One core problem, which is referred to as the *equal-valued contour* problem, occurs in many widely-used metrics such as signal-to-noise ratio (SNR) and scale-invariant signal-to-distortion ratio (SI-SDR). Equal-valued contour problem denotes the issue that given a reference signal and a metric, there are infinite numbers of estimated signals that can achieve the same performance. Certain estimations among this “contour” might be more preferred than the others, however an end-to-end model may lack the ability to distinguish the “good” estimations from the “bad” ones. As an example of the equal-valued contour problem in reverberant separation, consider an ideal model that always separates the direct-path targets from the reverberant mixture. When evaluated by the signal-level metric between the separation outputs and the reverberant targets, the model will not obtain a high performance especially when the energy of the late reverberation component is large (e.g. with a large reverberation time). However, such an ideal model can achieve very good performance on both word-error-rate (WER) and subjective perceptual quality measures. Suppose there is another model that achieves similar performance as this ideal model when evaluated by the signal-level metric while performs noisy, distorted separation, it is easy to imagine that this model will achieve a much worse performance.

The equal-valued contour problem mainly comes from the training configurations where a single end-to-end training objective is used without further regularizations on the distortion introduced to components such as the direct-path signals. It is natural to investigate how such regularizations can be incorporated into the training procedure in a simple way. The focus here is on the end-to-end systems where the separation is done by applying a linear mapping, e.g. a multiplicative mask, on the input mixture. This framework includes many recently proposed systems, including the TasNet-series of works in Chapter 2 and any linear neural beamformers in Chapter 3. With the linearity between the input and output, an additional auxiliary autoencoding loss is added, which forces the linear mapping to also perform autoencoding on the direct-path target signal. For example, given a mixture signal which contains one target signal $\mathbf{x}$ and $K \geq 1$ additional interference signals $\{\mathbf{n}_i\}_{i=1}^{K}$, standard training configuration attempts to optimize the model to learn a linear mapping $\mathcal{M}(\cdot)$ such that $\mathcal{M}(\mathbf{x} + \sum_{i=1}^{K} \mathbf{n}_i) \approx \mathbf{x}$. The auxiliary autoencoding term corresponds to the reconstruction of the direct-path signal of $\mathbf{x}$, denoted by $\mathbf{x}_d$, i.e. $\mathcal{M}(\mathbf{x}_d) \approx \mathbf{x}_d$. This training configuration is referred to as the *auxiliary autoencoding training (A2T)*.

5.3.1 Motivation and Design

The problem formulation of end-to-end reverberant speech enhancement and separation is briefly reviewed first. Given M channels of inputs and C signal-of-interests (SOIs), the mixture signal at channel i is represented as:

$$\mathbf{y}_i = \sum_{j=1}^{C} \mathbf{x}_i^{(j)} + \mathbf{n}_i, \quad i \in 1, \ldots, M \tag{5.5}$$

where $\mathbf{x}_i^{(j)} \in \mathbb{R}^{1\times T}$ is the j-th SOI at channel i and $\mathbf{n}_i \in \mathbb{R}^{1\times T}$ is the interference at channel i. In reverberant environment, each SOI is obtained by convolving a clean signal $\mathbf{c}_i^{(j)} \in \mathbb{R}^{1\times(T-K+1)}$ with a room impulse response (RIR) filter $\mathbf{h}_i^{(j)} \in \mathbb{R}^{1\times K}$:

$$\mathbf{x}_i^{(j)} = \mathbf{c}_i^{(j)} * \mathbf{h}_i^{(j)} \tag{5.6}$$

By decomposing the RIR filter $\mathbf{h}_i^{(j)}$ into a direct path RIR $\mathbf{hd}_i^{(j)}$ and a late reverberation RIR $\mathbf{hr}_i^{(j)}$, the SOI $\mathbf{x}_i^{(j)}$ can be decomposed into a direct path signal $\mathbf{x}_{d,i}^{(j)}$ and a late reverberation signal $\mathbf{x}_{r,i}^{(j)}$:

$$\begin{aligned} \mathbf{x}_i^{(j)} &= \mathbf{c}_i^{(j)} * \mathbf{h}_i^{(j)} \\ &= \mathbf{c}_i^{(j)} * (\mathbf{hd}_i^{(j)} + \mathbf{hr}_i^{(j)}) \\ &\triangleq \mathbf{x}_{d,i}^{(j)} + \mathbf{x}_{r,i}^{(j)} \end{aligned} \tag{5.7}$$

The task of speech enhancement or separation is to extract the SOIs given the mixtures. Here the end-to-end systems that generate a linear mapping $T(\cdot)$ between the mixture and each estimated SOI is considered:

$$\left\{\hat{\mathbf{x}}^{(j)}\right\}_{j=1}^{C} = T\left(\{\mathbf{y}_i\}_{i=1}^{M}\right) \tag{5.8}$$

In typical configurations, the training objective is to minimize the discrepancy between the estimated and the target SOIs at a specific reference microphone:

$$\mathcal{L}_{obj} = \sum_{j=1}^{C} D\left(\hat{\mathbf{x}}^{(j)}, \mathbf{x}_1^{(j)}\right) \tag{5.9}$$

where $D(\cdot)$ is a metric on the two signals, and it is assumed that the first channel is selected as the reference channel without loss of generality.

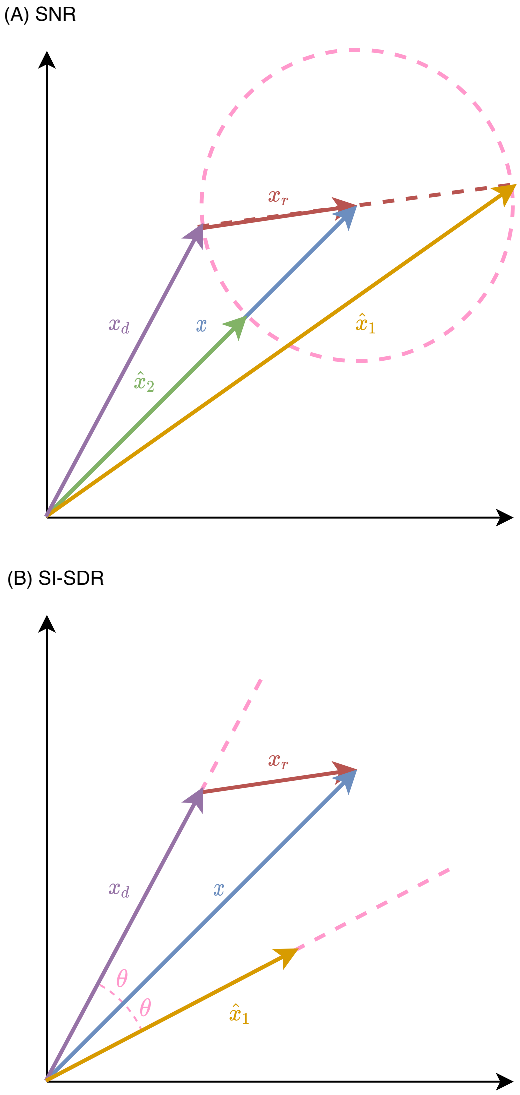

Figure 5.2: Simplified illustrations for equal-valued contours in (A) SNR metric, and (B) SI-SDR metric.

The equal-valued contour problem can then be demonstrated in two widely-used metrics, namely the SNR and the SI-SDR. SNR between the estimated and target SOIs is defined as:

$$\begin{aligned}\text{SNR}\left(\hat{\mathbf{x}}, \mathbf{x}\right) &= 10\log_{10}\frac{||\mathbf{x}||_2^2}{||\mathbf{x}-\hat{\mathbf{x}}||_2^2} && (5.10)\\ &= 10\log_{10}||\mathbf{x}||_2^2 - 10\log_{10}||\mathbf{x}-\hat{\mathbf{x}}||_2^2 && (5.11)\end{aligned}$$

where the notations are the same as equation 5.9 despite that the subscripts and superscripts are omitted for the sake of simplicity. SNR metric is equivalent to a logarithm-mean square error (log-MSE) metric on the distance between the estimated and target SOIs, thus its equal-valued contours can be defined by the surface of hyperballs whose centers are determined by $\mathbf{x}$. Figure 5.2 (A) shows a simplified example of an equal-valued contour in two-dimensional space. The radius of the equal-valued contour in the figure is defined by the reverberation component $\mathbf{x}_r$, and it's easy to see that $\hat{\mathbf{x}}_1$, $\hat{\mathbf{x}}_2$ and $\mathbf{x}_d$ are on the same contour and have the same SNR value with respect to the reverberant target $\mathbf{x}$. Moreover, $\hat{\mathbf{x}}_1 = \mathbf{x}_d + 2\mathbf{x}_r$ adds an additional reverberation component, $\hat{\mathbf{x}}_2$ is a rescaled version of $\mathbf{x}$, and $\mathbf{x}_d$ is the direct-path target. It's obvious that $\mathbf{x}_d$ is preferred than $\hat{\mathbf{x}}_2$ and $\hat{\mathbf{x}}_2$ is preferred than $\hat{\mathbf{x}}_1$, even though they share a same SNR value.

Another widely-used metric, the SI-SDR, is defined as:

$$\text{SI-SDR}\left(\hat{\mathbf{x}}, \mathbf{x}\right) = 10\log_{10}\frac{||\alpha\mathbf{x}||_2^2}{||\hat{\mathbf{x}}-\alpha\mathbf{x}||_2^2} \tag{5.12}$$

where $\alpha = \hat{\mathbf{x}}\mathbf{x}^\top/\mathbf{x}\mathbf{x}^\top$ corresponds to the optimal rescaling factor towards the estimated signal. It has been shown in Chapter 5.2 that the definition can be rewritten as:

$$\text{SI-SDR}(\hat{\mathbf{x}}, \mathbf{x}) = 10\log_{10}\left(\frac{c(\mathbf{x}, \hat{\mathbf{x}})^2}{1-c(\mathbf{x}, \hat{\mathbf{x}})^2}\right) \tag{5.13}$$

where $c(\mathbf{x}, \hat{\mathbf{x}}) \triangleq b/\sqrt{ac} = \hat{\mathbf{x}}\mathbf{x}^\top/\sqrt{(\mathbf{x}\mathbf{x}^\top)(\hat{\mathbf{x}}\hat{\mathbf{x}}^\top)}$ is the cosine similarity between $\mathbf{x}$ and $\hat{\mathbf{x}}$. SI-SDR is thus equivalent to the angular distance between the estimated and target SOIs, and its equal-valued contours can be defined by the boundary of cones whose symmetrical axes are defined by $\mathbf{x}$. Figure 5.2 (B) shows an example of an equal-valued contour with angle $\theta > 0$. Similarly, $\hat{\mathbf{x}}_1$

and $\mathbf{x}_d$ share the same value of SI-SDR, while $\mathbf{x}_d$ is always preferred than $\hat{\mathbf{x}}_1$.

Note that the definition of equal-valued contours in other metrics, e.g. L1-norm or MSE, can be easily defined in the same way by decoupling the direct-path and reverberation components in the SOIs.

Auxiliary autoencoding Training (A2T) adds one objective term to control the system outputs on the equal-valued contours. Take $\mathbf{x}^{(1)}$ as the SOI and omit the subscripts for channel indices where there is no ambiguity. Under the linearity assumption of $T(\cdot)$ in equation 5.8, the equation can be rewritten as:

$$\begin{aligned}\hat{\mathbf{x}}_1 &= T\left(\mathbf{y}\right) \\ &= T\left(\mathbf{x}^{(1)} + \sum_{j=2}^{C} \mathbf{x}^{(j)} + \mathbf{n}\right) \\ &= T\left(\mathbf{x}^{(1)}\right) + T\left(\sum_{j=2}^{C} \mathbf{x}^{(j)}\right) + T\left(\mathbf{n}\right)\end{aligned} \tag{5.14}$$

where the system output consist of three parts generated from the direct path, the late reverberation, and the interference, respectively. The conventional training objective sets the reverberant SOI $\mathbf{x}^{(1)}$ as the training target, and equation 2.6 becomes:

$$\mathcal{L}_{obj} = D\left(T\left(\mathbf{x}^{(1)}\right) + T\left(\sum_{j=2}^{C} \mathbf{x}^{(j)}\right) + T\left(\mathbf{n}\right), \mathbf{x}^{(1)}\right) \tag{5.15}$$

A2T adds an auxiliary autoencoding term on the direct-path signal to the objective:

$$\mathcal{L}_{A2T} = \underbrace{D\left(T\left(\mathbf{x}^{(1)}\right) + T\left(\sum_{j=2}^{C} \mathbf{x}^{(j)}\right) + T\left(\mathbf{n}\right), \mathbf{x}^{(1)}\right)}_{separation} \tag{5.16}$$

$$+ \underbrace{D\left(T\left(\mathbf{x}_d^{(1)}\right), \mathbf{x}_d^{(1)}\right)}_{preservation} \tag{5.17}$$

where the auxiliary autoencoding term controls the distortion introduces to the direct-path signal and preserves its signal quality.

To apply permutation invariant training (PIT) in A2T, the output permutations of the two objective terms need to be aligned. In the training phase, PIT is first applied on the separation term to obtain the best label permutation, and the permutation is then applied to the preservation term for auxiliary autoencoding.

Logarithm-scale objective functions such as SNR and SI-SDR are unbounded and may lead to infinitely large gradients. As autoencoding is a much easier task than separation with a much faster convergence speed, the A2T term may easily dominate the gradients and prevents the standard separation term to be in effect. Thus proper gradient balancing methods need to be applied to ensure successful training. The α-skewed SI-SDR (α-SI-SDR) objective introduced in Chapter 5.2 is applied here:

$$\alpha\text{-SI-SDR}(\mathbf{x}, \hat{\mathbf{x}}) \triangleq 10\log_{10}\left(\frac{c(\mathbf{x}, \hat{\mathbf{x}})^2}{1+\alpha - c(\mathbf{x}, \hat{\mathbf{x}})^2}\right) \tag{5.18}$$

where the gradient scale with respect to the cosine similarity term can be controlled by $\alpha \geq 0$. Similarly, [310] proposed the α-thresholded SNR (α-SNR):

$$\begin{aligned}\alpha\text{-SNR}(\mathbf{x}, \hat{\mathbf{x}}) &\triangleq 10\log_{10}\frac{||\mathbf{x}||_2^2}{||\mathbf{x}-\hat{\mathbf{x}}||_2^2 + \alpha||\mathbf{x}||_2^2} \\ &= 10\log_{10}||\mathbf{x}||_2^2 - 10\log_{10}\left(||\mathbf{x}-\hat{\mathbf{x}}||_2^2 + \alpha||\mathbf{x}||_2^2\right)\end{aligned} \tag{5.19}$$

As A2T only serves as a regularization term, $\alpha > 0$ is forced on the A2T term and $\alpha = 0$ is applied in the separation term.

The A2T objective term can be directly connected to the optimization target of distortionless response beamformers, such as the MVDR and MPDR beamformers [23], where a distortionless constraint is imposed on the direction of the SOI. A2T does not use such explicit hard constraint, but adds an auxiliary term in the objective as a soft constraint to control the distortion introduced to the direct-path signal. Literatures on imposing constraints on differential frameworks, e.g. the problem of constrained differential optimization [6], have been investigated in neural net-

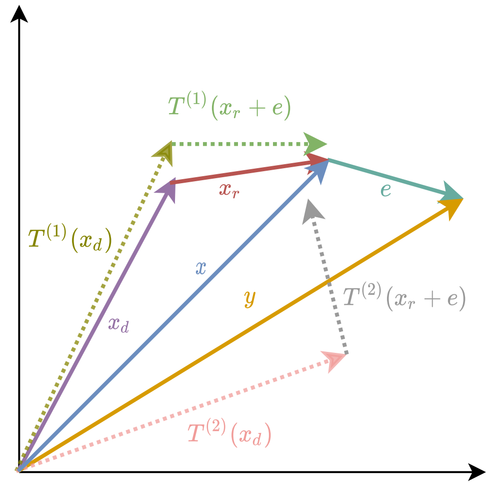

Figure 5.3: Illustration of two possible linear mappings $T^{(1)}(\cdot)$ and $T^{(2)}(\cdot)$. $T^{(1)}(\cdot)$ denotes the one learned with A2T with a controlled distortion on the direct-path signal $\mathbf{x}_d$. $T^{(2)}(\cdot)$ corresponds to an unconstrained mapping where the distortion on $\mathbf{x}_d$ can be significant.

works [110], however soft constraints have shown better performance and easier implementation than hard constraints [153]. Moreover, unlike MVDR/MPDR which are designed only for multi-channel systems, A2T can be easily applied to any end-to-end system which satisfies the linearity assumption of the mapping.

On the other hand, forcing the outputs to meet the A2T constraint may help with the generalization of the model. Figure 5.3 shows two example mappings $T^{(1)}(\cdot)$ and $T^{(2)}(\cdot)$ with and without A2T, respectively. When the distortion introduced to the direct-path $\mathbf{x}_d$ is significant, the mapping on the other sources and the noise, i.e. $\mathbf{e} = \mathbf{y} - \mathbf{x}$, needs to compensate for the distortion in order to map to the SOI $\mathbf{x}$. As the SOI and the interferences are in general uncorrelated, learning such a mapping may hurt the performance and the generalization ability of the system. Another point to clarify is that empirically $T^{(2)}(\cdot)$ might not be the usual case for models without A2T, as the experiment results will show that standard objectives inherently preserve the direct-path signal to some extent. Nevertheless, properly adding the A2T term can almost always achieve on par or better separation performance with a significantly lower distortion on the direct-path signal. This indicates that A2T is able to find “better” outputs on the equal-valued contours.

For the consideration of extra computational costs during training, applying autoencoding on the direct-path signal only requires the calculation of the linear transform on the direct-path targets. The complexity for the backward pass is slightly increased as the gradients with respect to the A2T term also need to be backpropagated, but the overall increase on the computational cost is minor.

5.3.2 Experiment Configurations and Results

The evaluation of the iFaSNet model is based on the same dataset used for the TAC-FaSNet in Chapter 3.2, while only the ad-hoc microphone array configuration is used for comparison. As the utterances in the dataset are randomly truncated and not suitable for speech recognition evaluation, another test set with 500 utterances simulated where the utterances are not truncated. In order to approximately match the length of the mixtures in the training set, the utterances are randomly sampled from the *test-clean* subset whose length is no longer than 4 seconds. All other configurations are the same as the original dataset.

DPRNN-TasNet is selected for all the models with the identical configuration in Chapter 2.3. The evaluation of the separation performance is done by both SNR and SI-SDR metrics. To evaluate the distortion introduced to the direct-path signals, the target-SNR (TSDR) and target-SI-SDR (TSI-SDR) is also applied, which are calculated between the transformed direct-path signal $T(\mathbf{x}_d)$ and the direct-path signal $\mathbf{x}_d$:

$$\text{TSNR}\left(\hat{\mathbf{x}}, \mathbf{x}\right) = \text{SNR}\left(T(\mathbf{x}_d), \mathbf{x}_d\right) \tag{5.20}$$

$$\text{TSI-SDR}\left(\hat{\mathbf{x}}, \mathbf{x}\right) = \text{SI-SDR}\left(T(\mathbf{x}_d), \mathbf{x}_d\right) \tag{5.21}$$

The evaluation of the speech recognition performance is done by word error rate (WER). The recognition engine used is directly taken from the pre-trained transformer model on Librispeech data from ESPNet [221][1].

Table 5.5 shows the experiment results of models trained with different objective functions,

[1] https://github.com/espnet/espnet/tree/master/egs/librispeech/asr1

Table 5.5: Comparison of DPRNN-TasNet models with objectives with and without A2T on the noisy reverberant separation task. “OR” stands for the overlap ratio between the two speakers.

Objective	α	SNR / TSNR / SI-SDR / TSI-SDR (dB)				
		OR $\in [0, 25)\%$	OR $\in [25, 50)\%$	OR $\in [50, 75)\%$	OR $\in [75, 100]\%$	Overall
SNR	–	14.0 / 18.4 / 13.7 / 18.3	10.3 / 12.9 / 9.7 / 12.6	8.0 / 10.3 / 6.9 / 9.7	6.1 / 8.4 / 4.5 / 7.7	9.6 / 12.5 / 8.7 / 12.1
+ A2T	0	-0.4 / **60.6** / -0.4 / **62.1**	-0.4 / **60.1** / -0.4 / **61.9**	-0.4 / **59.6** / -0.4 / **61.7**	-0.5 / **58.8** / -0.5 / **61.3**	-0.4 / **59.8** / -0.4 / **61.8**
	0.01	12.8 / 26.0 / 12.6 / 26.0	8.3 / 23.3 / 7.9 / 23.4	5.3 / 23.4 / 4.8 / 23.5	2.8 / 24.0 / 2.3 / 24.3	7.3 / 24.2 / 6.9 / 24.3
	0.03	13.8 / 23.0 / 13.5 / 23.2	9.8 / 18.9 / 9.3 / 19.0	7.3 / 16.9 / 6.4 / 16.9	5.2 / 15.6 / 3.9 / 15.7	9.0 / 18.6 / 8.3 / 18.7
	0.1	14.0 / 21.4 / 13.7 / 21.5	10.1 / 16.8 / 9.5 / 16.8	7.8 / 14.6 / 6.9 / 14.5	5.9 / 13.1 / 4.5 / 13.0	9.5 / 16.5 / 8.7 / 16.5
	0.3	14.2 / 20.3 / 13.9 / 20.4	**10.5** / 15.7 / **10.0** / 15.6	**8.2** / 13.2 / **7.2** / 13.1	**6.2** / 11.5 / **4.8** / 11.2	**9.8** / 15.2 / **9.0** / 15.1
	1	14.2 / 19.3 / 13.9 / 19.2	10.4 / 14.5 / 9.9 / 14.4	8.1 / 12.0 / 7.1 / 11.8	6.0 / 10.1 / 4.5 / 9.8	9.7 / 14.0 / 8.9 / 13.8
	3	**14.3** / 18.9 / **14.0** / 18.9	**10.5** / 13.5 / 9.9 / 13.3	8.1 / 10.9 / **7.2** / 10.5	6.1 / 9.0 / 4.5 / 8.5	**9.8** / 13.1 / 8.9 / 12.8
	10	14.1 / 18.5 / 13.7 / 18.4	10.2 / 13.0 / 9.6 / 12.7	7.8 / 10.3 / 6.7 / 9.7	5.7 / 8.3 / 4.0 / 7.5	9.4 / 12.6 / 8.5 / 12.1
SI-SDR	–	– / – / 13.9 / 16.9	– / – / 9.8 / 10.5	– / – / 6.9 / 7.6	– / – / 4.4 / 5.5	– / – / 8.8 / 10.2
+ A2T	0	– / – / -0.5 / **62.2**	– / – / -0.4 / **62.2**	– / – / -0.4 / **62.3**	– / – / -0.5 / **62.5**	– / – / -0.4 / **62.3**
	0.01	– / – / 12.4 / 27.0	– / – / 7.6 / 24.9	– / – / 4.3 / 26.3	– / – / 1.8 / 28.3	– / – / 6.6 / 26.6
	0.03	– / – / 13.2 / 23.5	– / – / 8.9 / 19.7	– / – / 5.9 / 19.0	– / – / 3.4 / 19.8	– / – / 7.9 / 20.5
	0.1	– / – / 13.6 / 21.3	– / – / 9.7 / 16.9	– / – / 6.9 / 14.6	– / – / 4.4 / 13.1	– / – / 8.7 / 16.5
	0.3	– / – / 14.0 / 20.8	– / – / 9.8 / 16.0	– / – / 7.0 / 13.6	– / – / 4.5 / 11.9	– / – / 8.8 / 15.6
	1	– / – / 13.9 / 19.8	– / – / **9.9** / 14.9	– / – / 7.2 / 12.3	– / – / 4.7 / 10.5	– / – / 8.9 / 14.4
	3	– / – / 13.9 / 19.5	– / – / **9.9** / 14.4	– / – / **7.3** / 11.9	– / – / **4.8** / 10.0	– / – / **9.0** / 14.0
	10	– / – / **14.1** / 19.4	– / – / **9.9** / 14.0	– / – / **7.3** / 11.5	– / – / 4.6 / 9.5	– / – / **9.0** / 13.6

Table 5.6: Comparison of WER from models trained with SNR with and without A2T. “OR” stands for the overlap ratio between the two speakers.

Objective	α	WER (%)				
		OR $\in [0, 25)\%$	OR $\in [25, 50)\%$	OR $\in [50, 75)\%$	OR $\in [75, 100]\%$	Overall
SNR	–	15.5	20.8	38.4	60.2	34.2
+ A2T	0.3	15.3	**17.5**	36.4	**57.7**	**32.1**
	1	15.2	18.4	36.5	58.8	32.6
	3	**14.8**	20.5	**34.5**	59.5	32.8
Noisy reverberant	–	–	–	–	–	17.7
Clean reverberant	–	–	–	–	–	8.1

with and without A2T, and with different values of α for gradient balancing in the A2T term. For the models trained with SI-SDR, the SNR and TSNR scores are not reported as SI-SDR does not preserve the scale of the outputs. First notice that the models trained with original SNR and SI-SDR objectives are able to inherently control the distortion introduced to the direct-path signals to some extent, and in low-overlapped utterances the distortion is significantly lower than high-overlapped utterances. On the one hand, the performance of TSNR and TSI-SDR in low-overlapped utterances is expected as in the nonoverlapped regions the separation model is equivalent to an autoencoding model. On the other hand, the worse performance in high-overlapped utterances shows that the equal-valued contour problem is practical and the separated outputs might not be the preferred ones. Moreover, SI-SDR objective even leads to a lower TSI-SDR score than the SNR objective across all overlap ratios. Since the SNR objective is also able to preserve the output scale, the results indicate that SNR can be a good replacement of SI-SDR as a training objective even when the evaluation is done by SI-SDR. This also matches the observation in [298] where SNR led to at least on par performance as SI-SDR.

It is then noticed that for $\alpha = 0$ in the A2T term, models trained with both objectives fail to converge and the gradients are dominated by the A2T term. It leads to a significantly higher performance on the TSNR and TSI-SDR scores but completely fails on separation. The TSNR and TSI-SDR scores gradually decrease as α increases, and are both higher than the models trained without A2T. The best separation performance is achieved at an intermediate value of α, e.g. $\alpha \in [0.3, 3]$, and a minor improvement on SNR and SI-SDR can be achieved at the best values of α across all overlap ratios. It confirms the ability of A2T to find "better" outputs on the equal-valued contours.

Table 5.6 presents the WER on the 500-utterance test set. Based on the observation in table 5.5, only the SNR-A2T results with $\alpha = 0.3, 1, 3$ are reported as they all achieve on par or better separation performance than the standard SNR while have a much lower distortion on the direc-path signal. It can be observed that adding the A2T term can always leads to improved WER across all overlap ratios. Moreover, the overall WER increases as α increases, and the best overall performance is achieved when $\alpha = 0.3$. Note that $\alpha = 0.3$ and $\alpha = 3$ both give the best separation performance in table 5.5, and $\alpha = 3$ leads to lower WER than $\alpha = 0.3$ in two overlap ratio ranges. This indicates that different α for different overlap ratios might further improve the overall performance, however it is left as a future work to verify. Nevertheless, the results confirm that with a similar level of SNR and SI-SDR, the actual WER can vary by as large as 16% relatively ($[25, 50)\%$ overlap ratio), and further emphasize the importance of the constraint on the equal-valued contours.

The definition of direct-path signal can vary in different literatures. Defining the direct-path RIR filter as ± 6 ms of the first peak in the RIR filter is the same as [205], however the range can be relaxed to cover more early reverberation components similar to [229]. Here the effect of different definitions of direct-path signals is also investigated. Table 5.7 shows the separation results on the

Table 5.7: Comparison of DPRNN-TasNet models with direct-path RIR filter defined as the ± 20 ms of the first peak in the RIR filter.

Objective	α	SNR / TSNR / SI-SDR / TSI-SDR (dB)				
		OR $\in [0, 25)\%$	OR $\in [25, 50)\%$	OR $\in [50, 75)\%$	OR $\in [75, 100]\%$	Overall
SNR	–	14.0 / 18.7 / 13.7 / 18.6	10.3 / 13.1 / 9.7 / 12.8	**8.0** / 10.5 / **6.9** / 10.0	**6.1** / 8.6 / **4.5** / 7.8	**9.6** / 12.8 / **8.7** / 12.3
+ A2T (± 20 ms)	0.3	**14.1 / 20.3 / 13.8 / 20.3**	10.2 / **15.3** / 9.7 / **15.2**	7.9 / **12.8** / **6.9** / **12.7**	5.9 / **10.9** / 4.3 / **10.7**	**9.6 / 14.9 / 8.7 / 14.7**
	1	**14.1** / 19.4 / **13.8** / 19.4	**10.4** / 14.2 / **9.8** / 14.0	7.9 / 11.5 / **6.9** / 11.1	5.8 / 9.5 / 4.2 / 9.1	**9.6** / 13.7 / **8.7** / 13.4
	3	14.0 / 19.1 / 13.7 / 19.2	10.1 / 13.7 / 9.5 / 13.5	7.8 / 11.0 / 6.7 / 10.7	5.8 / 9.0 / 4.1 / 8.6	9.4 / 13.3 / 8.5 / 13.0

Table 5.8: Comparison of WER from models trained with direct-path RIR filter defined as the ± 20 ms of the first peak in the RIR filter.

Objective	α	WER (%)				
		OR $\in [0, 25)\%$	OR $\in [25, 50)\%$	OR $\in [50, 75)\%$	OR $\in [75, 100]\%$	Overall
SNR	–	15.5	20.8	38.4	60.2	34.2
SNR+A2T (± 6 ms)	0.3	15.3	**17.5**	**36.4**	**57.7**	**32.1**
SNR+A2T (± 20 ms)	0.3	**14.8**	19.2	38.2	62.1	34.0
	1	15.4	19.2	36.5	61.1	33.4
	3	15.0	19.3	36.8	60.2	33.2

same datasets as above, while the direct-path RIR filter is defined as ± 20 ms of the first peak in the RIR filter. Interestingly, the separation performance measured by SNR and SI-SDR are both worse than those in table 5.5, and the autoencoding performance measured by TSNR and TSI-SDR, although on a different definition of direct-path signal, are also worse. The reason might be that autoencoding on the ± 20 ms direct-path signal also suffers the equal-valued contour problem, as the early reverberations may also cause minor distortions on the overall reconstruction. The recognition performance presented in table 5.8 also show that the WERs on ± 20 ms A2T are in general worse than those on ± 6 ms A2T, while still better than the standard SNR objective. Moreover, unlike the observation in ± 6 ms A2T that a larger α leads to worse WER, a larger α here leads to better performance. The reason behind this observation is yet to be revealed. To summarize, A2T prefers a more aggressive definition of direct-path signal.

5.4 Discussions

Both A2PIT and A2T make use of the concept of auxiliary autoencoding. Since the two training objectives are designed for different purposes, they can be jointly applied in the separation of varying number of sources in a reverberant environment, which better matches the requirements in real-world applications.

On the other hand, A2T requires the linearity assumption in the separation process, which might contradict with certain problem definitions which I will introduce in the next chapter. Although A2T is only evaluated on the end-to-end single-channel separation task, its application on mask-based neural beamformers might also be promising, as the masking operation is a linear operation and mask-based beamformers have proven effective in tasks such as ASR. Moreover, although the auxiliary autoencoding loss in A2T is applied on the direct-path signal, it can also be applied on the interference signal to put constraints on the equal-valued contours on the entire SOI. The effect of such application is left for future works.

Chapter 6: Rethinking the Problem Formulations of End-to-end Speech Separation

The previous chapters put the focus on new designs for model architectures and training objectives. In this chapter, I take a step back and empirically revisit some of the problem formulations in the end-to-end separation pipeline. I select three topics in the general end-to-end separation pipeline: (1) the role and necessity of *separation layers* [323], where an explicit "separation" operation defined as a single-input-multi-output (SIMO) operation happens at the end of the "separation" layers; (2) the performance of *generalized iterative separation* [325], where multiple rounds of separation is cascaded to form a multi-pass separation procedure; (3) the effect of *end-to-end training*, where a time-domain training objective is applied to networks with both time-domain and frequency-domain encoder and decoder. The dataset used for all the experiments in this chapter is identical with the one in Chapter 3.2.

6.1 Rethinking the Roles of Separation Layers in Speech Separation Networks

6.1.1 Motivation and Experiment Design

Speech separation models can be broadly categorized into single-input-single-output (*SISO*) systems and single-input-multi-output (*SIMO*) systems. A SISO system usually consists a stack of one to one mapping layers, extracting one speaker from the mixture at each time. SISO networks are typically designed for guided source separation (GSS) or speech enhancement tasks [88], [183], [217], [232], [258], [262], where a bias is often needed to distinguish the target speaker. When there are more than one source that need to be estimated, the single output separation needs to be performed multiple times, one for each source. In certain iterative separation methods, a mask can be estimated from the last layer in the model representing one target source, and a residual signal can be calculated by subtracting the separated output from the mixture [251]. The residual signal is then used as the input for next iteration. In contrast, the SIMO systems are the standard design for blind source separation (BSS) [148], [211], [293], [313], which target at separating C sources simultaneously. To fulfill this task, on top of the one to one mapping layers, there always exists one or more one-to-many mapping layers that convert the single input signal to multiple source output, i.e. one to many mapping. For example, in standard masking-based BSS models, C masks are generally estimated from the last layer in the network. In [227], though named as "MIMO" network, the system is essentially a SIMO system where the input feature consist of multi-microphone information.

Researchers have also explored the combination of SIMO and SIMO architecture for further performance improvement. A commonly applied integration is to use a SISO network for post-enhancement module on the output of the SIMO separation result [148], [228], [256], [261], while typically the two modules are not jointly optimized. However, as the combination systems usually contain a significantly larger parameter size which could also results in potential performance improvement for a pure SIMO network, little is known about the roles of SIMO and SISO modules in a BSS separation system. Why performance improvements can be achieved by incorporating the SISO modules? For a given model size, how to properly arrange the sizes of SIMO and SISO modules to achieve a best performance? Are SIMO modules always necessary? Those are the motivations for an empirical analysis on different model configurations, including the standard SIMO-only model, the mixed SIMO-SISO models, and the SISO-only models, on their effectiveness on the separation performance.

The three configurations are compared with a similar model architecture. For model configuration, the same DPRNN-TasNet architecture introduced in Chapter 2.3 is adopted in all formulations. The linear mapping function defined by the waveform encoder in the DPRNN-TasNet is denoted as $\mathcal{E}(\cdot)$, and the waveform encoder and decoder in Figure 6.1 are omitted for the sake of simplicity.

Figure 6.1 (A) shows the flowchart for the SIMO-only model design, which is the default

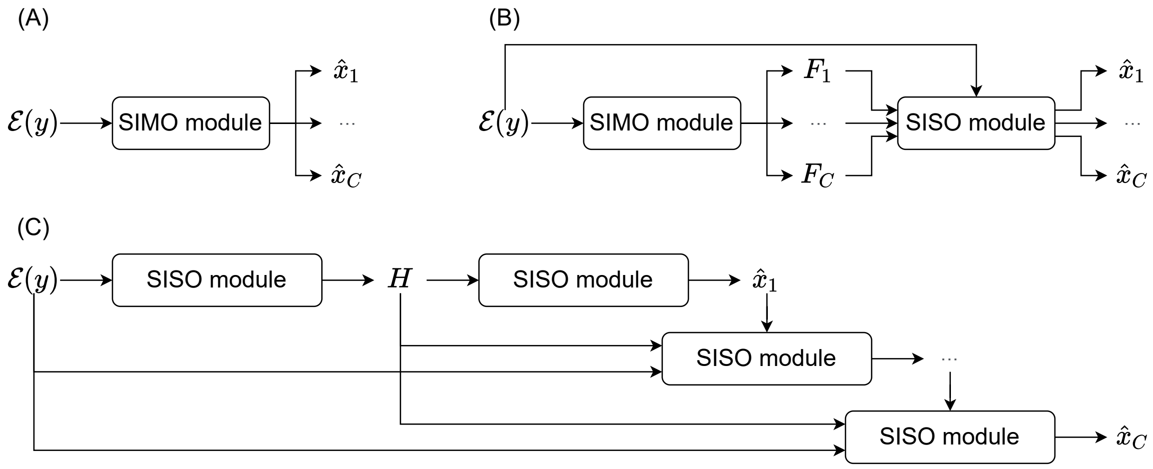

Figure 6.1: Flowchart of different configurations on the separation models. (A) Standard separation model with a single SIMO module that estimates C target sources. (B) A SIMO module first generates C intermediate features for the C sources, and a SISO module takes each of the feature as input and estimates the target sources. (C) A SISO encoder module first generates one intermediate feature from the input mixture. A SISO decoder module takes the feature as input and estimates the first target source. The input mixture, intermediate feature, and the target source are passed again to the decoder module to estimate the second target source. Such procedure is repeated until all sources are separated.

design of almost all current separation models. The M DPRNN blocks all belong to the SIMO module, and the C targets are estimated from the output layer of the module, which is typically a fully-connected (FC) layer with C output heads.

Figure 6.1 (B) illustrates the flowchart for the mixed SIMO-SISO design. The M DPRNN blocks are split into a SIMO module and a SISO module, where each module contains K and $M - K$ blocks, respectively. Similar to the SIMO-only design, the SIMO module is first applied on the input mixture $\mathbf{y}$ to create C intermediate features $\{\mathbf{F}_i\}_{i=1}^{C} \in \mathbb{R}^{N\times L}$. Each of the intermediate feature $\mathbf{F}_i$, together with the encoder output of the mixture signal $\mathcal{E}(\mathbf{y}) \in \mathbb{R}^{M}$, are concatenated and passed to the SISO module, which is shared by all SIMO output features, to generate the final estimations $\{\hat{\mathbf{x}}_i\}_{i=1}^{C}$. The two modules are jointly optimized and no extra training objective is applied to the intermediate features.

Note that unlike the SIMO-only design where the outputs of the SIMO module are typically C masks applied to the input mixture, here the output layer for the SIMO module can simply be a linear FC layer and the outputs do not need to be applied to the mixture. The setting where the outputs from the SIMO module are indeed the C masks and the masked mixture encoder output is directly used as $\{\mathbf{F}_i\}_{i=1}^{C}$ is also tested. $\{\mathbf{F}_i\}_{i=1}^{C}$ is directly added to the SISO outputs to form the final separated sources. This matches the standard pipeline in pre-separation and post-enhancement models, where the SIMO module servers as the pre-separation module and the SISO module is the post-enhancement module. Empirically such setting leads to identical performance as the simpler pipeline in Figure 6.1 (B).

Figure 6.1 (C) presents the flowchart for the SISO-only design. Since no SIMO module is present in the entire model, iterative separation has to be applied in order to separate all C targets. The M layers in the SISO module are split into K *encoder layers* and $M-K$ *decoder layers*, where the encoder layers are applied only once and the decoder layers are applied in every iteration. In other words, the encoder layers map the mixture into a latent representation shared by all iterations, and the decoder layers separate different targets based on the representation.

The mixture $\mathbf{y}$ is passed to the encoder and a SISO feature extractor to generate one sequence of intermediate feature $\mathbf{H} \in \mathbb{R}^{N \times L}$. In the first iteration, the encoder output of the mixture $\mathcal{E}(\mathbf{y})$, the intermediate feature $\mathbf{H}$, and an all-zero feature with the same shape as $\mathcal{E}(\mathbf{y})$ are passed to decoder layers to generate the first output $\hat{\mathbf{x}}_1$. In the j-th iteration where $j > 1$, $\mathcal{E}(\mathbf{y})$, $\mathbf{H}$ and the encoder output of the residual signal $\mathcal{E}(\mathbf{y} - \sum_{k=1}^{j-1} \hat{\mathbf{x}}_k)$ are concatenated and passed to a SISO feature decoder layers to generate the j-th output $\hat{\mathbf{x}}_j$. Note that here the number of target sources is assumed known in advance, but the same procedure can also be applied in the task of separating unknown number of speakers.

The iterative SISO-only design can be connected to the GSS framework, where the bias information comes from the residual signal in the previous iteration. The main difference here is that in GSS frameworks the bias information is typically related to the target to be extracted, e.g. speaker-related feature or content-related feature, while in the SISO-only design the bias information is related to all the signals that have not been separated. There could be other configurations of feature fusion, e.g. using all the separated signals instead of the residual signal as the bias.

Also note that in a recent literature, a newly proposed training method, the serialized output training (SOT) [281], applies the SISO-only configuration without iterative separation. SOT is designed for multi-talker automatic speech recognition (ASR), and it concatenates all target output sequences in to a single sequence as the training target. Together with an encoder-decoder architecture, the decoder sequentially generates the predicted labels for all speakers. Although SOT can also be extended to the task of speech separation, one main difference between ASR and separation is that the length of the output sequences in separation tasks is always the same as the input, while the length of the output sequences in ASR tasks can vary for different speakers. Such generative decoding mechanism might have trouble in the separation outputs as the total length of the output sequence can be significantly longer than that in ASR tasks.

6.1.2 Results and Discussions

The total number of DPRNN blocks M in the DPRNN-TasNet is set to 6 in all models. The window size in the waveform encoder and decoder is set to 2 ms (32 samples), and the number of filters in the encoder and decoder is always 128. The input size and hidden size of the LSTM layers in the DPRNN blocks are set to 64 and 128, respectively. Note that in the mixed SIMO-SISO design, the SIMO module can contain no DPRNN blocks but simply a single FC layer to generate the C intermediate features. In this case, the SISO module contains all 6 DPRNN blocks similar to the SISO-only design. This configuration is excluded from the SISO-only design as it does not perform iterative separation. The training procedure is the same as the one introduced in Chapter 5.2.

Table 6.1 presents the separation performance of the models in the SIMO-only and mixed SIMO-SISO designs across different overlap ratios between the speakers. The first row presents the standard SIMO-only design, which is also the design for the original DPRNN-TasNet. All other rows show the performance of mixed SIMO-SISO design with different numbers of blocks in each module. First notice that despite the configuration of 0 SIMO blocks, all other SIMO-SISO configurations lead to better performance than the standard SIMO-only design. Moreover, best performance is achieved at the 4-block configuration, and the 2- and 3-block configurations

SIMO blocks	SISO blocks	Overlap ratio (%)				Average
		<25	25-50	50-75	>75	
6	0	13.9	10.0	7.2	4.8	9.0
5	1	14.0	10.1	7.3	4.9	9.1
4	2	14.2	10.4	7.6	**5.0**	9.4
3	3	14.4	10.5	7.6	**5.0**	9.4
2	4	**14.6**	**10.6**	**7.8**	4.9	**9.5**
1	5	14.3	10.3	7.5	4.8	9.2
0	6	13.5	9.5	6.8	4.5	8.6

Table 6.1: Separation performance of different configurations in the SIMO-only and mixed SIMO-SISO designs across different overlap ratios between the two speakers. SI-SDR is reported in decibel scale.

also lead to comparable performance. The worst performance is observed at the 6-block configuration. This indicates that a deeper design in the SISO module is able to improve the performance, while the separation layers in the SIMO module also play an important role. A balance can be found on the arrangement of the number of layers in the SIMO and SISO modules, and it can be empirically observed here that assigning 70% of the total blocks to the SISO module can be a good configuration.

Another finding from the table is that the performance improvement obtained by the mixed SIMO-SISO design mainly comes from the low-overlap utterances. The performance on the utterance with higher than 75% overlap ratio is consistent across all configurations, however the performance on utterances with lower than 25% overlap ratio can vary by 1 dB. This implies that the mixed SIMO-SISO design might be more important for the single-speaker regions. One possible explanation comes from the role of the output layer of the SIMO module. In the standard SIMO-only design where the output FC layer estimates the C masks, the values for the masks have to be zero for inactive speakers in the single-speaker regions. Since the C output heads in the FC layer all receive a same feature from the output of the second last layer in the SIMO module, the estimation of the C masks not only requires the feature to be linearly separable in the latent space defined by the parameters of the FC layer, but also forces the same set of parameters to be able to reconstruct salient and silent regions across different regions. This may introduce difficulties on the optimization and put extra requirements on the feature dimension in order to achieve such constraints. Using a deeper SISO module removes the second constraint on the single-speaker regions and does not harm the first constraint on the separability. As more and more recent models consider data distributions with partially-overlap utterances [231], [268], [269], such mixed SIMO-SISO design should be more practical and beneficial than the standard designs.

Encoder blocks	Decoder blocks	Overlap ratio (%)				Average
		<25	25-50	50-75	>75	
1	5	**14.3**	**10.3**	7.3	**4.9**	**9.3**
2	4	14.2	10.2	**7.4**	4.8	9.1
3	3	14.0	10.0	7.1	4.4	8.9
4	2	13.4	9.3	6.5	3.8	8.3
5	1	13.0	8.9	6.2	3.3	7.9

Table 6.2: Separation performance of different configurations in the SISO-only design across different overlap ratios between the two speakers. SI-SDR is reported in decibel scale.

Table 6.2 shows the separation performance on different numbers of encoding and decoding layers in the SISO-only design. The performance is getting consistently worse as the number of decoder blocks decreases, implying that the model capacity in the decoder blocks need to be large enough in such iterative separation scheme. The best performance, on the other hand, is still slightly better than the standard SIMO-only design, especially on the low-overlap utterances. This matches the discussions in the previous section about the importance of deeper architectures for the single-speaker regions in the mixture.

The results provide another perspective on the role of the SIMO separation layers in a BSS network and rise new questions. If the SIMO module is not even necessary for successful separation, then what are the roles of the separation layers in a separation network? How are the speaker-dependent features, including speaker identity and contents of the context, separated by the SISO-only models? If unbiased speech extraction can replace speech separation, can there be a unified SISO framework for both GSS and BSS? Such questions may open new discussions on the understanding of separation networks and motivate new design paradigms for new architectures.

6.2 Empirical Analysis of Generalized Iterative Speech Separation Networks

6.2.1 Motivation and Experiment Design

The design of a wide range of speech separation networks follows a general *one-pass* pipeline, where the input mixture waveform is passed to a neural network to directly estimate the target sources [80], [121], [173], [187], [201], [243]. On the other hand, recent developments on the *multi-pass* or *iterative* pipeline have shown improved separation performance [123], [148], [234], [253], [306]. Conventional iterative separation pipelines were typically designed by certain iterative algorithms, such as Expectation-Maximization (EM) and nonnegative matrix factorization (NMF) [49], [105], [169], where multiple iterations are required for the algorithms to converge and achieve a satisfying performance. In neural network-based systems, an iterative speech separation pipeline can be defined as a system that contains multiple rounds of the separation process, where (1) each iteration performs a full separation pipeline, and (2) the separation outputs from a previous iteration can be used as additional information in an upcoming iteration. In single-channel applications, the iterative pipeline has proven better than one-pass pipelines with comparable model complexity [234], [306]. In multi-channel applications, the iterative pipeline can improve the performance of either a vocal activity detector (VAD) or a beamformer [183], [253], [333]. Different features such as speaker-specific embeddings can also be extracted from the previous separation outputs and serve as the additional feature for following iterations [216], [254], [307], [313].

A common configuration for such iterative separation pipeline is that the training objective, typically the discrepancy between the estimated and target sources, is applied to all the iterations. By unfolding the iterations into additional layers or modules in a deeper network, such training objective corresponds to a *layer-wise* objective in one-pass pipelines [293], [303]. Moreover, the objective can be further extended to models where a *post-enhancement* stage is applied to each of the separation outputs [118], [148], [171], [241], [272]. This gives a *generalized* iterative separation pipeline where the same training objective is applied to different parts of the network. Different model design and architecture configurations in such generalized iterative separation pipelines may result in different effects on the separation performance. However, a better understanding on the components as well as their combinations is still beneficial for the investigation of the reason behind their effectiveness and the design of improved pipelines. The target here is to empirically evaluate the effect and performance of different configurations of the generalized iterative separation pipelines.

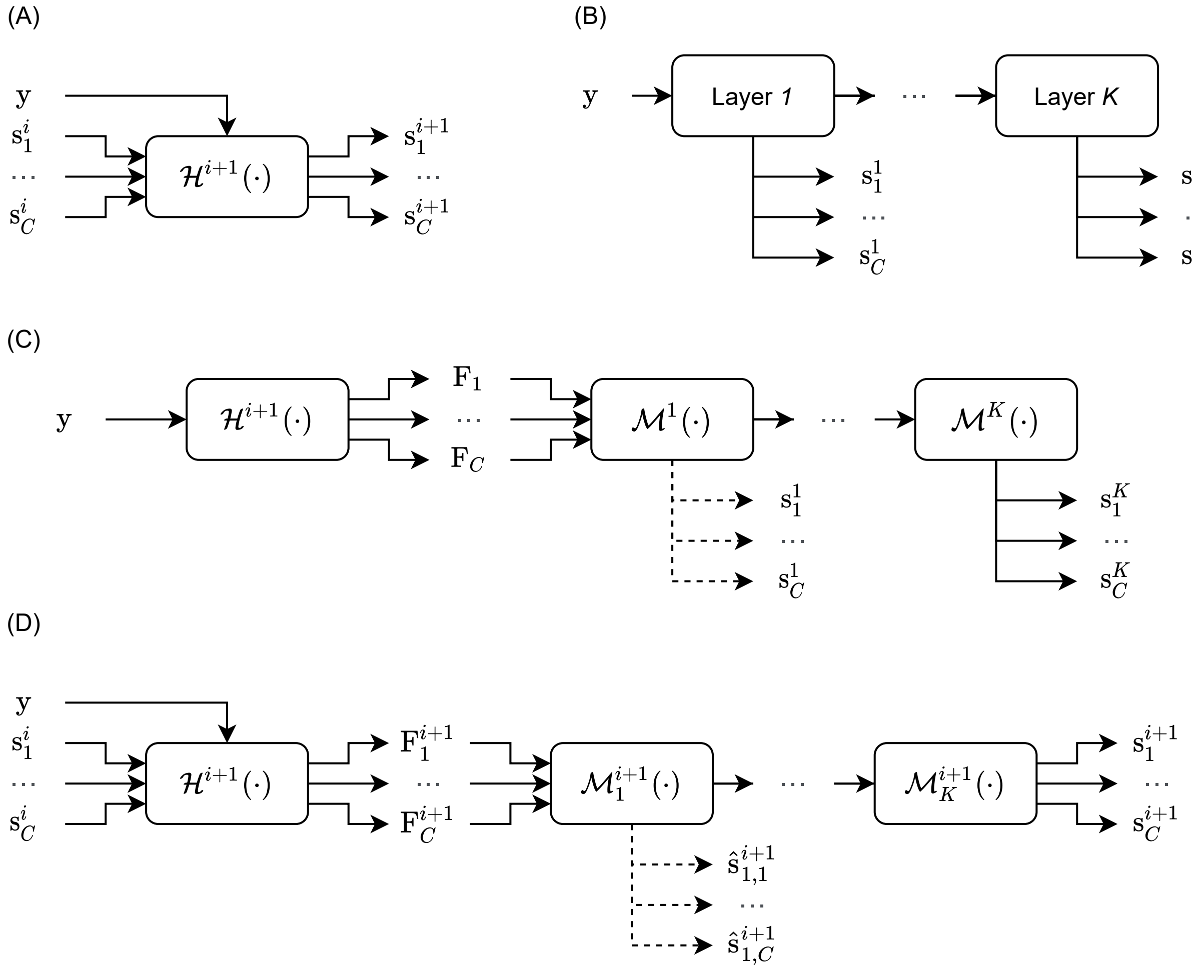

Figure 6.2: Standard pipelines for iterative speech separation networks. (A) The separation outputs at iteration i is used as auxiliary inputs at iteration $i+1$. (B) An output layer is added to each layer in the network to generate intermediate separation outputs, and the training objective is applied to each of them. (C) A single-input-multi-output (SIMO) separation module first separates the mixture into either outputs or intermediate features, and K single-input-single-output (SISO) post-enhancement layers is further applied to each of the outputs to generate the targets. (D) The combination of the three aforementioned pipelines.

Figure 6.2 (A) shows the most common pipeline for iterative separation. The mixture signal $\mathbf{y}$, together with the separation output from i-th iteration $\{\mathbf{s}_c^i\}_{c=1}^C$, is passed to the $(i+1)$-th single-input-multi-output (SIMO) mapping $\mathcal{H}^{(i+1)}(\cdot)$ defined by a neural network, to generate the separation outputs at the $(i+1)$-th iteration $\{\mathbf{s}_c^{i+1}\}_{c=1}^C$. For the first iteration, $\{\mathbf{s}_c^0\}_{c=1}^C$ are initialized as zero signals. The output permutation at the i-th iteration is used as the input permutation at the $(i+1)-th$ iteration, and empirically this can maintain the output permutation across all iterations without affecting the separation performance.

There are two optional designs in this pipeline. First, the model parameters across different iterations can be either shared or different. This can be related to the general definition of time-invariant and time-variant systems. Second, when performing backpropagation, the gradient of the input to the $(i+1)$-th iteration can either pass to the i-th iteration or be discarded. In the latter case, each iteration can be viewed as an independent process, and the output from the previous iteration can be treated as additional bias information for data augmentation.

Figure 6.2 (B) shows a typical generalized iterative separation pipeline where the training objective is applied to all the layers in the separator. For the k-th layer where $K = 1, \ldots, K$, a shared output layer is applied to its output to generate intermediate separation outputs $\{\mathbf{s}_c^k\}_{c=1}^C$. The pipeline is defined as a generalized iterative separation network because all layers in the separator are directly optimized with the same training objective to minimize the discrepancy between the (intermediate) separation outputs and the target sources, hence layer k with $k \geq 2$ can be treated as iterative separation layers receiving separation outputs from layer $k-1$. This is unlike the standard pipeline where the training objective is only applied to the output at layer K and the outputs at other layers do not have a clear and explicit meaning.

Figure 6.2 (C) shows the pipeline with a pre-separation module and a post-enhancement module. The pre-separation module receives the mixture as input and generates C outputs $\{\mathbf{F}_c\}_{c=1}^C$ for the C target sources. Note that $\{\mathbf{F}_c\}_{c=1}^C$ can either be intermediate features or the estimated targets themselves. Each feature $\mathbf{F}_c$ is then passed to a post-enhancement module with K SISO layers for output refinement, and the separation outputs can be generated from either each SISO layer (i.e., layer-wise objective) or the last SISO layer only. It is defined as a generalized iterative separation pipeline when the training objective is applied to each of the post-enhancement layers. Moreover, the training objective can also be applied to $\{\mathbf{F}_c\}_{c=1}^{C}$ when they correspond to the separation outputs.

Figure 6.2 (D) shows a combined pipeline for the three pipelines above. The separation-enhancement pipeline is inserted into the standard iterative pipeline, where the SISO enhancement layers together with optional layer-wise objectives are jointly applied together with the SIMO separation module. The outputs at the k-th SISO enhancement layer at the $(i+1)$-th iteration become $\{\hat{\mathbf{s}}_{k,c}^{i+1}\}_{c=1}^{C}$.

For the experiments, the combined pipeline is used following the same architecture in Chapter 6.1. Both time-domain and frequency-domain models are evaluated by selecting either learnable encoder and decoder or short-time Fourier transform (STFT) and its inverse (ISTFT). For STFT/ISTFT, only the magnitude spectrogram is used as the input, and the mixture's phase spectrogram is directly used for the ISTFT of the separation outputs. The window size for the learnable encoder/decoder and STFT/ISTFT is set to 2 ms (32 points) and 32 ms (512 points), respectively. The number of filters in the encoder and decoder for the learnable encoder/decoder and STFT/ISTFT is set to 128 and 257, respectively. A linear bottleneck layer with 64 hidden units is always applied to the encoder output for dimension reduction. The number of hidden units in each of the LSTM layers in the DPRNN modules is set to 128. The segment size for DPRNN is set to 100 frames and 24 frames for the learnable encoder/decoder and STFT/ISTFT, respectively.

6.2.2 Results and Discussions

Table 6.3: Experiment results for different configurations in the iterative separation pipeline.

SIMO layers	SISO layers	Iteration	Effective network depth	Output detach	SI-SDR (dB)	
					Time domain	Freq domain
3	0	1	3	–	8.7	8.4
2	1				9.0	8.7
1	2				9.2	9.1
1	2	2	6	✓	9.8	9.6
				✗	9.7	9.5
2	4	1		–	10.0	9.5
1	2	3	9	✓	10.1	**9.8**
				✗	9.6	9.5
3	6	1		–	**10.2**	9.4

Table 6.3 shows the experiment results of the networks with different configurations. The model parameters are assumed shared across all iterations in the models. Each SIMO and SISO layer corresponds to a DPRNN block, and 0 SISO layers means that the output of the SIMO layers are the separation outputs. First notice that for both time-domain and frequency-domain models, a deeper SISO module leads to better performance. Since Chapter 6.1 already showed that a deep SISO module improves the performance of time-domain networks, here the results further confirm that frequency-domain networks can also benefit from this configuration. For iterative networks with the number of iterations larger than 1, they are also compared with one-pass models with a same effective network depth. The "output detach" column corresponds to the configuration where the gradient is constrained within each iteration (which can be implemented by *detach* function in Pytorch or *stop_gradient* function in Tensorflow). It can be observed that for the 2-iteration configuration, both time-domain and frequency-domain models have comparable performance with their corresponding one-pass models. Moreover, detaching the gradient from the previous output leads to a minor improvement. For the 3-iteration configuration, the improvement introduced by gradient detachment becomes more salient, and the frequency-domain model even outperform the one-pass counterpart. The results here show that the iterative separation pipeline can serve as an effective way to reduce the storage requirement of the separation networks.

Table 6.4: Effect of layer-wise training objective.

SIMO layers	SISO layers	Iteration	SI-SDR (dB)	
			Time domain	Freq domain
1	2	3	9.9	9.4
3	6	1	10.1	9.2

Table 6.4 provides the separation performance of the iterative systems with layer-wise training objective. The output at each SISO layer in each iteration is passed to the shared mask estimation layer to generate the separated waveforms, and the negative SNR objective is applied to all outputs in the entire pipeline. The configuration where output detachment is applied and parameters are shared across iterations is selected here. Comparing the results with the ones in Table 6.3, layer-wise objective does not further improve the performance in either one-pass or iterative configurations. [293] and [303] reported that layer-wise objective leads to a performance improvement

in both monaural and binaural separation tasks, however here it can be observed that the objective may not be a universal option and its effect can vary in different problem settings and architectures. Since layer-wise objective belongs to the definition of a generalized iterative separation pipeline in the discussion, the results also show that the way the iterative separation is performed also needs to be carefully designed.

Table 6.5: Effect of iteration-specific SIMO modules with STFT/ISTFT.

SIMO layers	SISO layers	Iteration	SI-SDR (dB)
1	2	2	9.6
		3	9.7

Table 6.5 presents the separation performance on the models with different parameters in different iterations with STFT/ISTFT. Here only the frequency-domain configuration is evaluated. Here the SIMO layers are iteration-specific while the SISO layers are still shared across iterations. The rationale behind this configuration is that the additional bias information, i.e., the separation outputs from the previous iteration, is directly used by the SIMO separator, and the bias information differs from iteration to iteration. Iteration-specific separator may then have the potential to perform better separation based on the characteristics of the separation outputs from each iteration. However, the performance obtained by iteration-specific SIMO layers is on par with that of shared SIMO layers. The results indicate that the use of iterative-specific model parameters, or more general, time-variant model parameters when each iteration is treated as a discrete time step, may require further investigation in the iterative separation pipelines.

Table 6.6: Effect of different number of inference iterations and oracle bias information.

Training iterations	Inference iterations	SI-SDR (dB)		
		Time	Freq	Freq + oracle bias
1	1	9.2	9.1	9.1
	2	5.4	3.4	8.9
	3	6.2	4.5	8.6
	4	5.5	3.7	8.3
2	1	9.4	9.2	9.1
	2	9.8	9.6	9.7
	3	9.7	9.6	9.7
	4	9.7	9.6	9.6
3	1	9.2	9.2	9.2
	2	9.4	9.7	9.8
	3	10.1	9.8	9.8
	4	10.1	9.8	9.8

Table 6.6 measures the effect of different inference iterations. For the models trained with 1, 2, and 3 iterations with 1 SIMO layer and 2 SISO layers, their performance is evaluated with 1 to 4 iterations in the inference phase. This experiment is conducted to look into the effect of a mismatched number of iterations on the training and inference phases. It can be observed that the model trained with 1 iteration completely fails when more than 1 iteration is applied in the inference phase, which is expected since the bias information starting from the second iteration is completely unseen for the SIMO separation. When the model is trained for no fewer than 2 iterations, the inference phase performance becomes stable even if the inference phase iteration is larger than the training phase iteration. Moreover, the evaluation is done on the performance of the frequency-domain model when the oracle bias information, i.e., the clean target sources, is used for the SIMO module, and an auxiliary training objective is added to the overall training objectives. Adding this oracle bias information allows the model trained with 1 iteration to perform much better in inference phase and does not harm the performance of the models trained with 2 and 3 iterations. However, no obvious performance improvement is achieved by the auxiliary loss. How to further improve the separation performance of those iterative models remains an important topic to explore.

6.3 Empirical Analysis of the Effect of Separation Network Components under a Time-domain Training Objective

6.3.1 Motivation and Experiment Design

Different configurations can be adjusted in the three components of a typical end-to-end speech separation system: an *encoder*, a *separator*, and a *decoder*. On the one hand, short-time Fourier transform (STFT) and its inverse can also be seamlessly incorporated to the end-to-end training pipelines [226], [234]. On the other hand, the output of the separator can either be a set of *multiplicative masks* applied to the mixture's latent representation, or the target sources' latent representations that can be directly decoded. These two types of outputs match to *masking-based configuration* and the *regression-based configuration*. It has been shown that regression-based configuration can be beneficial than masking-based configuration in various problem settings [266], [293]. The target here is to empirically revisit the effect of different combinations of the component-level configurations on the separation performance.

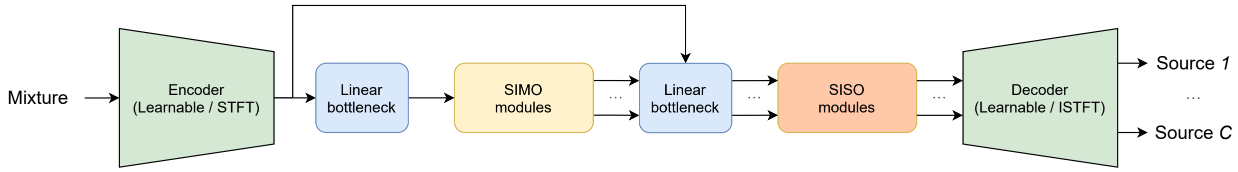

Figure 6.3: Flowchart for a standard speech separation pipeline. An encoder first transforms the mixture into a latent representation, and a linear bottleneck layer reduces its dimension. A single-input-multi-output (SIMO) separation module generates C features correspond to the C target sources. Each output is concatenated with the encoder output and passed to another linear bottleneck layer for dimension reduction, and a single-input-single-output (SISO) module is applied to estimate either a multiplicative mask for the encoder output or the latent representation for the target source directly. A decoder is finally used to reconstruct the target waveforms.

Figure 6.3 shows the general pipeline for an end-to-end speech separation system, which is identical to the pipeline introduced in Chapter 2. An encoder first transforms the mixture waveform into a latent representation. A layer normalization operation [114] is then applied on the representation, and a linear bottleneck layer reduces the feature dimension of the representation. The feature is then sent to a single-input-multi-output (SIMO) module to generate 2 outputs. Each of the outputs is then concatenated with the normalized mixture latent representation and sent to another linear bottleneck layer for dimension reduction, and a single-input-single-output (SISO) module follows to estimate either a multiplicative mask applied to the mixture's latent representation or the latent representation of the target signals directly. A decoder is finally applied to reconstruct the target waveforms.

Within the DPRNN-TasNet framework, different configurations of the pipeline are evaluated:

1. *Encoder/Decoder*: Both learnable encoder/decoder and STFT/ISTFT can be used. For learnable encoder/decoder, 1-D linear convolutional/transposed-convolutional layers identical to the ones in Chapter 2.2 are used. For STFT/ISTFT, either the magnitude spectrogram (i.e., *mag-spec configuration*) or the concatenation of real and imaginary parts of the complex-

valued spectrogram is used as the model input (i.e., *complex-spec configuration*).

2. *Window size*: Two window sizes, 2 ms (32 points) and 32 ms (512 points), are selected in the encoder/decoder. A 50% hop size is always applied when encoding/decoding. For learnable encoder/decoder, 128 and 512 convolutional kernels are used with the two window sizes, respectively. The chunk size for the DPRNN modules are 100 frames and 24 frames for the two window sizes, respectively.

3. *Window function*: Hann window is selected as the default window function, and the effect of Hamming window, Kaiser window, Blackman window, and learnable window are further compared on the separation performance. For an N-point learnable window where N is even, it is assumed that the window function is always symmetric and the first half of the window is set as the learnable part. During initialization, each entry in the learnable parameters is sampled from a uniform distribution $\mathcal{U}(0, 1)$.

4. *SIMO and SISO module organization*: The total number of DPRNN modules is fixed for all configurations, and different numbers of modules to the SIMO and SISO modules similar to Chapter 6.1.

5. *Output of SISO module*: The SISO module can either estimate multiplicative masks (*masking-based configuration*) or latent representations for the targets (*regression-based configuration*). For masking-based configuration, it is assumed that the masks are nonnegative for the learnable encoder/decoder and mag-spec configuration, and a ReLU function is applied to enforce it. For complex-spec configuration, unbounded real and imaginary parts for the complex-valued masks are estimated. For regression-based configuration, unbounded outputs without any nonlinear functions are generated for learnable encoder/decoder and complex-spec configuration, and the frame-level energy (evaluated by L_2-norm) of the mixture is multiplied to the SISO outputs since the layer normalization operation does not preserve the input energy throughout the network. For mag-spec configuration, a ReLU activation is still selected to ensure the estimated magnitude spectrograms are nonnegative.

Beyond the configurations above, the encoder bottleneck layer and the SISO bottleneck layer always contain 64 hidden units, and each LSTM in the DPRNN modules always has 128 hidden units.

6.3.2 Results and Discussions

Table 6.7, 6.8 and 6.9 provide the separation performance of models with different pipeline configurations. The experiments are first conducted with the total number of DPRNN modules fixed to 3, and then the model sizes are doubled for the best organizations. For learnable encoder/decoder configuration, regression-based configuration leads to better performance than masking-based configuration with 2 ms window, and the performance improves as the number of SISO layers increases. Moreover, increasing the total model size further improves the separation performance in both configurations. However, masking-based configuration performs consistently better than regression-based configuration with 32 ms window, and the performance does not increase with a larger network size. For the mag-spec configuration, the performance of both masking-based and regression-based configurations are stable across the two window sizes, while masking-based configuration prefers a larger window and regression-based configuration prefers a smaller window. The best performance is also achieved by the masking-based configuration with 32 ms window, which is similar to the best performance in learnable encoder/decoder configuration with a much lower model complexity due to the use of a larger window size. For the complex-spec configuration, a similar overall performance as the learnable encoder/decoder can be observed, while the performance for masking-based configuration is slightly higher. The best performance is still achieved by regression-based configuration with 2 ms window, but it is still slightly worse than that with learnable encoder/decoder.

Then the necessity of the nonnegativity constraint in magnitude T-F masks is revisited. The ReLU nonlinearity in the output layer is removed and the performance of unbounded magnitude masks is evaluated. Table 6.10 shows that the performance of nonnegative masks and unbounded masks has little or no difference in different model and window sizes, which indicates that the

Table 6.7: Experiment results for learnable encoder/decoder with different configurations.

Formulation	SIMO layer	SISO layer	SI-SDR (dB)	
			2 ms	32 ms
Masking	3	0	8.1	5.7
	2	1	8.5	6.3
	1	2	8.5	**6.7**
Regression	3	0	8.7	3.4
	2	1	9.0	3.9
	1	2	9.2	3.7
Masking	2	4	9.2	**6.7**
Regression	2	4	**10.0**	–
	4	2	–	4.2

Table 6.8: Experiment results for mag-spec configuration with different configurations.

Formulation	SIMO layer	SISO layer	SI-SDR (dB)	
			2 ms	32 ms
Masking	3	0	8.0	8.4
	2	1	8.1	8.7
	1	2	8.3	9.1
Regression	3	0	8.1	8.0
	2	1	8.1	7.7
	1	2	8.2	7.6
Masking	2	4	8.6	**9.5**
Regression	2	4	**8.7**	–
	6	0	–	8.4

Table 6.9: Experiment results for complex-spec configuration with different configurations.

Formulation	SIMO layer	SISO layer	SI-SDR (dB)	
			2 ms	32 ms
Masking	3	0	8.2	6.9
	2	1	8.4	6.7
	1	2	8.9	7.0
Regression	3	0	8.6	3.5
	2	1	8.6	3.7
	1	2	9.0	3.5
Masking	2	4	9.3	7.3
Regression	2	4	**9.6**	3.9

conventional constraint that magnitude T-F masks should be nonnegative is no longer necessary in the end-to-end training pipeline.

Table 6.10: Effect of nonnegative and unbounded magnitude time-frequency masks with 32 ms window size.

Masks	SIMO layer	SISO layer	SI-SDR (dB)
Nonnegative	1	2	9.1
Unbounded			9.0
Nonnegative	2	4	9.5
Unbounded			9.5

Finally the effect of different window functions in STFT/ISTFT on the separation performance is compared. The mag-spec configuration with unbounded masks is applied here, and the number of SIMO and SISO DPRNN layers are set to 1 and 2, respectively, according to the best configurations above. It can be observed that the choice of window function does affect the separation performance, while the model without a window function has the worst performance. Interestingly, the learnable window function achieves a relatively better performance comparing with all other well-defined window functions even with a random initialization. Figure 6.4 visualizes the learned window function and its frequency response.

Table 6.11: Effect of window functions in mag-spec configuration with unbounded magnitude T-F masks and 32 ms window size.

Window	SI-SDR (dB)
None	8.5
Hann	9.0
Hamming	9.1
Kaiser	8.6
Blackman	8.8
Learnable	**9.2**

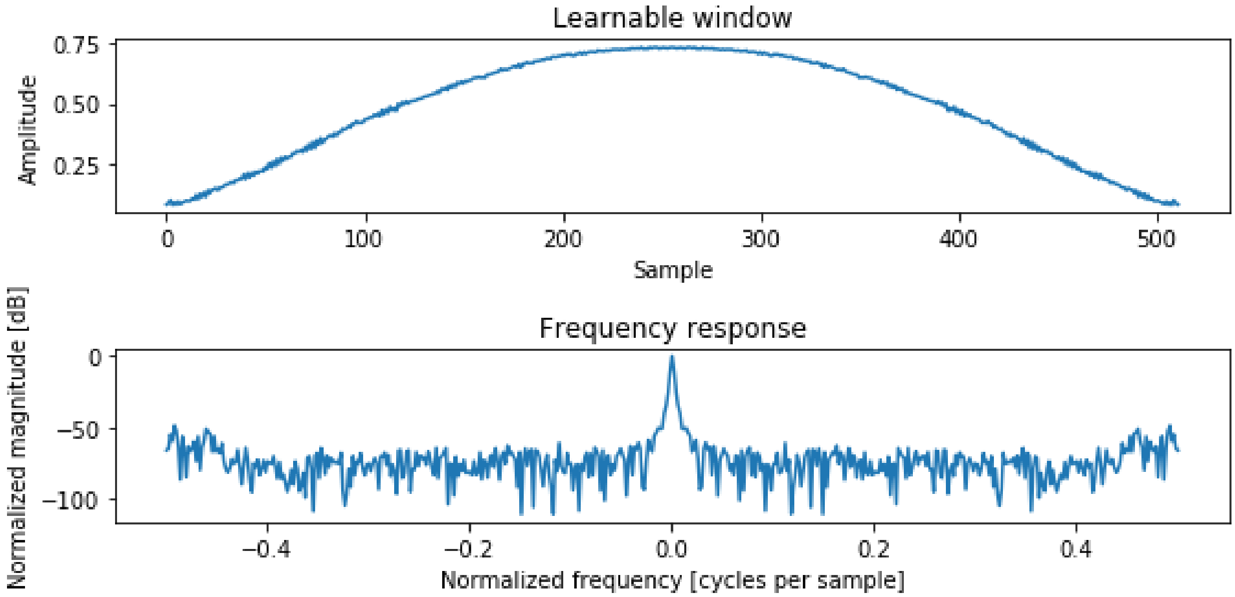

Figure 6.4: Visualization of the learned window function and its frequency response.

Multiple analysis and discussions can be made based on the results above:

1. It can be found from the results that proper organizations of SIMO and SISO modules can improve the separation performance in both masking-based and regression-based configurations. This matches the observation in Chapter 6.1. Moreover, the SISO module can

be considered as a *neural vocoder* jointly optimized with the separator in regression-based configurations, which builds connections to the recent works on synthesis-based speech enhancement and separation methods [244], [266], [271], [292].

2. Compare the performance of masking-based configuration between learnable encoder/decoder and complex-spec configurations, the performance of complex-spec configuration is consistently better than the learnable encoder/decoder across both window sizes. Since the main differences between the complex-spec configuration and the learanble encoder/decoder are the use of fixed orthogonal basis kernels (i.e., sinusoids) and the minimum mean-square error (MMSE) estimation of the waveform in ISTFT [4], it implies that domain-specific knowledge can still be beneficial in the design of encoder and decoder. Moreover, the performance in small window size is significantly better than that in large window size, which matches the observation in previous studies [234], [287].

3. In contrast to the results above, the performance of mag-spec configuration with large window is better than that with small window. Moreover, its performance in large window is also better than the complex-spec configuration. Since the phase spectrogram is unmodified in this pipeline, it becomes more interesting to investigate the role phase information in masking-based pipelines. It has been shown in other literature that T-F domain training objectives can be successfully applied with complex-valued input and outputs [133], [239], [308], hence it is necessary to learn more about the behavior of STFT/ISTFT representations with a time-domain objective. The conventional definition of magnitude T-F masks also needs to be reconsidered, as in end-to-end pipelines the ISTFT process as well as the overlap-add operation for waveform reconstruction both contributes to the backpropagation process and can greatly change the behavior of magnitude T-F masks. As an evidence, unbounded magnitude masks achieve same performance as nonnegative magnitude masks. Note that since a negative-valued mask corresponds to a phase shift of π as $-e^{i\theta} = e^{i(\theta+\pi)}$, such unbounded masks can be viewed as constrained complex-valued masks where the phase

at each T-F bin can be modified by either 0 degree or 180 degree. These results indicate that the conventional definition and analysis of T-F masks needs a revision in the end-to-end pipeline, and the role and effect of T-F masking needs to be reconsidered.

4. One core advantage for regression-based configuration is that it bypasses the issue in masking-based configuration which binds the separation outputs with the mixture's encoder output. It can be observed that regression-based configuration performs consistently better in a smaller window than a larger window, and the best system across all possible configurations (10.0 dB SI-SDR) is achieved by the regression-based configuration with a small window size. This shows that when properly configured, regression-based configuration has the potential to outperform masking-based configuration. This matches the conclusion in a prior work [266].

5. The performance comparison on different encoder/decode types gives a mixed conclusion. On the one hand, both learnable encoder/decoder and complex-spec configurations use a phase information different than the mixture phase during reconstruction, which confirms that the ability for accurate phase reconstruction can lead towards a better separation performance. On the other hand, the performance gap between small and large windows in those two encoder/decoder configurations is significantly larger than that in mag-spec configuration, which implies again that it is not always beneficial to modify the phase when a large window is selected. Another observation is that the performance of learnable encoder/decoder and the complex-spec configuration is comparable across all experiments. This also implies that the actual choice of kernel parameters in the learnable encoder/decoder might not be an important factor, especially in the regression-based configuration where the output waveforms are directly generated.

6. [264] has considered trainable STFT window functions in the speech enhancement task. However, it used different window functions for STFT and ISTFT without symmetric constraint and applied a frequency-domain training objective, and did not compare the perfor-

mance with different types of existing window functions. Here it is further confirmed that the choice of window function is indeed a factor that can be optimized, and certain window functions may not even be helpful (e.g., the Kaiser window). Moreover, it is showed that the learned window function does “look like” a standard window function with random initialization and without a nonnegativity constraint. It is obvious that its frequency response is not ideal comparing with other well-defined window functions such as the Hann or Hamming windows, however it achieves a slightly better performance than any other windows. This also serves as a proof showing that the behavior of STFT/ISTFT can be complicated in the end-to-end training pipeline.

Conclusion and Future Works

This dissertation focused on advancing the state-of-the-art methods on the problem of speech separation with neural networks. The contributions of this dissertation can be categorized into three classes: *problem formulations*, *network architectures*, and *training objectives*.

1. *Problem formulations*: The formulation of end-to-end speech separation in time domain was proposed and validated. STFT and its inverse were replaced by real-valued, learnable 1-D convolutional and transposed convolutional layers, and time-domain training objectives were applied to directly optimize the evaluation metrics. In the single-channel scenario, the TasNet framework introduced in Chapter 2 has achieved higher performance than multiple oracle T-F masks and has become a benchmark in the general problem of speech separation. In the multi-channel scenario, the FaSNet framework introduced in Chapter 3 has achieved superior performance compared to multiple oracle beamformers in terms of signal quality measures. Moreover, by revisiting the commonly-used model configurations for speech separation in Chapter 6, additional questions were raised for a better understanding on the intrinsic mechanisms of the end-to-end speech separation pipelines.

2. *Network architectures*: Multiple network architectures were proposed to not only improve the separation performance but also decrease the model complexity. The TCN and DPRNN architectures introduced in Chapter 2 have been widely adopted in the community, and the GC3 architecture introduced in Chapter 4 has the potential to become a general design paradigm in low-resource platforms and applications.

3. *Training objectives*: Training objectives were proposed in Chapter 5 to improve the robustness of the separation networks under reverberation and to allow the systems to separate arbitrary numbers of sources with a single model. Both of the proposed training objectives, A2T and A2PIT, utilized the idea of auxiliary autoencoding loss, and a modification to the commonly-used SI-SDR and SNR functions were also proposed to control the range of the gradients when the auxiliary autoencoding loss was applied.

There remains many interesting problems in the general context of speech separation to solve:

1. *Separation of unsegmented speech*: The systems introduced in this dissertation were all evaluated on utterance-level datasets, where the length of the mixtures are typically small than 10 seconds. Real-world communications often involve unsegmented speech with time-varying characteristics of speaker overlaps, speaker locations, and speaker activations. How to properly perform speech separation in such long recordings is a critical problem for the deployment of speech separation systems to real-world applications such as meeting transcription systems. Recent studies have started investigating this direction [267], [268], [275], [309], [321], [322], [328], [331], [332], and it is expected that the development of the systems on this task can be accelerated when more realistic meeting-style data with multiple overlapped speakers is collected and released [330].

2. *Separation under strong reverberation*: Although the A2T training objective was proposed to improve the system robustness under reverberation, it did not significantly improve the overall separation performance in terms of signal quality. It is unclear whether time-domain training objectives such as SNR and SI-SDR are still good training objectives under strong reverberation, since such objectives do not consider frequency-dependent properties of the sources and are highly phase-sensitive. Recent works have attempted to propose new time-domain training objectives for reverberant speech separation [263], while the proposed function has the same drawback as the SDR metric introduced in Chapter 1.3. On the other hand, current model architectures for reverberant speech separation are almost always

identical to the ones for anechoic speech separation, and new model architectures that better reflect the properties of the reverberant signals may be beneficial in this task. It it thus worth exploring new training objectives and model architectures for this problem.

3. *Separation with preserved spatial cues*: Spatial cues are important features that allow human beings to precisely perceive the spatial location of the sound sources. Preserving the spatial cues during separation can result in a more realistic hearing experience in either real-world or virtual environments. Recent works have started to investigate this problem with different neural network architectures on various artificially simulated binaural speech datasets [276], [303], [318]. However, the performance of such systems on real-world conversations with moving sources remains unclear, and whether the existing systems satisfy the latency and complexity requirements in real-world devices and applications also needs further verification. Moreover, spatial cues can be hard to accurately measure in noisy reverberant environments, and how to properly define both the evaluation metrics and the training objectives of the systems is also an interesting problem.

4. *Separation as a front-end*: The recognition of overlapped speech can be done by a multi-talker ASR system without an explicit speech separation model [172], [182], [281], [317]. However, it is natural to first apply a speech separation model as a front-end module and use a standard single-channel ASR system as a back-end [139], [206], [209], [227], [295], [296]. Current pipelines that use a separation model as a front-end still cannot achieve on-par performance as a plain ASR system trained on clean single-speaker utterances, and it is important to continue investigating this direction and mitigate the performance gap.

5. *Multi-modal speech separation*: The entire dissertation focused on the audio-only speech separation task. Researchers have also studied the design of multi-modal source separation models in the audio-visual [186], [257], [274], [327], audio-textual [104], [285], [336], and audio-motion [158], [301] modalities. There are two main directions to further explore this

topic. The first one is to continue developing novel system designs to better connect the data from different modalities in a joint embedding space, and existing works in multi-modal data modeling and understanding have shown potentials on it [61], [84], [86], [128], [329]. The second one is how to alleviate the inconsistency between different modalities. Consider a meeting-style conversation with speakers moving their heads while talking. A camera may miss the location of the speaker's face, and a sound localization module may generate rapidly changing DOA information with a moving head. A separation system that relies on these two features may easily get confused when the face information is lost or when the DOA information has a clear mismatch with the location of the face. How to ensure the robustness of the multi-modal system with such inaccurate or even inconsistent features is an important topic for practical applications.

6. *A theoretical understanding on end-to-end separation*: Chapter 6 has empirically analyzed the effect of different model configurations with a time-domain training objective. It is natural to further explore a theoretical understanding on the behaviors of the models, especially on the role of different encoder and decoder configurations in the entire separation pipelines.

References

[1] R. R. Sokal, “A statistical method for evaluating systematic relationship,” *University of Kansas science bulletin*, vol. 28, pp. 1409–1438, 1958.

[2] C. Knapp and G. Carter, “The generalized correlation method for estimation of time delay,” *IEEE/ACM Transactions on Audio, Speech, and Language Processing (TASLP)*, vol. 24, no. 4, pp. 320–327, 1976.

[3] J. B. Allen and D. A. Berkley, “Image method for efficiently simulating small-room acoustics,” *The Journal of the Acoustical Society of America*, vol. 65, no. 4, pp. 943–950, 1979.

[4] D. Griffin and J. Lim, “Signal estimation from modified short-time fourier transform,” *IEEE Transactions on Acoustics, Speech, and Signal Processing*, vol. 32, no. 2, pp. 236–243, 1984.

[5] R. Mucci, “A comparison of efficient beamforming algorithms,” *IEEE/ACM Transactions on Audio, Speech, and Language Processing (TASLP)*, vol. 32, no. 3, pp. 548–558, 1984.

[6] J. C. Platt and A. H. Barr, “Constrained differential optimization,” in *Neural Information Processing Systems*, 1988, pp. 612–621.

[7] B. D. Van Veen and K. M. Buckley, “Beamforming: A versatile approach to spatial filtering,” *IEEE assp magazine*, vol. 5, no. 2, pp. 4–24, 1988.

[8] J. S. Garofolo, L. F. Lamel, W. M. Fisher, J. G. Fiscus, and D. S. Pallett, “Timit acoustic-phonetic continous speech corpus cd-rom. nist speech disc 1-1.1,” *NASA STI/Recon technical report n*, vol. 93, 1993.

[9] G. J. Brown and M. Cooke, “Computational auditory scene analysis,” *Computer Speech & Language*, vol. 8, no. 4, pp. 297–336, 1994.

[10] M. S. Brandstein and H. F. Silverman, “A robust method for speech signal time-delay estimation in reverberant rooms,” in *Acoustics, Speech and Signal Processing (ICASSP), 1997 IEEE International Conference on*, IEEE, vol. 1, 1997, pp. 375–378.

[11] S. Hochreiter and J. Schmidhuber, “Long short-term memory,” *Neural computation*, vol. 9, no. 8, pp. 1735–1780, 1997.

[12] T.-W. Lee, M. S. Lewicki, M. Girolami, and T. J. Sejnowski, “Blind source separation of more sources than mixtures using overcomplete representations,” *IEEE Signal Processing Letters*, vol. 6, no. 4, pp. 87–90, 1999.

[13] P. Bofill and M. Zibulevsky, “Underdetermined blind source separation using sparse representations,” *Signal processing*, vol. 81, no. 11, pp. 2353–2362, 2001.

[14] S. Gannot, D. Burshtein, and E. Weinstein, “Signal enhancement using beamforming and nonstationarity with applications to speech,” *IEEE Transactions on Signal Processing*, vol. 49, no. 8, pp. 1614–1626, 2001.

[15] D. D. Lee and H. S. Seung, “Algorithms for non-negative matrix factorization,” in *Advances in neural information processing systems*, 2001, pp. 556–562.

[16] A. W. Rix, J. G. Beerends, M. P. Hollier, and A. P. Hekstra, “Perceptual evaluation of speech quality (PESQ)-a new method for speech quality assessment of telephone networks and codecs,” in *Acoustics, Speech and Signal Processing (ICASSP), 2001 IEEE International Conference on*, IEEE, vol. 2, 2001, pp. 749–752.

[17] M. Zibulevsky and B. A. Pearlmutter, “Blind source separation by sparse decomposition in a signal dictionary,” *Neural computation*, vol. 13, no. 4, pp. 863–882, 2001.

[18] L. Benaroya, L. M. Donagh, F. Bimbot, and R. Gribonval, “Non negative sparse representation for wiener based source separation with a single sensor,” in *Acoustics, Speech and Signal Processing (ICASSP), 2003 IEEE International Conference on*, IEEE, vol. 6, 2003, pp. VI–613.

[19] G. Hu and D. Wang, “Monaural speech separation,” in *Advances in neural information processing systems*, 2003, pp. 1245–1252.

[20] N. Mitianoudis and M. E. Davies, “Using beamforming in the audio source separation problem,” in *Seventh International Symposium on Signal Processing and Its Applications, 2003. Proceedings.*, IEEE, vol. 2, 2003, pp. 89–92.

[21] S. Araki, S. Makino, A. Blin, R. Mukai, and H. Sawada, “Underdetermined blind separation for speech in real environments with sparseness and ICA,” in *Acoustics, Speech and Signal Processing (ICASSP), 2004 IEEE International Conference on*, IEEE, vol. 3, 2004, pp. iii–881.

[22] P. Divenyi, *Speech separation by humans and machines*. Springer Science & Business Media, 2004.

[23] H. L. Van Trees, *Optimum array processing: Part IV of detection, estimation, and modulation theory*. John Wiley & Sons, 2004.

[24] O. Yilmaz and S. Rickard, “Blind separation of speech mixtures via time-frequency masking,” *IEEE Transactions on Signal Processing*, vol. 52, no. 7, pp. 1830–1847, 2004.

[25] G. J. Brown and D. Wang, "Separation of speech by computational auditory scene analysis," in *Speech enhancement*, Springer, 2005, pp. 371–402.

[26] S. Choi, A. Cichocki, H.-M. Park, and S.-Y. Lee, "Blind source separation and independent component analysis: A review," *Neural Information Processing-Letters and Reviews*, vol. 6, no. 1, pp. 1–57, 2005.

[27] D. P. Ellis, "Evaluating speech separation systems," in *Speech Separation by Humans and Machines*, Springer, 2005, pp. 295–304.

[28] P. D. O'grady, B. A. Pearlmutter, and S. T. Rickard, "Survey of sparse and non-sparse methods in source separation," *International Journal of Imaging Systems and Technology*, vol. 15, no. 1, pp. 18–33, 2005.

[29] D. Wang, "On ideal binary mask as the computational goal of auditory scene analysis," in *Speech separation by humans and machines*, Springer, 2005, pp. 181–197.

[30] Ö. Çetin and E. Shriberg, "Analysis of overlaps in meetings by dialog factors, hot spots, speakers, and collection site: Insights for automatic speech recognition," in *Ninth International Conference on Spoken Language Processing*, 2006.

[31] T. Kim, T. Eltoft, and T.-W. Lee, "Independent vector analysis: An extension of ICA to multivariate components," in *International Conference on Independent Component Analysis and Signal Separation*, Springer, 2006, pp. 165–172.

[32] Y. Li, S.-I. Amari, A. Cichocki, D. W. Ho, and S. Xie, "Underdetermined blind source separation based on sparse representation," *IEEE Transactions on Signal Processing*, vol. 54, no. 2, pp. 423–437, 2006.

[33] M. N. Schmidt and R. K. Olsson, "Single-channel speech separation using sparse nonnegative matrix factorization," in *Ninth International Conference on Spoken Language Processing*, 2006.

[34] P. Smaragdis, "Convolutive speech bases and their application to supervised speech separation," *IEEE/ACM Transactions on Audio, Speech, and Language Processing (TASLP)*, vol. 15, no. 1, pp. 1–12, 2006.

[35] E. Vincent, R. Gribonval, and C. Févotte, "Performance measurement in blind audio source separation," *IEEE/ACM Transactions on Audio, Speech, and Language Processing (TASLP)*, vol. 14, no. 4, pp. 1462–1469, 2006.

[36] D. Wang and G. J. Brown, *Computational auditory scene analysis: Principles, algorithms, and applications*. Wiley-IEEE Press, 2006.

[37] M. E. Davies and C. J. James, “Source separation using single channel ICA,” *Signal Processing*, vol. 87, no. 8, pp. 1819–1832, 2007.

[38] I. Himawan, I. McCowan, and M. Lincoln, “Microphone array beamforming approach to blind speech separation,” in *International Workshop on Machine Learning for Multimodal Interaction*, Springer, 2007, pp. 295–305.

[39] Z. Koldovskỳ and P. Tichavskỳ, “Time-domain blind audio source separation using advanced ICA methods,” in *Eighth Annual Conference of the International Speech Communication Association*, 2007.

[40] I. Lee, T. Kim, and T.-W. Lee, “Independent vector analysis for convolutive blind speech separation,” in *Blind speech separation*, Springer, 2007, pp. 169–192.

[41] S. Makino, T.-W. Lee, and H. Sawada, *Blind speech separation*. Springer, 2007, vol. 615.

[42] P. Smaragdis, “Convolutive speech bases and their application to supervised speech separation,” *IEEE/ACM Transactions on Audio, Speech, and Language Processing (TASLP)*, vol. 15, no. 1, pp. 1–12, 2007.

[43] E. Vincent, “Complex nonconvex Lp norm minimization for underdetermined source separation,” in *International Conference on Independent Component Analysis and Signal Separation*, Springer, 2007, pp. 430–437.

[44] T. Virtanen, “Monaural sound source separation by nonnegative matrix factorization with temporal continuity and sparseness criteria,” *IEEE/ACM Transactions on Audio, Speech, and Language Processing (TASLP)*, vol. 15, no. 3, pp. 1066–1074, 2007.

[45] D. Wang, “Time-frequency masking for speech separation and its potential for hearing aid design,” *Trends in amplification*, vol. 12, no. 4, pp. 332–353, 2008.

[46] S. Arberet, A. Ozerov, R. Gribonval, and F. Bimbot, “Blind spectral-gmm estimation for underdetermined instantaneous audio source separation,” in *International Conference on Independent Component Analysis and Signal Separation*, 2009, pp. 751–758.

[47] Y. Bengio, J. Louradour, R. Collobert, and J. Weston, “Curriculum learning,” in *Proc. ICML*, 2009, pp. 41–48.

[48] Y. Li and D. Wang, “On the optimality of ideal binary time–frequency masks,” *Speech Communication*, vol. 51, no. 3, pp. 230–239, 2009.

[49] M. I. Mandel, R. J. Weiss, and D. P. Ellis, “Model-based expectation-maximization source separation and localization,” *IEEE/ACM Transactions on Audio, Speech, and Language Processing (TASLP)*, vol. 18, no. 2, pp. 382–394, 2009.

[50] A. Ozerov and C. Févotte, “Multichannel nonnegative matrix factorization in convolutive mixtures for audio source separation,” *IEEE/ACM Transactions on Audio, Speech, and Language Processing (TASLP)*, vol. 18, no. 3, pp. 550–563, 2009.

[51] H. Christensen, J. Barker, N. Ma, and P. D. Green, “The CHiME corpus: A resource and a challenge for computational hearing in multisource environments,” in *Eleventh Annual Conference of the International Speech Communication Association*, 2010.

[52] S. Doclo, S. Gannot, M. Moonen, and A. Spriet, “Acoustic beamforming for hearing aid applications,” *Handbook on array processing and sensor networks*, pp. 269–302, 2010.

[53] A. B. Gershman, N. D. Sidiropoulos, S. Shahbazpanahi, M. Bengtsson, and B. Ottersten, “Convex optimization-based beamforming,” *IEEE Signal Processing Magazine*, vol. 27, no. 3, pp. 62–75, 2010.

[54] J. Hao, I. Lee, T.-W. Lee, and T. J. Sejnowski, “Independent vector analysis for source separation using a mixture of gaussians prior,” *Neural computation*, vol. 22, no. 6, pp. 1646–1673, 2010.

[55] G. Hu and D. Wang, “A tandem algorithm for pitch estimation and voiced speech segregation,” *IEEE/ACM Transactions on Audio, Speech, and Language Processing (TASLP)*, vol. 18, no. 8, pp. 2067–2079, 2010.

[56] Z. Koldovsky and P. Tichavskỳ, “Time-domain blind separation of audio sources on the basis of a complete ICA decomposition of an observation space,” *IEEE/ACM Transactions on Audio, Speech, and Language Processing (TASLP)*, vol. 19, no. 2, pp. 406–416, 2010.

[57] E. Sarradj, “A fast signal subspace approach for the determination of absolute levels from phased microphone array measurements,” *Journal of Sound and Vibration*, vol. 329, no. 9, pp. 1553–1569, 2010.

[58] C. H. Taal, R. C. Hendriks, R. Heusdens, and J. Jensen, “A short-time objective intelligibility measure for time-frequency weighted noisy speech,” in *Acoustics, Speech and Signal Processing (ICASSP), 2010 IEEE International Conference on*, IEEE, 2010, pp. 4214–4217.

[59] V. Emiya, E. Vincent, N. Harlander, and V. Hohmann, “Subjective and objective quality assessment of audio source separation,” *IEEE/ACM Transactions on Audio, Speech, and Language Processing (TASLP)*, vol. 19, no. 7, pp. 2046–2057, 2011.

[60] K. Han and D. Wang, “An SVM based classification approach to speech separation,” in *Acoustics, Speech and Signal Processing (ICASSP), 2011 IEEE International Conference on*, IEEE, 2011, pp. 4632–4635.

[61] J. Ngiam, A. Khosla, M. Kim, J. Nam, H. Lee, and A. Y. Ng, “Multimodal deep learning,” in *ICML*, 2011.

[62] H. Sawada, H. Kameoka, S. Araki, and N. Ueda, “Formulations and algorithms for multichannel complex nmf,” in *Acoustics, Speech and Signal Processing (ICASSP), 2011 IEEE International Conference on*, IEEE, 2011, pp. 229–232.

[63] ——, “New formulations and efficient algorithms for multichannel NMF,” in *2011 IEEE Workshop on Applications of Signal Processing to Audio and Acoustics (WASPAA)*, IEEE, 2011, pp. 153–156.

[64] I. Tošić and P. Frossard, “Dictionary learning,” *IEEE Signal Processing Magazine*, vol. 28, no. 2, pp. 27–38, 2011.

[65] T. Xu and W. Wang, “Methods for learning adaptive dictionary in underdetermined speech separation,” in *2011 IEEE International Workshop on Machine Learning for Signal Processing*, IEEE, 2011, pp. 1–6.

[66] H. Adel, M. Souad, A. Alaqeeli, and A. Hamid, “Beamforming techniques for multichannel audio signal separation,” *arXiv preprint arXiv:1212.6080*, 2012.

[67] M. Bai, J.-G. Ih, and J. Benesty, “Time-domain MVDR array filter for speech enhancement,” in *Acoustic Array Systems: Theory, Implementation, and Application*. IEEE, 2013, ch. 7, pp. 287–314, ISBN: 9780470827253.

[68] J. Barker, E. Vincent, N. Ma, H. Christensen, and P. Green, “The PASCAL CHiME speech separation and recognition challenge,” *Computer Speech & Language*, vol. 27, no. 3, pp. 621–633, 2013.

[69] K. Hu and D. Wang, “An unsupervised approach to cochannel speech separation,” *IEEE/ACM Transactions on Audio, Speech, and Language Processing (TASLP)*, vol. 21, no. 1, pp. 122–131, 2013.

[70] Y. Liang, G. Chen, S. Naqvi, and J. A. Chambers, “Independent vector analysis with multivariate student’s t-distribution source prior for speech separation,” *Electronics Letters*, vol. 49, no. 16, pp. 1035–1036, 2013.

[71] T. Mikolov, I. Sutskever, K. Chen, G. S. Corrado, and J. Dean, “Distributed representations of words and phrases and their compositionality,” in *Advances in neural information processing systems*, 2013, pp. 3111–3119.

[72] H. Sawada, H. Kameoka, S. Araki, and N. Ueda, “Multichannel extensions of non-negative matrix factorization with complex-valued data,” *IEEE/ACM Transactions on Audio, Speech, and Language Processing (TASLP)*, vol. 21, no. 5, pp. 971–982, 2013.

[73] E. Vincent, J. Barker, S. Watanabe, J. Le Roux, F. Nesta, and M. Matassoni, "The second 'CHiME'speech separation and recognition challenge: Datasets, tasks and baselines," in *Acoustics, Speech and Signal Processing (ICASSP), 2013 IEEE International Conference on*, IEEE, 2013, pp. 126–130.

[74] Y. Wang and D. Wang, "Towards scaling up classification-based speech separation," *IEEE/ACM Transactions on Audio, Speech, and Language Processing (TASLP)*, vol. 21, no. 7, pp. 1381–1390, 2013.

[75] T. Xu, W. Wang, and W. Dai, "Sparse coding with adaptive dictionary learning for underdetermined blind speech separation," *Speech Communication*, vol. 55, no. 3, pp. 432–450, 2013.

[76] Y. Xu, J. Du, L.-R. Dai, and C.-H. Lee, "An experimental study on speech enhancement based on deep neural networks," *IEEE Signal Processing Letters*, vol. 21, no. 1, pp. 65–68, 2013.

[77] G. Bao, Y. Xu, and Z. Ye, "Learning a discriminative dictionary for single-channel speech separation," *IEEE/ACM Transactions on Audio, Speech, and Language Processing (TASLP)*, vol. 22, no. 7, pp. 1130–1138, 2014.

[78] U. Hamid, R. A. Qamar, and K. Waqas, "Performance comparison of time-domain and frequency-domain beamforming techniques for sensor array processing," in *Proceedings of 2014 11th International Bhurban Conference on Applied Sciences & Technology (IBCAST) Islamabad, Pakistan, 14th-18th January, 2014*, IEEE, 2014, pp. 379–385.

[79] J. R. Hershey, J. L. Roux, and F. Weninger, "Deep unfolding: Model-based inspiration of novel deep architectures," *arXiv preprint arXiv:1409.2574*, 2014.

[80] P.-S. Huang, M. Kim, M. Hasegawa-Johnson, and P. Smaragdis, "Deep learning for monaural speech separation," in *Acoustics, Speech and Signal Processing (ICASSP), 2014 IEEE International Conference on*, IEEE, 2014, pp. 1562–1566.

[81] C. Hummersone, T. Stokes, and T. Brookes, "On the ideal ratio mask as the goal of computational auditory scene analysis," in *Blind source separation*, Springer, 2014, pp. 349–368.

[82] T. G. Kang, K. Kwon, J. W. Shin, and N. S. Kim, "NMF-based target source separation using deep neural network," *IEEE Signal Processing Letters*, vol. 22, no. 2, pp. 229–233, 2014.

[83] D. Kingma and J. Ba, "Adam: A method for stochastic optimization," *arXiv preprint: 1412.6980*, 2014.

[84] R. Kiros, R. Salakhutdinov, and R. Zemel, “Multimodal neural language models,” in *International conference on machine learning*, PMLR, 2014, pp. 595–603.

[85] Y. Liang, J. Harris, S. M. Naqvi, G. Chen, and J. A. Chambers, “Independent vector analysis with a generalized multivariate gaussian source prior for frequency domain blind source separation,” *Signal Processing*, vol. 105, pp. 175–184, 2014.

[86] J. Mao, W. Xu, Y. Yang, J. Wang, Z. Huang, and A. Yuille, “Deep captioning with multimodal recurrent neural networks (m-rnn),” *arXiv preprint arXiv:1412.6632*, 2014.

[87] C. Raffel, B. McFee, E. J. Humphrey, J. Salamon, O. Nieto, D. Liang, D. P. Ellis, and C. C. Raffel, “Mir_eval: A transparent implementation of common MIR metrics,” in *In Proceedings of the 15th International Society for Music Information Retrieval Conference, ISMIR*, Citeseer, 2014.

[88] E. Vincent, N. Bertin, R. Gribonval, and F. Bimbot, “From blind to guided audio source separation: How models and side information can improve the separation of sound,” *IEEE Signal Processing Magazine*, vol. 31, no. 3, pp. 107–115, 2014.

[89] Y. Wang, A. Narayanan, and D. Wang, “On training targets for supervised speech separation,” *IEEE/ACM Transactions on Audio, Speech and Language Processing (TASLP)*, vol. 22, no. 12, pp. 1849–1858, 2014.

[90] Z. Wang and F. Sha, “Discriminative non-negative matrix factorization for single-channel speech separation,” in *Acoustics, Speech and Signal Processing (ICASSP), 2014 IEEE International Conference on*, IEEE, 2014, pp. 3749–3753.

[91] F. Weninger, J. R. Hershey, J. Le Roux, and B. Schuller, “Discriminatively trained recurrent neural networks for single-channel speech separation,” in *2014 IEEE Global Conference on Signal and Information Processing (GlobalSIP)*, IEEE, 2014, pp. 577–581.

[92] F. Weninger, J. L. Roux, J. R. Hershey, and S. Watanabe, “Discriminative NMF and its application to single-channel source separation,” in *Fifteenth Annual Conference of the International Speech Communication Association*, 2014.

[93] Y. Xu, J. Du, L.-R. Dai, and C.-H. Lee, “A regression approach to speech enhancement based on deep neural networks,” *IEEE/ACM Transactions on Audio, Speech, and Language Processing (TASLP)*, vol. 23, no. 1, pp. 7–19, 2014.

[94] S. Araki, T. Hayashi, M. Delcroix, M. Fujimoto, K. Takeda, and T. Nakatani, “Exploring multi-channel features for denoising-autoencoder-based speech enhancement,” in *Acoustics, Speech and Signal Processing (ICASSP), 2015 IEEE International Conference on*, IEEE, 2015, pp. 116–120.

[95] J. Barker, R. Marxer, E. Vincent, and S. Watanabe, “The third ‘chime’ speech separation and recognition challenge: Dataset, task and baselines,” *Automatic Speech Recognition and Understanding (ASRU), 2015 IEEE Workshop on*, pp. 504–511, 2015.

[96] ——, “The third ‘CHiME’speech separation and recognition challenge: Dataset, task and baselines,” in *2015 IEEE Workshop on Automatic Speech Recognition and Understanding (ASRU)*, IEEE, 2015, pp. 504–511.

[97] X. Chen, X. Qiu, C. Zhu, P. Liu, and X.-J. Huang, “Long short-term memory neural networks for chinese word segmentation,” in *Proceedings of the 2015 Conference on Empirical Methods in Natural Language Processing*, 2015, pp. 1197–1206.

[98] H. Erdogan, J. R. Hershey, S. Watanabe, and J. Le Roux, “Phase-sensitive and recognition-boosted speech separation using deep recurrent neural networks,” in *Acoustics, Speech and Signal Processing (ICASSP), 2015 IEEE International Conference on*, IEEE, 2015, pp. 708–712.

[99] K. He, X. Zhang, S. Ren, and J. Sun, “Delving deep into rectifiers: Surpassing human-level performance on imagenet classification,” in *Proceedings of the IEEE international conference on computer vision*, 2015, pp. 1026–1034.

[100] J. Heymann, L. Drude, A. Chinaev, and R. Haeb-Umbach, “BLSTM supported GEV beamformer front-end for the 3rd chime challenge,” in *Automatic Speech Recognition and Understanding (ASRU), 2015 IEEE Workshop on*, IEEE, 2015, pp. 444–451.

[101] G. Hinton, O. Vinyals, and J. Dean, “Distilling the knowledge in a neural network,” *arXiv preprint: 1503.02531*, 2015.

[102] P.-S. Huang, M. Kim, M. Hasegawa-Johnson, and P. Smaragdis, “Joint optimization of masks and deep recurrent neural networks for monaural source separation,” *IEEE/ACM Transactions on Audio, Speech and Language Processing (TASLP)*, vol. 23, no. 12, pp. 2136–2147, 2015.

[103] D. Kitamura, N. Ono, H. Sawada, H. Kameoka, and H. Saruwatari, “Efficient multichannel nonnegative matrix factorization exploiting rank-1 spatial model,” in *Acoustics, Speech and Signal Processing (ICASSP), 2015 IEEE International Conference on*, IEEE, 2015, pp. 276–280.

[104] L. Le Magoarou, A. Ozerov, and N. Q. Duong, “Text-informed audio source separation. example-based approach using non-negative matrix partial co-factorization,” *Journal of Signal Processing Systems*, vol. 79, no. 2, pp. 117–131, 2015.

[105] J. Le Roux, J. R. Hershey, and F. Weninger, “Deep NMF for speech separation,” in *Acoustics, Speech and Signal Processing (ICASSP), 2015 IEEE International Conference on*, IEEE, 2015, pp. 66–70.

[106] J. Le Roux, F. J. Weninger, and J. R. Hershey, “Sparse NMF–half-baked or well done?” *Mitsubishi Electric Research Labs (MERL), Cambridge, MA, USA, Tech. Rep., no. TR2015-023*, vol. 11, pp. 13–15, 2015.

[107] J. Li, A. Mohamed, G. Zweig, and Y. Gong, “LSTM time and frequency recurrence for automatic speech recognition,” in *Automatic Speech Recognition and Understanding (ASRU), 2015 IEEE Workshop on*, IEEE, 2015, pp. 187–191.

[108] J. Li, M.-T. Luong, and D. Jurafsky, “A hierarchical neural autoencoder for paragraphs and documents,” *arXiv preprint: 1506.01057*, 2015.

[109] V. Panayotov, G. Chen, D. Povey, and S. Khudanpur, “Librispeech: An ASR corpus based on public domain audio books,” in *Acoustics, Speech and Signal Processing (ICASSP), 2015 IEEE International Conference on*, IEEE, 2015, pp. 5206–5210.

[110] D. Pathak, P. Krahenbuhl, and T. Darrell, “Constrained convolutional neural networks for weakly supervised segmentation,” in *Proceedings of the IEEE international conference on computer vision*, 2015, pp. 1796–1804.

[111] T. N. Sainath, R. J. Weiss, K. W. Wilson, A. Narayanan, M. Bacchiani, *et al.*, “Speaker location and microphone spacing invariant acoustic modeling from raw multichannel waveforms,” in *Automatic Speech Recognition and Understanding (ASRU), 2015 IEEE Workshop on*, IEEE, 2015, pp. 30–36.

[112] T. N. Sainath, R. J. Weiss, A. Senior, K. W. Wilson, and O. Vinyals, “Learning the speech front-end with raw waveform CLDNNs,” in *Sixteenth Annual Conference of the International Speech Communication Association*, 2015.

[113] D. S. Williamson, Y. Wang, and D. Wang, “Complex ratio masking for monaural speech separation,” *IEEE/ACM Transactions on Audio, Speech, and Language Processing (TASLP)*, vol. 24, no. 3, pp. 483–492, 2015.

[114] J. L. Ba, J. R. Kiros, and G. E. Hinton, “Layer normalization,” *arXiv preprint: 1607.06450*, 2016.

[115] F. Chollet, “Xception: Deep learning with depthwise separable convolutions,” *arXiv preprint*, 2016.

[116] J. Chung, S. Ahn, and Y. Bengio, “Hierarchical multiscale recurrent neural networks,” *arXiv preprint: 1609.01704*, 2016.

[117] H. Erdogan, T. Hayashi, J. R. Hershey, T. Hori, C. Hori, W.-N. Hsu, S. Kim, J. Le Roux, Z. Meng, and S. Watanabe, “Multi-channel speech recognition: LSTMs all the way through,” in *CHiME-4 workshop*, 2016.

[118] H. Erdogan, J. R. Hershey, S. Watanabe, M. I. Mandel, and J. Le Roux, "Improved MVDR beamforming using single-channel mask prediction networks.," in *Proc. Interspeech*, 2016, pp. 1981–1985.

[119] K. He, X. Zhang, S. Ren, and J. Sun, "Deep residual learning for image recognition," in *Proceedings of the IEEE conference on computer vision and pattern recognition*, 2016, pp. 770–778.

[120] ——, "Identity mappings in deep residual networks," in *European Conference on Computer Vision*, Springer, 2016, pp. 630–645.

[121] J. R. Hershey, Z. Chen, J. Le Roux, and S. Watanabe, "Deep clustering: Discriminative embeddings for segmentation and separation," in *Acoustics, Speech and Signal Processing (ICASSP), 2016 IEEE International Conference on*, IEEE, 2016, pp. 31–35.

[122] J. Heymann, L. Drude, and R. Haeb-Umbach, "Neural network based spectral mask estimation for acoustic beamforming," in *Acoustics, Speech and Signal Processing (ICASSP), 2016 IEEE International Conference on*, IEEE, 2016, pp. 196–200.

[123] Y. Isik, J. Le Roux, Z. Chen, S. Watanabe, and J. R. Hershey, "Single-channel multi-speaker separation using deep clustering," *Proc. Interspeech*, pp. 545–549, 2016.

[124] C. Lea, R. Vidal, A. Reiter, and G. D. Hager, "Temporal convolutional networks: A unified approach to action segmentation," in *European Conference on Computer Vision*, Springer, 2016, pp. 47–54.

[125] B. Li, T. N. Sainath, R. J. Weiss, K. W. Wilson, and M. Bacchiani, "Neural network adaptive beamforming for robust multichannel speech recognition.," in *Proc. Interspeech*, 2016, pp. 1976–1980.

[126] H. Li, S. Nie, X. Zhang, and H. Zhang, "Jointly optimizing activation coefficients of convolutive NMF using dnn for speech separation.," in *Proc. Interspeech*, 2016, pp. 550–554.

[127] J. Li, A. Mohamed, G. Zweig, and Y. Gong, "Exploring multidimensional LSTMs for large vocabulary ASR," in *Acoustics, Speech and Signal Processing (ICASSP), 2016 IEEE International Conference on*, IEEE, 2016, pp. 4940–4944.

[128] L. Ma, Z. Lu, and H. Li, "Learning to answer questions from image using convolutional neural network," in *Proceedings of the AAAI Conference on Artificial Intelligence*, vol. 30, 2016.

[129] S. Mehri, K. Kumar, I. Gulrajani, R. Kumar, S. Jain, J. Sotelo, A. Courville, and Y. Bengio, "SampleRNN: An unconditional end-to-end neural audio generation model," *arXiv preprint: 1612.07837*, 2016.

[130] A. v. d. Oord, S. Dieleman, H. Zen, K. Simonyan, O. Vinyals, A. Graves, N. Kalchbrenner, A. Senior, and K. Kavukcuoglu, “Wavenet: A generative model for raw audio,” *arXiv preprint: 1609.03499*, 2016.

[131] D. Pathak, P. Krahenbuhl, J. Donahue, T. Darrell, and A. A. Efros, “Context encoders: Feature learning by inpainting,” in *Proceedings of the IEEE conference on computer vision and pattern recognition*, 2016, pp. 2536–2544.

[132] T. N. Sainath and B. Li, “Modeling time-frequency patterns with LSTM vs. convolutional architectures for lvcsr tasks,” *Proc. Interspeech*, pp. 813–817, 2016.

[133] D. S. Williamson, Y. Wang, and D. Wang, “Complex ratio masking for monaural speech separation,” *IEEE/ACM Transactions on Audio, Speech, and Language Processing (TASLP)*, vol. 24, no. 3, pp. 483–492, 2016.

[134] X. Xiao, S. Watanabe, E. S. Chng, and H. Li, “Beamforming networks using spatial covariance features for far-field speech recognition,” in *Signal and Information Processing Association Annual Summit and Conference (APSIPA), 2016 Asia-Pacific*, IEEE, 2016, pp. 1–6.

[135] X. Xiao, S. Watanabe, H. Erdogan, L. Lu, J. Hershey, M. L. Seltzer, G. Chen, Y. Zhang, M. Mandel, and D. Yu, “Deep beamforming networks for multi-channel speech recognition,” in *Acoustics, Speech and Signal Processing (ICASSP), 2016 IEEE International Conference on*, IEEE, 2016, pp. 5745–5749.

[136] C. Boeddeker, P. Hanebrink, L. Drude, J. Heymann, and R. Haeb-Umbach, “Optimizing neural-network supported acoustic beamforming by algorithmic differentiation,” in *Acoustics, Speech and Signal Processing (ICASSP), 2017 IEEE International Conference on*, IEEE, 2017, pp. 171–175.

[137] P. Chandna, M. Miron, J. Janer, and E. Gómez, “Monoaural audio source separation using deep convolutional neural networks,” in *International conference on latent variable analysis and signal separation*, Springer, 2017, pp. 258–266.

[138] S. Chang, Y. Zhang, W. Han, M. Yu, X. Guo, W. Tan, X. Cui, M. Witbrock, M. A. Hasegawa-Johnson, and T. S. Huang, “Dilated recurrent neural networks,” in *Advances in Neural Information Processing Systems*, 2017, pp. 77–87.

[139] Z. Chen, J. Droppo, J. Li, and W. Xiong, “Progressive joint modeling in unsupervised single-channel overlapped speech recognition,” *IEEE/ACM Transactions on Audio, Speech, and Language Processing (TASLP)*, vol. 26, no. 1, pp. 184–196, 2017.

[140] Z. Chen, Y. Luo, and N. Mesgarani, “Deep attractor network for single-microphone speaker separation,” in *Acoustics, Speech and Signal Processing (ICASSP), 2017 IEEE International Conference on*, IEEE, 2017, pp. 246–250.

[141] S. Erateb, M. Naqvi, and J. Chambers, “Online IVA with adaptive learning for speech separation using various source priors,” in *2017 Sensor Signal Processing for Defence Conference (SSPD)*, IEEE, 2017, pp. 1–5.

[142] S. Gannot, E. Vincent, S. Markovich-Golan, and A. Ozerov, “A consolidated perspective on multimicrophone speech enhancement and source separation,” *IEEE/ACM Transactions on Audio, Speech, and Language Processing (TASLP)*, vol. 25, no. 4, pp. 692–730, 2017.

[143] J. Heymann, L. Drude, C. Boeddeker, P. Hanebrink, and R. Haeb-Umbach, “Beamnet: End-to-end training of a beamformer-supported multi-channel ASR system,” in *Acoustics, Speech and Signal Processing (ICASSP), 2017 IEEE International Conference on*, IEEE, 2017, pp. 5325–5329.

[144] A. G. Howard, M. Zhu, B. Chen, D. Kalenichenko, W. Wang, T. Weyand, M. Andreetto, and H. Adam, “Mobilenets: Efficient convolutional neural networks for mobile vision applications,” *arXiv preprint: 1704.04861*, 2017.

[145] S. Ishiwatari, J. Yao, S. Liu, M. Li, M. Zhou, N. Yoshinaga, M. Kitsuregawa, and W. Jia, “Chunk-based decoder for neural machine translation,” in *Proceedings of the 55th Annual Meeting of the Association for Computational Linguistics (Volume 1: Long Papers)*, 2017, pp. 1901–1912.

[146] A. Jansson, E. Humphrey, N. Montecchio, R. Bittner, A. Kumar, and T. Weyde, “Singing voice separation with deep u-net convolutional networks.,” in *ISMIR*, 2017, pp. 745–751.

[147] L. Kaiser, A. N. Gomez, and F. Chollet, “Depthwise separable convolutions for neural machine translation,” *arXiv preprint: 1706.03059*, 2017.

[148] M. Kolbæk, D. Yu, Z.-H. Tan, and J. Jensen, “Multitalker speech separation with utterance-level permutation invariant training of deep recurrent neural networks,” *IEEE/ACM Transactions on Audio, Speech, and Language Processing (TASLP)*, vol. 25, no. 10, pp. 1901–1913, 2017.

[149] C. Lea, M. D. Flynn, R. Vidal, A. Reiter, and G. D. Hager, “Temporal convolutional networks for action segmentation and detection,” in *proceedings of the IEEE Conference on Computer Vision and Pattern Recognition*, 2017, pp. 156–165.

[150] J.-H. Luo, J. Wu, and W. Lin, “Thinet: A filter level pruning method for deep neural network compression,” in *Proceedings of the IEEE international conference on computer vision*, 2017, pp. 5058–5066.

[151] Y. Luo, Z. Chen, J. R. Hershey, J. Le Roux, and N. Mesgarani, “Deep clustering and conventional networks for music separation: Stronger together,” in *Acoustics, Speech and Signal Processing (ICASSP), 2017 IEEE International Conference on*, IEEE, 2017, pp. 61–65.

[152] P. Magron, R. Badeau, and B. David, “Phase-dependent anisotropic gaussian model for audio source separation,” in *Acoustics, Speech and Signal Processing (ICASSP), 2017 IEEE International Conference on*, IEEE, 2017, pp. 531–535.

[153] P. Márquez-Neila, M. Salzmann, and P. Fua, “Imposing hard constraints on deep networks: Promises and limitations,” *arXiv preprint arXiv:1706.02025*, 2017.

[154] Z. Meng, S. Watanabe, J. R. Hershey, and H. Erdogan, “Deep long short-term memory adaptive beamforming networks for multichannel robust speech recognition,” in *Acoustics, Speech and Signal Processing (ICASSP), 2017 IEEE International Conference on*, IEEE, 2017, pp. 271–275.

[155] G. Naithani, T. Barker, G. Parascandolo, L. Bramsl, N. H. Pontoppidan, T. Virtanen, *et al.*, “Low latency sound source separation using convolutional recurrent neural networks,” in *2017 IEEE Workshop on Applications of Signal Processing to Audio and Acoustics (WASPAA)*, IEEE, 2017, pp. 71–75.

[156] T. Ochiai, S. Watanabe, T. Hori, and J. R. Hershey, “Multichannel end-to-end speech recognition,” *arXiv preprint: 1703.04783*, 2017.

[157] T. Ochiai, S. Watanabe, T. Hori, J. R. Hershey, and X. Xiao, “Unified architecture for multichannel end-to-end speech recognition with neural beamforming,” *IEEE Journal of Selected Topics in Signal Processing*, vol. 11, no. 8, pp. 1274–1288, 2017.

[158] S. Parekh, S. Essid, A. Ozerov, N. Q. Duong, P. Pérez, and G. Richard, “Motion informed audio source separation,” in *Acoustics, Speech and Signal Processing (ICASSP), 2017 IEEE International Conference on*, IEEE, 2017, pp. 6–10.

[159] L. Pfeifenberger, M. Zöhrer, and F. Pernkopf, “DNN-based speech mask estimation for eigenvector beamforming,” in *Acoustics, Speech and Signal Processing (ICASSP), 2017 IEEE International Conference on*, IEEE, 2017, pp. 66–70.

[160] T. Pham, Y.-S. Lee, S. Mathulaprangsan, and J.-C. Wang, “Source separation using dictionary learning and deep recurrent neural network with locality preserving constraint,” in *2017 IEEE International Conference on Multimedia and Expo (ICME)*, IEEE, 2017, pp. 151–156.

[161] T. N. Sainath, R. J. Weiss, K. W. Wilson, B. Li, A. Narayanan, E. Variani, M. Bacchiani, I. Shafran, A. Senior, K. Chin, *et al.*, “Multichannel signal processing with deep neural networks for automatic speech recognition,” *IEEE/ACM Transactions on Audio, Speech, and Language Processing (TASLP)*, vol. 25, no. 5, pp. 965–979, 2017.

[162] A. Santoro, D. Raposo, D. G. Barrett, M. Malinowski, R. Pascanu, P. Battaglia, and T. Lillicrap, “A simple neural network module for relational reasoning,” in *Advances in neural information processing systems*, 2017, pp. 4967–4976.

[163] P. Smaragdis and S. Venkataramani, “A neural network alternative to non-negative audio models,” in *Acoustics, Speech and Signal Processing (ICASSP), 2017 IEEE International Conference on*, IEEE, 2017, pp. 86–90.

[164] L. Sun, J. Du, L.-R. Dai, and C.-H. Lee, “Multiple-target deep learning for LSTM-RNN based speech enhancement,” in *2017 Hands-free Speech Communications and Microphone Arrays (HSCMA)*, IEEE, 2017, pp. 136–140.

[165] N. Takahashi and Y. Mitsufuji, “Multi-scale multi-band densenets for audio source separation,” in *2017 IEEE Workshop on Applications of Signal Processing to Audio and Acoustics (WASPAA)*, IEEE, 2017, pp. 21–25.

[166] A. Vaswani, N. Shazeer, N. Parmar, J. Uszkoreit, L. Jones, A. N. Gomez, Ł. Kaiser, and I. Polosukhin, “Attention is all you need,” in *Advances in neural information processing systems*, 2017, pp. 5998–6008.

[167] S. Venkataramani, C. Subakan, and P. Smaragdis, “Neural network alternatives toconvolutive audio models for source separation,” in *2017 IEEE 27th International Workshop on Machine Learning for Signal Processing (MLSP)*, IEEE, 2017, pp. 1–6.

[168] Q. Wang, J. Du, L.-R. Dai, and C.-H. Lee, “Joint noise and mask aware training for DNN-based speech enhancement with sub-band features,” in *2017 Hands-free Speech Communications and Microphone Arrays (HSCMA)*, IEEE, 2017, pp. 101–105.

[169] S. Wisdom, T. Powers, J. Pitton, and L. Atlas, “Deep recurrent nmf for speech separation by unfolding iterative thresholding,” in *2017 IEEE Workshop on Applications of Signal Processing to Audio and Acoustics (WASPAA)*, IEEE, 2017, pp. 254–258.

[170] X. Xiao, S. Zhao, D. L. Jones, E. S. Chng, and H. Li, “On time-frequency mask estimation for MVDR beamforming with application in robust speech recognition,” in *Acoustics, Speech and Signal Processing (ICASSP), 2017 IEEE International Conference on*, IEEE, 2017, pp. 3246–3250.

[171] Y. Xu, J. Du, Z. Huang, L.-R. Dai, and C.-H. Lee, “Multi-objective learning and mask-based post-processing for deep neural network based speech enhancement,” *arXiv preprint arXiv:1703.07172*, 2017.

[172] D. Yu, X. Chang, and Y. Qian, “Recognizing multi-talker speech with permutation invariant training,” *Proc. Interspeech*, pp. 2456–2460, 2017.

[173] D. Yu, M. Kolbæk, Z.-H. Tan, and J. Jensen, “Permutation invariant training of deep models for speaker-independent multi-talker speech separation,” in *Acoustics, Speech and Signal Processing (ICASSP), 2017 IEEE International Conference on*, IEEE, 2017, pp. 241–245.

[174] M. Zaheer, S. Kottur, S. Ravanbakhsh, B. Poczos, R. R. Salakhutdinov, and A. J. Smola, "Deep sets," in *Advances in neural information processing systems*, 2017, pp. 3391–3401.

[175] X. Zhang and D. Wang, "Deep learning based binaural speech separation in reverberant environments," *IEEE/ACM Transactions on Audio, Speech, and Language Processing (TASLP)*, vol. 25, no. 5, pp. 1075–1084, 2017.

[176] X. Zhang, Z.-Q. Wang, and D. Wang, "A speech enhancement algorithm by iterating single-and multi-microphone processing and its application to robust ASR," in *Acoustics, Speech and Signal Processing (ICASSP), 2017 IEEE International Conference on*, IEEE, 2017, pp. 276–280.

[177] H. Zhou, Z. Tu, S. Huang, X. Liu, H. Li, and J. Chen, "Chunk-based bi-scale decoder for neural machine translation," *arXiv preprint: 1705.01452*, 2017.

[178] J. Azcarreta, N. Ito, S. Araki, and T. Nakatani, "Permutation-free CGMM: Complex gaussian mixture model with inverse wishart mixture model based spatial prior for permutation-free source separation and source counting," in *Acoustics, Speech and Signal Processing (ICASSP), 2018 IEEE International Conference on*, IEEE, 2018, pp. 51–55.

[179] S. Bai, J. Z. Kolter, and V. Koltun, "An empirical evaluation of generic convolutional and recurrent networks for sequence modeling," *arXiv preprint: 1803.01271*, 2018.

[180] J. Barker, S. Watanabe, E. Vincent, and J. Trmal, "The fifth 'CHiME'speech separation and recognition challenge: Dataset, task and baselines," in *Interspeech 2018-19th Annual Conference of the International Speech Communication Association*, 2018.

[181] C. Boeddeker, H. Erdogan, T. Yoshioka, and R. Haeb-Umbach, "Exploring practical aspects of neural mask-based beamforming for far-field speech recognition," in *Acoustics, Speech and Signal Processing (ICASSP), 2018 IEEE International Conference on*, IEEE, 2018, pp. 6697–6701.

[182] X. Chang, Y. Qian, and D. Yu, "Monaural multi-talker speech recognition with attention mechanism and gated convolutional networks.," in *Proc. Interspeech*, 2018, pp. 1586–1590.

[183] Z. Chen, X. Xiao, T. Yoshioka, H. Erdogan, J. Li, and Y. Gong, "Multi-channel overlapped speech recognition with location guided speech extraction network," in *2018 IEEE Spoken Language Technology Workshop (SLT)*, IEEE, 2018, pp. 558–565.

[184] L. Dong, S. Xu, and B. Xu, "Speech-transformer: A no-recurrence sequence-to-sequence model for speech recognition," in *Acoustics, Speech and Signal Processing (ICASSP), 2018 IEEE International Conference on*, IEEE, 2018, pp. 5884–5888.

[185] L. Drude, T. von Neumann, and R. Haeb-Umbach, "Deep attractor networks for speaker re-identification and blind source separation," in *Acoustics, Speech and Signal Processing (ICASSP), 2018 IEEE International Conference on*, IEEE, 2018, pp. 11–15.

[186] A. Ephrat, I. Mosseri, O. Lang, T. Dekel, K. Wilson, A. Hassidim, W. T. Freeman, and M. Rubinstein, "Looking to listen at the cocktail party: A speaker-independent audio-visual model for speech separation," *ACM Transactions on Graphics (TOG)*, vol. 37, no. 4, pp. 1–11, 2018.

[187] S.-W. Fu, T.-W. Wang, Y. Tsao, X. Lu, and H. Kawai, "End-to-end waveform utterance enhancement for direct evaluation metrics optimization by fully convolutional neural networks," *IEEE/ACM Transactions on Audio, Speech and Language Processing (TASLP)*, vol. 26, no. 9, pp. 1570–1584, 2018.

[188] J. Heymann, M. Bacchiani, and T. N. Sainath, "Performance of mask based statistical beamforming in a smart home scenario," in *Acoustics, Speech and Signal Processing (ICASSP), 2018 IEEE International Conference on*, IEEE, 2018, pp. 6722–6726.

[189] N. Ito, C. Schymura, S. Araki, and T. Nakatani, "Noisy cGMM: Complex gaussian mixture model with non-sparse noise model for joint source separation and denoising," in *2018 26th European Signal Processing Conference (EUSIPCO)*, IEEE, 2018, pp. 1662–1666.

[190] M. J. Jo, G. W. Lee, J. M. Moon, C. Cho, and H. K. Kim, "Estimation of MVDR beamforming weights based on deep neural network," in *Audio Engineering Society Convention 145*, Audio Engineering Society, 2018.

[191] H. Kameoka, H. Sawada, and T. Higuchi, "General formulation of multichannel extensions of NMF variants," in *Audio Source Separation*, Springer, 2018, pp. 95–124.

[192] M. Kim and P. Smaragdis, "Bitwise neural networks for efficient single-channel source separation," in *Acoustics, Speech and Signal Processing (ICASSP), 2018 IEEE International Conference on*, IEEE, 2018, pp. 701–705.

[193] K. Kinoshita, L. Drude, M. Delcroix, and T. Nakatani, "Listening to each speaker one by one with recurrent selective hearing networks," in *Acoustics, Speech and Signal Processing (ICASSP), 2018 IEEE International Conference on*, IEEE, 2018, pp. 5064–5068.

[194] C. Li, L. Zhu, S. Xu, P. Gao, and B. Xu, "CBLDNN-based speaker-independent speech separation via generative adversarial training," in *Acoustics, Speech and Signal Processing (ICASSP), 2018 IEEE International Conference on*, IEEE, 2018.

[195] J. Li, B. M. Chen, and G. Hee Lee, "So-net: Self-organizing network for point cloud analysis," in *Proceedings of the IEEE conference on computer vision and pattern recognition*, 2018, pp. 9397–9406.

[196] S. Li, W. Li, C. Cook, C. Zhu, and Y. Gao, "Independently recurrent neural network (indrnn): Building a longer and deeper rnn," in *Proceedings of the IEEE Conference on Computer Vision and Pattern Recognition*, 2018, pp. 5457–5466.

[197] H. Liu, K. Simonyan, and Y. Yang, "DARTS: Differentiable architecture search," in *International Conference on Learning Representations*, 2018.

[198] Y. Luo, Z. Chen, and N. Mesgarani, "Speaker-independent speech separation with deep attractor network," *IEEE/ACM Transactions on Audio, Speech, and Language Processing (TASLP)*, vol. 26, no. 4, pp. 787–796, 2018.

[199] ——, "Speaker-independent speech separation with deep attractor network," *IEEE/ACM Transactions on Audio, Speech, and Language Processing (TASLP)*, vol. 26, no. 4, pp. 787–796, 2018.

[200] Y. Luo and N. Mesgarani, "Real-time single-channel dereverberation and separation with time-domain audio separation network," *Proc. Interspeech*, pp. 342–346, 2018.

[201] ——, "TasNet: Time-domain audio separation network for real-time, single-channel speech separation," in *Acoustics, Speech and Signal Processing (ICASSP), 2018 IEEE International Conference on*, IEEE, 2018.

[202] Y. Matsui, T. Nakatani, M. Delcroix, K. Kinoshita, N. Ito, S. Araki, and S. Makino, "Online integration of DNN-based and spatial clustering-based mask estimation for robust MVDR beamforming," in *2018 16th International Workshop on Acoustic Signal Enhancement (IWAENC)*, IEEE, 2018, pp. 71–75.

[203] S. Nie, S. Liang, W. Liu, X. Zhang, and J. Tao, "Deep learning based speech separation via NMF-style reconstructions," *IEEE/ACM Transactions on Audio, Speech, and Language Processing (TASLP)*, vol. 26, no. 11, pp. 2043–2055, 2018.

[204] S. Park, T. Kim, K. Lee, and N. Kwak, "Music source separation using stacked hourglass networks.," in *ISMIR*, 2018, pp. 289–296.

[205] K. Qian, Y. Zhang, S. Chang, X. Yang, D. Florencio, and M. Hasegawa-Johnson, "Deep learning based speech beamforming," in *Acoustics, Speech and Signal Processing (ICASSP), 2018 IEEE International Conference on*, IEEE, 2018, pp. 5389–5393.

[206] Y. Qian, X. Chang, and D. Yu, "Single-channel multi-talker speech recognition with permutation invariant training," *Speech Communication*, vol. 104, pp. 1–11, 2018.

[207] M. Sandler, A. Howard, M. Zhu, A. Zhmoginov, and L.-C. Chen, "Mobilenetv2: Inverted residuals and linear bottlenecks," in *Proceedings of the IEEE Conference on Computer Vision and Pattern Recognition*, 2018, pp. 4510–4520.

[208] R. Scheibler, E. Bezzam, and I. Dokmanić, "Pyroomacoustics: A python package for audio room simulation and array processing algorithms," in *Acoustics, Speech and Signal Processing (ICASSP), 2018 IEEE International Conference on*, IEEE, 2018, pp. 351–355.

[209] S. Settle, J. Le Roux, T. Hori, S. Watanabe, and J. R. Hershey, "End-to-end multi-speaker speech recognition," in *Acoustics, Speech and Signal Processing (ICASSP), 2018 IEEE International Conference on*, IEEE, 2018, pp. 4819–4823.

[210] J. Shi, J. Xu, G. Liu, and B. Xu, "Listen, think and listen again: Capturing top-down auditory attention for speaker-independent speech separation," in *Proceedings of the 27th International Joint Conference on Artificial Intelligence*, AAAI Press, 2018, pp. 4353–4360.

[211] D. Stoller, S. Ewert, and S. Dixon, "Wave-U-Net: A multi-scale neural network for end-to-end audio source separation.," in *ISMIR*, 2018, pp. 334–340.

[212] N. Takahashi, N. Goswami, and Y. Mitsufuji, "MMDenseLSTM: An efficient combination of convolutional and recurrent neural networks for audio source separation," in *2018 16th International Workshop on Acoustic Signal Enhancement (IWAENC)*, IEEE, 2018, pp. 106–110.

[213] K. Tan and D. Wang, "A convolutional recurrent neural network for real-time speech enhancement.," in *Proc. Interspeech*, 2018, pp. 3229–3233.

[214] S. Venkataramani, J. Casebeer, and P. Smaragdis, "End-to-end source separation with adaptive front-ends," in *2018 52nd Asilomar Conference on Signals, Systems, and Computers*, IEEE, 2018, pp. 684–688.

[215] D. Wang and J. Chen, "Supervised speech separation based on deep learning: An overview," *IEEE/ACM Transactions on Audio, Speech, and Language Processing (TASLP)*, 2018.

[216] J. Wang, J. Chen, D. Su, L. Chen, M. Yu, Y. Qian, and D. Yu, "Deep extractor network for target speaker recovery from single channel speech mixtures," *Proc. Interspeech*, pp. 307–311, 2018.

[217] Q. Wang, H. Muckenhirn, K. Wilson, P. Sridhar, Z. Wu, J. Hershey, R. A. Saurous, R. J. Weiss, Y. Jia, and I. L. Moreno, "Voicefilter: Targeted voice separation by speaker-conditioned spectrogram masking," *arXiv preprint arXiv:1810.04826*, 2018.

[218] Z.-Q. Wang, J. Le Roux, and J. R. Hershey, "Alternative objective functions for deep clustering," in *Acoustics, Speech and Signal Processing (ICASSP), 2018 IEEE International Conference on*, 2018.

[219] ——, “Multi-channel deep clustering: Discriminative spectral and spatial embeddings for speaker-independent speech separation,” in *Acoustics, Speech and Signal Processing (ICASSP), 2018 IEEE International Conference on*, 2018.

[220] Z.-Q. Wang, J. L. Roux, D. Wang, and J. R. Hershey, “End-to-end speech separation with unfolded iterative phase reconstruction,” *arXiv preprint: 1804.10204*, 2018.

[221] S. Watanabe, T. Hori, S. Karita, T. Hayashi, J. Nishitoba, Y. Unno, N. E. Y. Soplin, J. Heymann, M. Wiesner, N. Chen, *et al.*, “ESPnet: End-to-end speech processing toolkit,” *arXiv preprint arXiv:1804.00015*, 2018.

[222] C. Xu, W. Rao, X. Xiao, E. S. Chng, and H. Li, “Single channel speech separation with constrained utterance level permutation invariant training using grid LSTM,” in *Acoustics, Speech and Signal Processing (ICASSP), 2018 IEEE International Conference on*, IEEE, 2018, pp. 6–10.

[223] K. Xu, W. Hu, J. Leskovec, and S. Jegelka, “How powerful are graph neural networks?” *arXiv preprint: 1810.00826*, 2018.

[224] H. Zhao, S. Zarar, I. Tashev, and C.-H. Lee, “Convolutional-recurrent neural networks for speech enhancement,” in *Acoustics, Speech and Signal Processing (ICASSP), 2018 IEEE International Conference on*, IEEE, 2018, pp. 2401–2405.

[225] R. Aihara, T. Hanazawa, Y. Okato, G. Wichern, and J. Le Roux, “Teacher-student deep clustering for low-delay single channel speech separation,” in *Acoustics, Speech and Signal Processing (ICASSP), 2019 IEEE International Conference on*, IEEE, 2019, pp. 690–694.

[226] F. Bahmaninezhad, J. Wu, R. Gu, S.-X. Zhang, Y. Xu, M. Yu, and D. Yu, “A comprehensive study of speech separation: Spectrogram vs waveform separation,” *arXiv preprint: 1905.07497*, 2019.

[227] X. Chang, W. Zhang, Y. Qian, J. Le Roux, and S. Watanabe, “MIMO-speech: End-to-end multi-channel multi-speaker speech recognition,” in *Automatic Speech Recognition and Understanding (ASRU), 2019 IEEE Workshop on*, IEEE, 2019, pp. 237–244.

[228] M. Delfarah and D. Wang, “Deep learning for talker-dependent reverberant speaker separation: An empirical study,” *IEEE/ACM Transactions on Audio, Speech, and Language Processing*, vol. 27, no. 11, pp. 1839–1848, 2019.

[229] L. Drude, J. Heitkaemper, C. Boeddeker, and R. Haeb-Umbach, “SMS-WSJ: Database, performance measures, and baseline recipe for multi-channel source separation and recognition,” *arXiv preprint arXiv:1910.13934*, 2019.

[230] S. Gao, M.-M. Cheng, K. Zhao, X.-Y. Zhang, M.-H. Yang, and P. H. Torr, “Res2net: A new multi-scale backbone architecture,” *IEEE transactions on pattern analysis and machine intelligence (TPAMI)*, 2019.

[231] R. Gu, J. Wu, S.-X. Zhang, L. Chen, Y. Xu, M. Yu, D. Su, Y. Zou, and D. Yu, “End-to-end multi-channel speech separation,” *arXiv preprint: 1905.06286*, 2019.

[232] N. Kanda, C. Boeddeker, J. Heitkaemper, Y. Fujita, S. Horiguchi, K. Nagamatsu, and R. Haeb-Umbach, “Guided source separation meets a strong ASR backend: Hitachi/paderborn university joint investigation for dinner party asr,” *arXiv preprint arXiv:1905.12230*, 2019.

[233] S. Karita, N. Chen, T. Hayashi, T. Hori, H. Inaguma, Z. Jiang, M. Someki, N. E. Y. Soplin, R. Yamamoto, X. Wang, *et al.*, “A comparative study on transformer vs rnn in speech applications,” in *Automatic Speech Recognition and Understanding (ASRU), 2019 IEEE Workshop on*, IEEE, 2019, pp. 449–456.

[234] I. Kavalerov, S. Wisdom, H. Erdogan, B. Patton, K. Wilson, J. L. Roux, and J. R. Hershey, “Universal sound separation,” *arXiv preprint: 1905.03330*, 2019.

[235] S. Kim, M. Maity, and M. Kim, “Incremental binarization on recurrent neural networks for single-channel source separation,” in *Acoustics, Speech and Signal Processing (ICASSP), 2019 IEEE International Conference on*, IEEE, 2019, pp. 376–380.

[236] J. Le Roux, S. Wisdom, H. Erdogan, and J. R. Hershey, “SDR–half-baked or well done?” In *Acoustics, Speech and Signal Processing (ICASSP), 2019 IEEE International Conference on*, IEEE, 2019, pp. 626–630.

[237] N. Li, S. Liu, Y. Liu, S. Zhao, and M. Liu, “Neural speech synthesis with transformer network,” in *Proceedings of the AAAI Conference on Artificial Intelligence*, vol. 33, 2019, pp. 6706–6713.

[238] X. Li and R. Horaud, “Multichannel speech enhancement based on time-frequency masking using subband long short-term memory,” in *2019 IEEE Workshop on Applications of Signal Processing to Audio and Acoustics (WASPAA)*, IEEE, 2019, pp. 298–302.

[239] Y. Liu and D. Wang, “Divide and conquer: A deep casa approach to talker-independent monaural speaker separation,” *arXiv preprint: 1904.11148*, 2019.

[240] F. Lluís, J. Pons, and X. Serra, “End-to-end music source separation: Is it possible in the waveform domain?” *Proc. Interspeech*, pp. 4619–4623, 2019.

[241] Y. Luo, E. Ceolini, C. Han, S.-C. Liu, and N. Mesgarani, “FaSNet: Low-latency adaptive beamforming for multi-microphone audio processing,” in *Automatic Speech Recognition and Understanding (ASRU), 2019 IEEE Workshop on*, IEEE, 2019.

[242] Y. Luo and N. Mesgarani, "Augmented time-frequency mask estimation in cluster-based source separation algorithms," in *Acoustics, Speech and Signal Processing (ICASSP), 2019 IEEE International Conference on*, IEEE, 2019, pp. 710–714.

[243] ——, "Conv-TasNet: Surpassing ideal time–frequency magnitude masking for speech separation," *IEEE/ACM Transactions on Audio, Speech, and Language Processing (TASLP)*, vol. 27, no. 8, pp. 1256–1266, 2019.

[244] S. Maiti and M. I. Mandel, "Parametric resynthesis with neural vocoders," in *2019 IEEE Workshop on Applications of Signal Processing to Audio and Acoustics (WASPAA)*, IEEE, 2019, pp. 303–307.

[245] A. Marafioti, N. Perraudin, N. Holighaus, and P. Majdak, "A context encoder for audio inpainting," *IEEE/ACM Transactions on Audio, Speech, and Language Processing (TASLP)*, vol. 27, no. 12, pp. 2362–2372, 2019.

[246] H. Mazzawi, X. Gonzalvo, A. Kracun, P. Sridhar, N. Subrahmanya, I. Lopez-Moreno, H.-J. Park, and P. Violette, "Improving keyword spotting and language identification via neural architecture search at scale.," in *Proc. Interspeech*, 2019, pp. 1278–1282.

[247] T. von Neumann, K. Kinoshita, M. Delcroix, S. Araki, T. Nakatani, and R. Haeb-Umbach, "All-neural online source separation, counting, and diarization for meeting analysis," in *Acoustics, Speech and Signal Processing (ICASSP), 2019 IEEE International Conference on*, IEEE, 2019, pp. 91–95.

[248] A. Pandey and D. Wang, "A new framework for cnn-based speech enhancement in the time domain," *IEEE/ACM Transactions on Audio, Speech, and Language Processing (TASLP)*, vol. 27, no. 7, pp. 1179–1188, 2019.

[249] J. Shi, J. Xu, and B. Xu, "Which ones are speaking? speaker-inferred model for multi-talker speech separation," *Interspeech 2019*, pp. 4609–4613, 2019.

[250] T. Simons and D.-J. Lee, "A review of binarized neural networks," *Electronics*, vol. 8, no. 6, p. 661, 2019.

[251] N. Takahashi, S. Parthasaarathy, N. Goswami, and Y. Mitsufuji, "Recursive speech separation for unknown number of speakers," *Interspeech 2019*, pp. 1348–1352, 2019.

[252] E. Tsunoo, Y. Kashiwagi, T. Kumakura, and S. Watanabe, "Transformer ASR with contextual block processing," in *Automatic Speech Recognition and Understanding (ASRU), 2019 IEEE Workshop on*, IEEE, 2019, pp. 427–433.

[253] Y.-H. Tu, J. Du, L. Sun, F. Ma, H.-K. Wang, J.-D. Chen, and C.-H. Lee, "An iterative mask estimation approach to deep learning based multi-channel speech recognition," *Speech Communication*, vol. 106, pp. 31–43, 2019.

[254] P. Wang, Z. Chen, X. Xiao, Z. Meng, T. Yoshioka, T. Zhou, L. Lu, and J. Li, "Speech separation using speaker inventory," in *2019 IEEE Automatic Speech Recognition and Understanding Workshop (ASRU)*, IEEE, 2019, pp. 230–236.

[255] Z.-Q. Wang, K. Tan, and D. Wang, "Deep learning based phase reconstruction for speaker separation: A trigonometric perspective," in *Acoustics, Speech and Signal Processing (ICASSP), 2019 IEEE International Conference on*, IEEE, 2019, pp. 71–75.

[256] G. Wichern, J. Antognini, M. Flynn, L. R. Zhu, E. McQuinn, D. Crow, E. Manilow, and J. L. Roux, "WHAM!: Extending speech separation to noisy environments," *arXiv preprint arXiv:1907.01160*, 2019.

[257] J. Wu, Y. Xu, S.-X. Zhang, L.-W. Chen, M. Yu, L. Xie, and D. Yu, "Time domain audio visual speech separation," in *2019 IEEE Automatic Speech Recognition and Understanding Workshop (ASRU)*, IEEE, 2019, pp. 667–673.

[258] C. Xu, W. Rao, E. S. Chng, and H. Li, "Time-domain speaker extraction network," in *Automatic Speech Recognition and Understanding (ASRU), 2019 IEEE Workshop on*, IEEE, 2019, pp. 327–334.

[259] T. Yoshioka, I. Abramovski, C. Aksoylar, Z. Chen, M. David, D. Dimitriadis, Y. Gong, I. Gurvich, X. Huang, Y. Huang, *et al.*, "Advances in online audio-visual meeting transcription," *arXiv preprint arXiv:1912.04979*, 2019.

[260] T. Yoshioka, Z. Chen, D. Dimitriadis, W. Hinthorn, X. Huang, A. Stolcke, and M. Zeng, "Meeting transcription using virtual microphone arrays," Microsoft Research, Tech. Rep. MSR-TR-2019-11, 2019, Available as https://arxiv.org/abs/1905.02545.

[261] T. Yoshioka, Z. Chen, C. Liu, X. Xiao, H. Erdogan, and D. Dimitriadis, "Low-latency speaker-independent continuous speech separation," in *Acoustics, Speech and Signal Processing (ICASSP), 2019 IEEE International Conference on*, IEEE, 2019, pp. 6980–6984.

[262] K. Žmolıéková, M. Delcroix, K. Kinoshita, T. Ochiai, T. Nakatani, L. Burget, and J. Černockỳ, "Speakerbeam: Speaker aware neural network for target speaker extraction in speech mixtures," *IEEE Journal of Selected Topics in Signal Processing*, vol. 13, no. 4, pp. 800–814, 2019.

[263] C. Boeddeker, W. Zhang, T. Nakatani, K. Kinoshita, T. Ochiai, M. Delcroix, N. Kamo, Y. Qian, S. Watanabe, and R. Haeb-Umbach, "Convolutive transfer function invariant sdr training criteria for multi-channel reverberant speech separation," *arXiv preprint arXiv:2011.15003*, 2020.

[264] J. Casebeer, U. Isik, S. Venkataramani, and A. Krishnaswamy, "Efficient trainable front-ends for neural speech enhancement," in *Acoustics, Speech and Signal Processing (ICASSP), 2020 IEEE International Conference on*, IEEE, 2020, pp. 6639–6643.

[265] J. Chen, Q. Mao, and D. Liu, "Dual-path transformer network: Direct context-aware modeling for end-to-end monaural speech separation," *Proc. Interspeech*, pp. 2642–2646, 2020.

[266] ——, "On synthesis for supervised monaural speech separation in time domain," *Proc. Interspeech*, pp. 2627–2631, 2020.

[267] S. Chen, Y. Wu, Z. Chen, T. Yoshioka, S. Liu, and J. Li, "Don't shoot butterfly with rifles: Multi-channel continuous speech separation with early exit transformer," *arXiv preprint arXiv:2010.12180*, 2020.

[268] Z. Chen, T. Yoshioka, L. Lu, T. Zhou, Z. Meng, Y. Luo, J. Wu, X. Xiao, and J. Li, "Continuous speech separation: Dataset and analysis," in *Acoustics, Speech and Signal Processing (ICASSP), 2020 IEEE International Conference on*, IEEE, 2020, pp. 7284–7288.

[269] J. Cosentino, M. Pariente, S. Cornell, A. Deleforge, and E. Vincent, "Librimix: An open-source dataset for generalizable speech separation," *arXiv preprint arXiv:2005.11262*, 2020.

[270] D. Diaz-Guerra, A. Miguel, and J. R. Beltran, "GpuRIR: A python library for room impulse response simulation with gpu acceleration," *Multimedia Tools and Applications*, pp. 1–19, 2020.

[271] Z. Du, X. Zhang, and J. Han, "A joint framework of denoising autoencoder and generative vocoder for monaural speech enhancement," *IEEE/ACM Transactions on Audio, Speech, and Language Processing (TASLP)*, vol. 28, pp. 1493–1505, 2020.

[272] C. Fan, J. Tao, B. Liu, J. Yi, Z. Wen, and X. Liu, "End-to-end post-filter for speech separation with deep attention fusion features," *IEEE/ACM Transactions on Audio, Speech, and Language Processing (TASLP)*, vol. 28, pp. 1303–1314, 2020.

[273] R. Gu, S.-X. Zhang, L. Chen, Y. Xu, M. Yu, D. Su, Y. Zou, and D. Yu, "Enhancing end-to-end multi-channel speech separation via spatial feature learning," in *Acoustics, Speech and Signal Processing (ICASSP), 2020 IEEE International Conference on*, IEEE, 2020, pp. 7319–7323.

[274] R. Gu, S.-X. Zhang, Y. Xu, L. Chen, Y. Zou, and D. Yu, "Multi-modal multi-channel target speech separation," *IEEE Journal of Selected Topics in Signal Processing*, vol. 14, no. 3, pp. 530–541, 2020.

[275] C. Han, Y. Luo, C. Li, T. Zhou, K. Kinoshita, S. Watanabe, M. Delcroix, H. Erdogan, J. R. Hershey, N. Mesgarani, *et al.*, "Continuous speech separation using speaker inventory for long multi-talker recording," *arXiv preprint arXiv:2012.09727*, 2020.

[276] C. Han, Y. Luo, and N. Mesgarani, "Real-time binaural speech separation with preserved spatial cues," in *Acoustics, Speech and Signal Processing (ICASSP), 2020 IEEE International Conference on*, IEEE, 2020, pp. 6404–6408.

[277] K. Han, Y. Wang, Q. Tian, J. Guo, C. Xu, and C. Xu, "Ghostnet: More features from cheap operations," in *Proceedings of the IEEE/CVF Conference on Computer Vision and Pattern Recognition*, 2020, pp. 1580–1589.

[278] S. Hu, X. Xie, S. Liu, M. Geng, X. Liu, and H. Meng, "Neural architecture search for speech recognition," *arXiv preprint: 2007.08818*, 2020.

[279] Y. Hu, Y. Liu, S. Lv, M. Xing, S. Zhang, Y. Fu, J. Wu, B. Zhang, and L. Xie, "DCCRN: Deep complex convolution recurrent network for phase-aware speech enhancement," *arXiv preprint: 2008.00264*, 2020.

[280] B. Kadıoğlu, M. Horgan, X. Liu, J. Pons, D. Darcy, and V. Kumar, "An empirical study of Conv-TasNet," in *Acoustics, Speech and Signal Processing (ICASSP), 2020 IEEE International Conference on*, IEEE, 2020, pp. 7264–7268.

[281] N. Kanda, Y. Gaur, X. Wang, Z. Meng, and T. Yoshioka, "Serialized output training for end-to-end overlapped speech recognition," *arXiv preprint arXiv:2003.12687*, 2020.

[282] S. Kim, H. Yang, and M. Kim, "Boosted locality sensitive hashing: Discriminative binary codes for source separation," in *Acoustics, Speech and Signal Processing (ICASSP), 2020 IEEE International Conference on*, IEEE, 2020, pp. 106–110.

[283] K. Kinoshita, T. von Neumann, M. Delcroix, T. Nakatani, and R. Haeb-Umbach, "Multi-path RNN for hierarchical modeling of long sequential data and its application to speaker stream separation," *Proc. Interspeech 2020*, pp. 2652–2656, 2020.

[284] M. Kolbæk, Z.-H. Tan, S. H. Jensen, and J. Jensen, "On loss functions for supervised monaural time-domain speech enhancement," *IEEE/ACM Transactions on Audio, Speech, and Language Processing (TASLP)*, 2020.

[285] C. Li and Y. Qian, "Listen, watch and understand at the cocktail party: Audio-visual-contextual speech separation," *Proc. Interspeech*, pp. 1426–1430, 2020.

[286] Y. Luo, Z. Chen, N. Mesgarani, and T. Yoshioka, "End-to-end microphone permutation and number invariant multi-channel speech separation," in *Acoustics, Speech and Signal Processing (ICASSP), 2020 IEEE International Conference on*, IEEE, 2020, pp. 6394–6398.

[287] Y. Luo, Z. Chen, and T. Yoshioka, "Dual-path RNN: Efficient long sequence modeling for time-domain single-channel speech separation," in *Acoustics, Speech and Signal Processing (ICASSP), 2020 IEEE International Conference on*, IEEE, 2020, pp. 46–50.

[288] Y. Luo, C. Han, and N. Mesgarani, "Ultra-lightweight speech separation via group communication," *arXiv preprint: 2011.08397*, 2020.

[289] Y. Luo and N. Mesgarani, "Implicit filter-and-sum network for multi-channel speech separation," *arXiv preprint: 2011.08401*, 2020.

[290] ——, "Separating varying numbers of sources with auxiliary autoencoding loss," *Proc. Interspeech*, 2020.

[291] M. Maciejewski, G. Wichern, E. McQuinn, and J. Le Roux, "WHAMR!: Noisy and reverberant single-channel speech separation," in *Acoustics, Speech and Signal Processing (ICASSP), 2020 IEEE International Conference on*, IEEE, 2020, pp. 696–700.

[292] S. Maiti and M. I. Mandel, "Speaker independence of neural vocoders and their effect on parametric resynthesis speech enhancement," in *Acoustics, Speech and Signal Processing (ICASSP), 2020 IEEE International Conference on*, IEEE, 2020, pp. 206–210.

[293] E. Nachmani, Y. Adi, and L. Wolf, "Voice separation with an unknown number of multiple speakers," *arXiv preprint: 2003.01531*, 2020.

[294] T. Nakamura and H. Saruwatari, "Time-domain audio source separation based on wave-u-net combined with discrete wavelet transform," in *Acoustics, Speech and Signal Processing (ICASSP), 2020 IEEE International Conference on*, IEEE, 2020, pp. 386–390.

[295] T. von Neumann, C. Boeddeker, L. Drude, K. Kinoshita, M. Delcroix, T. Nakatani, and R. Haeb-Umbach, "Multi-talker ASR for an unknown number of sources: Joint training of source counting, separation and ASR," *Proc. Interspeech*, pp. 3097–3101, 2020.

[296] T. von Neumann, K. Kinoshita, L. Drude, C. Boeddeker, M. Delcroix, T. Nakatani, and R. Haeb-Umbach, "End-to-end training of time domain audio separation and recognition," in *Acoustics, Speech and Signal Processing (ICASSP), 2020 IEEE International Conference on*, IEEE, 2020, pp. 7004–7008.

[297] A. Novoselov, P. Balazs, and G. Bokelmann, "Separating and denoising seismic signals with dual-path recurrent neural network architecture," 2020.

[298] T. Ochiai, M. Delcroix, R. Ikeshita, K. Kinoshita, T. Nakatani, and S. Araki, "Beam-TasNet: Time-domain audio separation network meets frequency-domain beamformer," in *Acoustics, Speech and Signal Processing (ICASSP), 2020 IEEE International Conference on*, IEEE, 2020, pp. 6384–6388.

[299] M. Pariente, S. Cornell, A. Deleforge, and E. Vincent, "Filterbank design for end-to-end speech separation," in *Acoustics, Speech and Signal Processing (ICASSP), 2020 IEEE International Conference on*, IEEE, 2020, pp. 6364–6368.

[300] C. Subakan, M. Ravanelli, S. Cornell, M. Bronzi, and J. Zhong, "Attention is all you need in speech separation," *arXiv preprint arXiv:2010.13154*, 2020.

[301] M. Tagliasacchi, Y. Li, K. Misiunas, and D. Roblek, "SEANet: A multi-modal speech enhancement network," *Proc. Interspeech*, pp. 1126–1130, 2020.

[302] N. Takahashi and Y. Mitsufuji, "D3net: Densely connected multidilated densenet for music source separation," *arXiv preprint: 2010.01733*, 2020.

[303] K. Tan, B. Xu, A. Kumar, E. Nachmani, and Y. Adi, "SAGRNN: Self-attentive gated rnn for binaural speaker separation with interaural cue preservation," *arXiv preprint: 2009.01381*, 2020.

[304] K. Tan, Y. Xu, S.-X. Zhang, M. Yu, and D. Yu, "Audio-visual speech separation and dereverberation with a two-stage multimodal network," *IEEE Journal of Selected Topics in Signal Processing*, vol. 14, no. 3, pp. 542–553, 2020.

[305] E. Tzinis, Z. Wang, and P. Smaragdis, "Sudo rm-rf: Efficient networks for universal audio source separation," in *2020 IEEE 30th International Workshop on Machine Learning for Signal Processing (MLSP)*, IEEE, 2020, pp. 1–6.

[306] E. Tzinis, S. Wisdom, J. R. Hershey, A. Jansen, and D. P. Ellis, "Improving universal sound separation using sound classification," in *Acoustics, Speech and Signal Processing (ICASSP), 2020 IEEE International Conference on*, IEEE, 2020, pp. 96–100.

[307] P. Wang, Z. Chen, D. Wang, J. Li, and Y. Gong, "Speaker separation using speaker inventories and estimated speech," *IEEE/ACM Transactions on Audio, Speech, and Language Processing (TASLP)*, 2020.

[308] Z.-Q. Wang, P. Wang, and D. Wang, "Complex spectral mapping for single-and multi-channel speech enhancement and robust asr," *IEEE/ACM Transactions on Audio, Speech, and Language Processing (TASLP)*, vol. 28, pp. 1778–1787, 2020.

[309] ——, "Multi-microphone complex spectral mapping for utterance-wise and continuous speaker separation," *arXiv preprint arXiv:2010.01703*, 2020.

[310] S. Wisdom, E. Tzinis, H. Erdogan, R. J. Weiss, K. Wilson, and J. R. Hershey, "Unsupervised sound separation using mixtures of mixtures," *arXiv preprint arXiv:2006.12701*, 2020.

[311] Y. Xu, M. Yu, S.-X. Zhang, L. Chen, C. Weng, J. Liu, and D. Yu, "Neural spatio-temporal beamformer for target speech separation," *Proc. Interspeech 2020*, pp. 56–60, 2020.

[312] D. Yin, C. Luo, Z. Xiong, and W. Zeng, "PHASEN: A phase-and-harmonics-aware speech enhancement network.," in *AAAI*, 2020, pp. 9458–9465.

[313] N. Zeghidour and D. Grangier, “Wavesplit: End-to-end speech separation by speaker clustering,” *arXiv preprint arXiv:2002.08933*, 2020.

[314] H. Zhang, C. Wu, Z. Zhang, Y. Zhu, Z. Zhang, H. Lin, Y. Sun, T. He, J. Mueller, R. Manmatha, *et al.*, “ResNeSt: Split-attention networks,” *arXiv preprint: 2004.08955*, 2020.

[315] L. Zhang, Z. Shi, J. Han, A. Shi, and D. Ma, “FurcaNeXt: End-to-end monaural speech separation with dynamic gated dilated temporal convolutional networks,” in *International Conference on Multimedia Modeling*, Springer, 2020, pp. 653–665.

[316] ——, “Furcanext: End-to-end monaural speech separation with dynamic gated dilated temporal convolutional networks,” in *International Conference on Multimedia Modeling*, Springer, 2020, pp. 653–665.

[317] W. Zhang, X. Chang, Y. Qian, and S. Watanabe, “Improving end-to-end single-channel multi-talker speech recognition,” *IEEE/ACM Transactions on Audio, Speech, and Language Processing (TASLP)*, vol. 28, pp. 1385–1394, 2020.

[318] B. J. Borgström, M. S. Brandstein, G. A. Ciccarelli, T. F. Quatieri, and C. J. Smalt, “Speaker separation in realistic noise environments with applications to a cognitively-controlled hearing aid,” *Neural Networks*, vol. 140, pp. 136–147, 2021.

[319] H. Chen and P. Zhang, “A 2-stage framework with iterative refinement for multi-channel speech separation,” *arXiv preprint arXiv:2102.02998*, 2021.

[320] R. Ikeshita and T. Nakatani, “Independent vector extraction for fast joint blind source separation and dereverberation,” *IEEE Signal Processing Letters*, 2021.

[321] N. Kanda, X. Chang, Y. Gaur, X. Wang, Z. Meng, Z. Chen, and T. Yoshioka, “Investigation of end-to-end speaker-attributed ASR for continuous multi-talker recordings,” in *2021 IEEE Spoken Language Technology Workshop (SLT)*, IEEE, 2021, pp. 809–816.

[322] C. Li, Y. Luo, C. Han, J. Li, T. Yoshioka, T. Zhou, M. Delcroix, K. Kinoshita, C. Boeddeker, Y. Qian, *et al.*, “Dual-path RNN for long recording speech separation,” in *2021 IEEE Spoken Language Technology Workshop (SLT)*, IEEE, 2021, pp. 865–872.

[323] Y. Luo, Z. Chen, C. Han, C. Li, T. Zhou, and N. Mesgarani, “Rethinking the separation layers in speech separation networks,” in *Acoustics, Speech and Signal Processing (ICASSP), 2021 IEEE International Conference on*, IEEE, 2021.

[324] Y. Luo, C. Han, and N. Mesgarani, “Distortion-controlled training for end-to-end reverberant speech separation with auxiliary autoencoding loss,” in *2021 IEEE Spoken Language Technology Workshop (SLT)*, IEEE, 2021.

[325] ——, "Empirical analysis of generalized iterative speech separation networks," *Proc. Interspeech 2021*, 2021.

[326] ——, "Group communication with context codec for lightweight source separation," *IEEE/ACM Transactions on Audio, Speech, and Language Processing (TASLP)*, 2021.

[327] D. Michelsanti, Z.-H. Tan, S.-X. Zhang, Y. Xu, M. Yu, D. Yu, and J. Jensen, "An overview of deep-learning-based audio-visual speech enhancement and separation," *IEEE/ACM Transactions on Audio, Speech, and Language Processing*, 2021.

[328] D. Raj, P. Denisov, Z. Chen, H. Erdogan, Z. Huang, M. He, S. Watanabe, J. Du, T. Yoshioka, Y. Luo, *et al.*, "Integration of speech separation, diarization, and recognition for multi-speaker meetings: System description, comparison, and analysis," in *2021 IEEE Spoken Language Technology Workshop (SLT)*, IEEE, 2021, pp. 897–904.

[329] A. Ramesh, M. Pavlov, G. Goh, S. Gray, C. Voss, A. Radford, M. Chen, and I. Sutskever, "Zero-shot text-to-image generation," *arXiv preprint arXiv:2102.12092*, 2021.

[330] W. Rao, Y. Fu, Y. Hu, X. Xu, Y. Jv, J. Han, Z. Jiang, L. Xie, Y. Wang, S. Watanabe, *et al.*, "INTERSPEECH 2021 ConferencingSpeech challenge: Towards far-field multi-channel speech enhancement for video conferencing," *arXiv preprint arXiv:2104.00960*, 2021.

[331] D. Wang, T. Yoshioka, Z. Chen, X. Wang, T. Zhou, and Z. Meng, "Continuous speech separation with ad hoc microphone arrays," *arXiv preprint arXiv:2103.02378*, 2021.

[332] X. Wang, N. Kanda, Y. Gaur, Z. Chen, Z. Meng, and T. Yoshioka, "Exploring end-to-end multi-channel asr with bias information for meeting transcription," in *2021 IEEE Spoken Language Technology Workshop (SLT)*, IEEE, 2021, pp. 833–840.

[333] Z.-Q. Wang, H. Erdogan, S. Wisdom, K. Wilson, D. Raj, S. Watanabe, Z. Chen, and J. R. Hershey, "Sequential multi-frame neural beamforming for speech separation and enhancement," in *2021 IEEE Spoken Language Technology Workshop (SLT)*, IEEE, 2021, pp. 905–911.

[334] G. Hu, *100 Nonspeech Sounds*, `http://web.cse.ohio-state.edu/pnl/corpus/HuNonspeech/HuCorpus.html`.

[335] *ITU-T Rec. P.10: Vocabulary for performance and quality of service*.

[336] K. Schulze-Forster, C. S. Doire, G. Richard, and R. Badeau, "Joint phoneme alignment and text-informed speech separation on highly corrupted speech," in *Acoustics, Speech and Signal Processing (ICASSP), 2020 IEEE International Conference on*, pp. 6404–6408.